

Copyright Warning & Restrictions

The copyright law of the United States (Title 17, United States Code) governs the making of photocopies or other reproductions of copyrighted material.

Under certain conditions specified in the law, libraries and archives are authorized to furnish a photocopy or other reproduction. One of these specified conditions is that the photocopy or reproduction is not to be “used for any purpose other than private study, scholarship, or research.” If a user makes a request for, or later uses, a photocopy or reproduction for purposes in excess of “fair use” that user may be liable for copyright infringement,

This institution reserves the right to refuse to accept a copying order if, in its judgment, fulfillment of the order would involve violation of copyright law.

Please Note: The author retains the copyright while the New Jersey Institute of Technology reserves the right to distribute this thesis or dissertation

Printing note: If you do not wish to print this page, then select “Pages from: first page # to: last page #” on the print dialog screen



The Van Houten library has removed some of the personal information and all signatures from the approval page and biographical sketches of theses and dissertations in order to protect the identity of NJIT graduates and faculty.

ABSTRACT

INVESTIGATION OF HEART RATE VARIABILITY DURING SLEEP APNEA

**by
Sekar Subramanian**

Sleep apnea is a disorder, where there are repetitive pauses in respiratory flow of at least 10 seconds or longer duration, and which occur more than five times per hour. Apnea has strong modulating effects on the autonomic nervous system, with prominent heart rate variation. It can be assumed that during sleep, internal influences (sympathetic and parasympathetic nervous system activities) dominate the autonomic nervous system; in addition repetitive apneas are accompanied by a pronounced increase in average heart rate. The aim of this study was to investigate the heart rate variability using spectral analysis and time-frequency analysis during sleep apnea.

A total of 22 subjects (18 males and 4 females, 49 ± 20 years) were studied who were experiencing both obstructive sleep apnea and central sleep apnea in whom sleep-disordered breathing was diagnosed. In addition 6 control subjects were studied where sleep apnea was not expected. Spectral and wavelet analysis were used to investigate the heart rate variability from the sleep apnea subjects and control subjects. The results of the wavelet analysis gave information about the parasympathetic (HF) and sympatho-vagal balance (LF: HF) changes as a function of time and frequency. The spectral parameters LF, HF and LF/HF confirmed reduced parasympathetic activity in patients with sleep apnea compared to normal subjects. In addition the repetitive apneas are accompanied by a pronounced increased cyclic variation of heart rate.

**INVESTIGATION OF HEART RATE VARIABILITY
DURING SLEEP APNEA**

by
Sekar Subramanian

**A Thesis
Submitted to the Faculty of
New Jersey Institute of Technology
In Partial Fulfillment of the Requirements for the Degree of
Master of Science in Biomedical Engineering**

Department of Biomedical Engineering

January 2004

APPROVAL PAGE

**INVESTIGATION OF HEART RATE VARIABILITY
DURING SLEEP APNEA**

Sekar Subramanian

Dr. Stanley S. Reisman, Thesis Advisor
Professor of Biomedical Engineering, NJIT

Date

Dr. David Kristol, Committee Member
Professor of Biomedical Engineering, NJIT

Date

Dr. Ronald H Rockland, Committee Member
Associate Professor of Engineering Technology, NJIT

Date

BIOGRAPHICAL SKETCH

Author: Sekar Subramanian

Degree: Master of Science

Date: January 2004

Date of Birth: July 4, 1972

Undergraduate and Graduate Education:

- **Master of Science in Biomedical Engineering**
New Jersey Institute of Technology, Newark, NJ, 2003.
- **Bachelor of Engineering in Electronics and Communication Engineering**
University of Madras, Salem, India, 1995.

**This Thesis is dedicated
to the memory of my Grandparents**

ACKNOWLEDGMENT

The author wishes to express his most sincere gratitude to his advisor, Dr. Stanley S. Reisman, for his patience, guidance, friendship, and moral support throughout this research.

Special thanks are extended to Dr. David Kristol and Dr. Ronald H. Rockland for serving as members of the thesis committee. Dr. Basner of Columbia University College of Physicians and Surgeons, provided ideas, much valuable information on sleep apnea, and data from sleep apnea subjects. These data were collected at the Pulmonary Function Test Laboratory at the Columbia Presbyterian Hospital, NY and used as the main resource for this thesis. Special gratitude and appreciation are extended to Mr. Paky Ngai and Mr. Xu Zhong of the Columbia Presbyterian Hospital, who performed the tedious task of data collection for this research.

Many thanks should go to Dr. Douglas A Newandee and Anne Marie Petrock for their ideas and technical assistance.

The author also appreciates former and present NJIT Master students: Jason Steffener, Kripa Jayraman and many others for their support and friendship. They have also been constant sources of ideas, suggestions and discussions for this research. Their immense enthusiasm has helped me getting over many ups and downs of master's level research.

Deepest gratitude and respect should go to my parents for all their support, love and encouragement throughout my education; to my brothers-in-law for their concern, constant encouragement; to my sister, Malathi, for always being ready to lend a helping hand.

This thesis simply could never have been completed without the love, understanding and support of my wife, Senthilvadivu. Thank you for all the time when you really needed my presence but I could not be there because of my devotion to this research. For all your patience and sacrifice, I am forever grateful.

And finally, much appreciation should go to Dr. Ronald S. Kane and Ms. Clarisa González-Lenahan for reviewing, making corrections, recommendations and approving the final draft of this thesis.

**INVESTIGATION OF HEART RATE VARIABILITY
DURING SLEEP APNEA**

TABLE OF CONTENTS

Chapter	Page
1 INTRODUCTION	1
1.1 Scope of Research	1
1.2 Goals and Contributions	6
1.3 Outline of the Thesis	7
2 PHYSIOLOGY BACKGROUND	8
2.1 Cardiovascular Systems and the Heart	8
2.2 Blood Pressure	14
2.3 Metabolic Function/Respiration.....	15
2.4 The Nervous System.....	16
2.4.1 The Autonomic Nervous System.....	17
2.4.2 Autonomic Nervous System and Sleep	22
2.5 Heart Rate and Heart Rate Variability	23
2.5.1 Physiology of Changes in Heart Rate.....	23
2.5.2 Heart Rate Variability as a Measure of Autonomic Function.....	25
2.6 The Electrocardiogram (ECG)	28
2.7 Electroencephalogram (EEG)	31
2.7.1 Brain Wave.....	31
2.7.2 Brain Wave during Sleep	32

TABLE OF CONTENTS
(Continued)

Chapter		Page
2.8	Sleep Physiology	33
	2.8.1 Sleep	33
	2.8.2 Types of Sleep – Sleep Stage	35
2.9	Sleep Apnea Diseases (SA).....	40
	2.9.1 Symptoms	40
	2.9.2 Severity of Sleep Apnea.....	40
	2.9.3 Types of Sleep Apnea	41
	2.9.4 Physiological Changes during an Apnea	45
3	ENGINEERING BACKGROUND.....	49
	3.1 The Need for Time-Frequency Distributions.....	49
	3.2 The Uncertainty Principle	49
	3.3 The Analytic Signal and Instantaneous Frequency	50
	3.4 Properties of Time-Frequency Distributions	52
	3.5 Power Spectrum Analysis of Heart Rate Variability	53
	3.6 The Wavelet Transform	61
	3.6.1 Continuous Wavelet Transform.....	63
	3.6.2 Parseval Relation of Wavelet Transform.....	68
	3.6.3 Discrete Wavelet Transform	69

TABLE OF CONTENTS
(Continued)

Chapter	Page
4 METHODS	72
4.1 Subjects Protocol	72
4.2 Protocol Analysis.....	73
4.3 Sleep Recording.....	73
4.4 Data Analysis.....	74
4.4.1 Power Spectrum Analysis	75
4.4.2 Wavelet Analysis.....	78
5 RESULTS	82
6 CONCLUSIONS AND FUTURE WORK	98
APPENDIX A: Equipment Setup.....	101
APPENDIX B: Computer Program.....	103
APPENDIX C: Example of Control Subjects	117
APPENDIX D: Example of Sleep Apnea Subjects	121
APPENDIX E: T-test.....	124
REFERENCES	129

LIST OF TABLES

Table		Page
2.1	The Nervous System.....	16
2.2	Autonomic Effects on Selected Organs of the Body.....	21
2.3	Symptoms associated with Sleep Apnea (SA).....	44
5.1	T-test for Normal and Apnea Subjects (with outlier).....	82
5.2	T-test for Normal and Apnea Subject (without outlier).....	85

LIST OF FIGURES

Figure	Page
2.1 The Heart	9
2.2 The Systemic and Pulmonary Circulations.....	10
2.3 The Intrinsic Conduction System of the Heart	11
2.4 The Sequence of Cardiac Excitation	13
2.5 The Sympathetic Nervous System and Parasympathetic Nervous System.....	20
2.6 Autonomic Innervation of the Heart	24
2.7 Effect of Autonomic Stimulation on the slope of the Pacemaker Potential.....	25
2.8 An Electrocardiogram Tracing (lead I).....	28
2.9 The Placement of the Positive and Negative Electrodes	30
2.9.1 Typical Hypnogram from a Healthy Young Subject.....	34
2.9.2 Stage I Sleep – Alpha Waves	35
2.9.3 EEG during Sleep Stage 1	36
2.9.4 EEG during Sleep Stage II	37
2.9.5 EEG Slow Wave Sleep during Stage 3 & 4.....	38
2.9.6 EEG – REM Sleep	39
2.9.7 Obstructive Sleep Apnea	42
2.9.8 Central Sleep Apnea Example.....	43
2.9.9 Transient Heart Rate and Blood Pressure Consequences of an Apnea.....	46
2.9.9.1 Heart Rate and Blood Pressure Consequences of an Apnea	47
3.1 Figure Depicting the Construction of the IBI signal	54

**LIST OF FIGURES
(Continued)**

Figure	Page
3.2 IBI and IIBI Signals of Heart Rate.....	56
3.3 Power Spectrum of IIBI Signal	58
3.4 Plot of the Split Cosine Bell Taper used as a Window in the FFT Calculation	58
3.5 Example of Power Spectral Density of HRV	59
3.6 The Time-Frequency Plane Resolution Cells of the STFT vs. Wavelet Trans...	65
3.7 The Role of Scaling Parameter in Wavelet Transform.....	68
4.1 Lab VIEW Program for Power Spectrum Analysis.....	74
4.2 Lab VIEW Program for Channel Identification	75
4.3 Lab VIEW Program to Identify the Channels.....	76
4.4 IIBI Plot using Morl Wavelet.....	77
4.5 Sympathetic and Parasympathetic activity of Apnea Subject	78
4.6 Normalized Symp. and Parasymp. Activity of Apnea Subject	79
5.1 Comparison of LF with Subject PW	83
5.2 Comparison of HF with Subject PW	83
5.3 Comparison of LF/HF with Subject PW.....	84
5.4 Comparison of LF without Subject PW	85
5.5 Comparison of HF without Subject PW	86
5.6 Comparison of LF/HF without Subject PW	86
5.7 Obstructive Apnea for a period of 10 seconds.....	87
5.8.a Airflow of Apnea Subject (HL)	88

LIST OF FIGURES
(Continued)

Figure	Page
5.8.b Wavelet output of Apnea Subject (HL)	88
5.9.a Airflow of Apnea Subject (SE)	89
5.9.b Wavelet output of Apnea Subject (SE)	89
5.10 Normal subject (L2) with a Single Central Apnea	91
5.11 Expanded Version of (Fig 5.10).....	92
5.12 IIBI plot of Normal Subject (L2)	93
5.13 Wavelet output of Normal Subject (L2)	94
5.14 Spectral output of a Sleep Apnea Subject (HL).....	95
5.15 Spectral output of a Normal Subject (GN).....	96
5.16 Spectral output of a Normal Subject (B).....	97
5.17 Spectral output of a Normal Subject (L)	97

Blank Page

Blank Page

Blank Page

ABBREVIATIONS

A

ABP	Arterial Blood Pressure
ANS	Autonomic Nervous System
ARMA	AutoRegressive Moving Average
AV	Atrial Venous Node

B

BP	Blood Pressure
BPV	Blood Pressure Variability
BRSI	Baroreflex Sensitivity Index

C

CHF	Congestive Heart Failure
CNS	Central Nervous System
CO	Cardiac Output

E

ECG	Electrocardiogram
EEG	Electroencephalogram
ED	Excessive Daytime Sleep

F

FFT	Fast Fourier Transform
FIR	Finite Impulse Response
FT	Fourier Transform

G

GUI	Graphical User Interface
GWN	Gaussian White Noise

H

HF	High Frequency Activity (0.15-0.4 Hz)
HR	Heart Rate
HRV	Heart Rate Variability
HS	Hypopnea Syndrome

I

IBI	Interbeat Interval
IIBI	Interpolated Interbeat Interval

L	
LF	Low Frequency Activity (0.04-0.15 Hz)
LF: HF	Sympatho-vagal Balance
M	
MAP	Mean Arterial Pressure
MLE	Maximum Likelihood Estimation
N	
O	
O ₂	30 % Oxygen supplementation
OE	Output Error
P	
PID	Proportional-integral-derivative
PNS	Peripheral Nervous System
PSG	Polysomnography
R	
RA	Room Air
RESP	Respiration Signal
RR	R-to-R peak interval of ECG
RSA	Respiratory Sinus Arrhythmia
S	
SA	Sino-Atrial Node
SAHS	Sleep Apnea Hypopnea Syndrome
SID	System Identification
STFT	Short Time Fourier Transform
SV	Stroke Volume
S/V	Sympatho-vagal Balance
T	
TFA	Time-Frequency Analysis
TFR	Time-Frequency Representation
TPR	Overall Arteriole Resistance
V	
VE	Ventilation
VLF	Very Low Frequency (<0.04 Hz)
VO ₂	Volume of Oxygen per unit time
W	
WD	Wavelet Distribution
WT	Wavelet Transform

CHAPTER 1

INTRODUCTION

1.1 Scope of research

The development of improved treatments for diseased patients is important, and the development of improved monitoring techniques to assess risk of morbidity and mortality, as well as to assess response to treatment is needed. One particular population of patients, which is used in this study, is the Sleep Apnea Hypopnea Syndrome. SAHS is characterized by repetitive punctuations or reductions of respiration during sleep.

Sleep apnea is a sleep disorder with high prevalence in the adult population. Sleep apnea is regarded as an independent risk factor for cardiovascular sequelae such as ischemic heart attacks and stroke. Early recognition and selection of patients with sleep related breathing disorder is an important task. It has been suggested that this can be done on the basis of the single channel ECG doing time-frequency analysis [1,20,23].

Sleep apnea / hypopnea syndrome is associated with a wide range of health implications and increased cardiovascular morbidity and mortality. The gold standard in diagnosing sleep apnea is polysomnography, an inconvenient, expensive and time consuming procedure which includes an overnight multi channel recording of blood oxygen saturation, blood pressure, EEG, ECG, EOG, EMG, nasal/oral airflow, chest effort, and abdominal effort. This study assesses the suitability of established time-frequency domain HRV measures, which are known to reflect ANS control [1, 7]. Investigation of heart rate variability during sleep apnea and through tests which measure the physiologic changes of sleep stage in the brain. However, the effects of severe sleep disease are not limited to the brain. Often there are serious accompanying

cardiac problems and severe alterations to the normal state of autonomic regulation [1]. Patients with sleep disease are subject to a hyperadrenergic state and have many alterations in their autonomic physiology that can be documented. There is a non-invasive measure of autonomic function, heart rate variability (HRV), which can be performed in a simple fashion and can offer a clear window into the state of the subject. In subject populations with cardiac disease, the abnormalities found in these measures were found to have very strong correlations with subsequent mortality and sudden death. Because of some of the similarities (ex: change in blood pressure, respiration rate etc) between patients with severe sleep disease and patients with severe heart disease, the systematic study of the autonomic disturbances in these individuals, along with an analysis of the survival of the patients with and without treatment should be undertaken [24].

Respiratory sinus arrhythmia (RSA) is a phenomenon that has been recognized and studied for years, and it has been described as a rhythmical fluctuation in R-R intervals that is characterized by a decrease in the R-R interval length during inspiration, and an increase in the R-R interval length during expiration. Spectral analysis techniques have allowed researchers to conclude that RSA can primarily be attributed to vagal activity [1] and can be used as an index of vagal control of the heart. It has been shown that the variation of blood pressure seen with respiration is also associated with the heart rate variability. The physiologic mechanism of heart rate variability is mediated through respiratory afferents synapsing in the medulla oblongata and entraining the central regulatory oscillator. Similarly, the mechanism of blood pressure variability (BPV) is entrained to respiration, and is a combination of the effects of the

changes of stroke volume and the increase in vagal tone with inspiration. With the use of spectral analysis, and time-frequency analysis, the raw data (ECG and BP) obtained can be broken down into useful investigation of sleep apnea subjects [1, 20].

Since the relationship of altered heart rate variability and increased mortality have been documented in cardiac populations, the population of patients with severe sleep apnea disease (SA) is an excellent candidate to be studied. Patients with sleep disease also have significant alterations of their autonomic regulation [1]. In SA patients breathing patterns are altered, causing abnormalities in the entrainment of the normal central oscillators.

With the correlations that are possible to see from the previous work that has been done in cardiac disease and heart failure, it should be possible to demonstrate that these autonomic tests are clear predictor of HRV in sleep apnea subject.

Further to the above discussion an article survey was conducted, which is discussed below.

1. Kim [5] reported that HRV was significantly higher in severe apnea patients, especially in REM and stage 2 sleep. Sleep apnea occurred more in REM sleep, and exclusively in supine position. The increased HRV during sleep was excited by sleep apnea. Having more stage 2 and REM sleep can contribute to higher HRV both in normal and apnea patients.

2. Penzel [8] compared the results of normal subjects with patients suffering from mild sleep apnea, modulating influence of sleep stages on heart rate variability remained very strong even though OSA caused additional fluctuations. The additional fluctuations are directly linked with the disturbed respiration during sleep.
3. Hilton [9] reported that spectral analysis of HRV is a better diagnostic than oximetry for the SAHS. The accuracy of HRV may be reduced with the association of the other sleep disorders that produce recurrent arousal or fluctuations in the heart rate. The article proposed that applying spectral analysis of HRV in conjunction with oximetry would provide much better diagnostic accuracy than oximetry alone.
4. Baharav [11] reported that the overall increased sympathetic activity during sleep and sympathetic predominance during SWS in apnea patients, as compared to control subjects. The degree of sympathetic predominance correlated well with the severity of sleep apnea.
5. Maier [7] reported that the best result from 28/30 subjects achieved when the median minute-by-minute values are considered. Calculation over the whole signal duration decreases the performance considerably, because the higher regulatory of the cyclic variation of heart rate during period of apnea is blunted by other fluctuations on this time scale. This author concluded, generally, lower, less complex heart rate variability is found in apnea patients.

This study has been designed to answer questions about interactions between the nervous system, the cardiovascular system, sleep physiology and the pulmonary system; and issues concerning heart rate variability activity.

1.2 Goals and Contributions

The goals of this research are:

1. To apply time-frequency analysis to heart rate variability in order to investigate the heart rate variability during subject sleep apnea.
2. To use time-frequency analysis to understand and to develop tools that can describe rapid changes in the time varying spectrum due to apnea. Expansion of the concept of spectral analysis of heart rate variability to time-frequency analysis gives us the ability to quantitatively assess the parasympathetic and sympatho-vagal balance changes as a function of time for the subjects with sleep apnea.
3. To investigate the Weighted coherence which is a technique to measure the total variance of one signal that is shared with the other signal within a certain frequency band. It can be computed easily from the values of the coherence function and the spectral density values of one of the signals in that frequency region.

This work clarified some of the questions about heart rate variability in sleep apnea subjects which are of fundamental importance in diagnosing the severity of the disease, in assessing the benefit of rehabilitation procedure and ultimately in determining who may benefit the most from sleep apnea disease.

1.3 Outline of the Thesis

Chapter 1 summarizes the scope of research involving the investigation of sleep apnea (SA) populations.

Chapter 2 summarizes the physiology background for studying the human cardiovascular system and sleep mechanism. The description and operating mechanism of the heart, lung, the electrocardiogram (ECG), the blood pressure, the respiration, the brain waves and the sleep physiology are presented.

Chapter 3 presents the engineering tools to analyze the biological signals of ECG, BP and respiration. The basic signal representation used in this thesis is the time-frequency representation.

Chapter 4 presents the experimental protocols used in the study.

Chapter 5 presents the results of the study.

Chapter 6 presents the discussion of all the results obtained in chapter 5 and conclusions as well as suggestion of topics for future study. Hopefully, these topics, in addition to this research work, will motivate the prospective researcher to explore further unresolved issues in the field of heart rate variability, biological modeling and disease severity classification in the direction of signal processing application to signal analysis using time-frequency representation techniques.

CHAPTER 2

PHYSIOLOGY BACKGROUND

Biomedical engineering is the application of the principles of engineering, science, and mathematics to biology and medicine. The physiological signals or waveforms (ECG, EEG, blood pressure) are examined because they can yield information of clinical significance about the biological systems. Therefore, in order to conduct biomedical research, the relevant physiological systems must be understood. The purpose of this section is to provide a general, but concise, background to the physiological systems that are relevant to the work in this research.

2.1 Cardiovascular Systems and the Heart

The cardiovascular system consists of the heart, which is a muscular pumping device, and a closed system of blood vessels called arteries, veins, and capillaries. The heart pumps blood around a closed circuit of vessels contained in the circulatory system as it repeatedly passes through the various “circulations” of the body. The vital role of the cardiovascular system in maintaining homeostasis is dependent upon the continuous and controlled movement of blood to reach every cell in the body. Regulation of blood pressure and flow must change in response to cellular activity. Consequently, numerous control mechanisms help to regulate and integrate the diverse functions and component parts of the cardiovascular system to supply blood to specific body areas according to need [1,2].

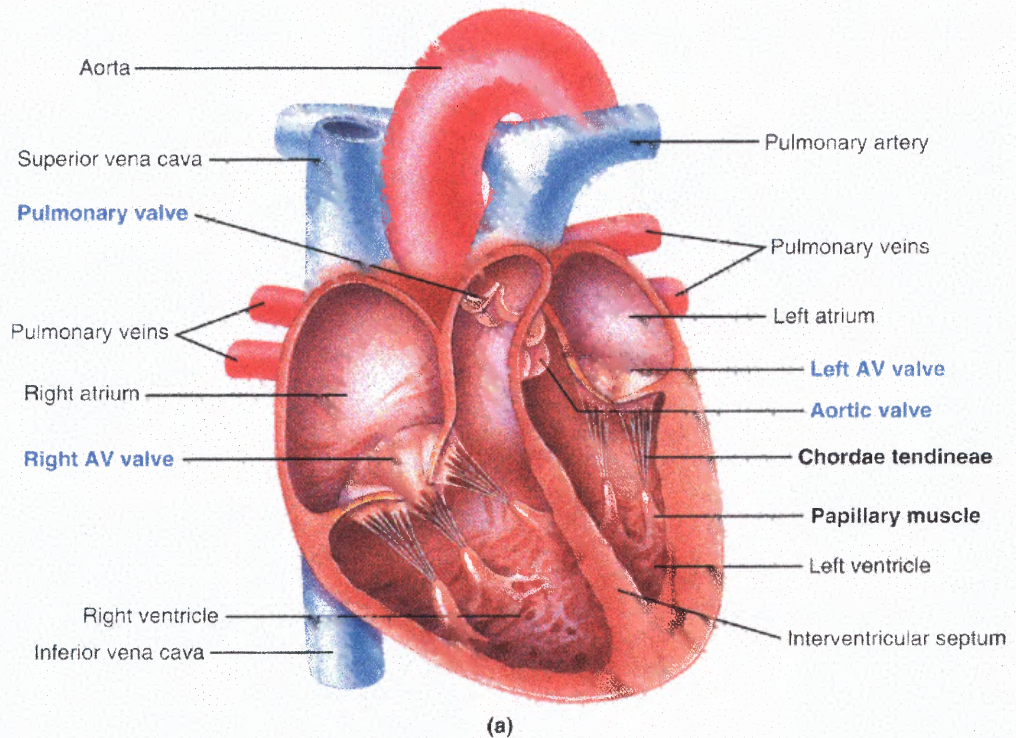


Figure 2.1 The Heart. (From Lauralee Sherwood, *Human Anatomy and Physiology*, 4th Ed. California: The Brooks/Cole Publishing Company, Inc., 2001.)

The heart, illustrated in Figure 2.1, is divided into two functional halves, each half containing two chambers: an atrium and a ventricle. The atrium of each side empties into the ventricle on that side. There is no direct flow between the two atria or the two ventricles in a healthy individual. Blood is pumped by the pulmonary circuit from the right ventricle through the lungs and then into the left atrium. The blood is then pumped by the systemic circuit, from the left ventricle, through all the tissues of the body except the lungs, and then to the right atrium [2].

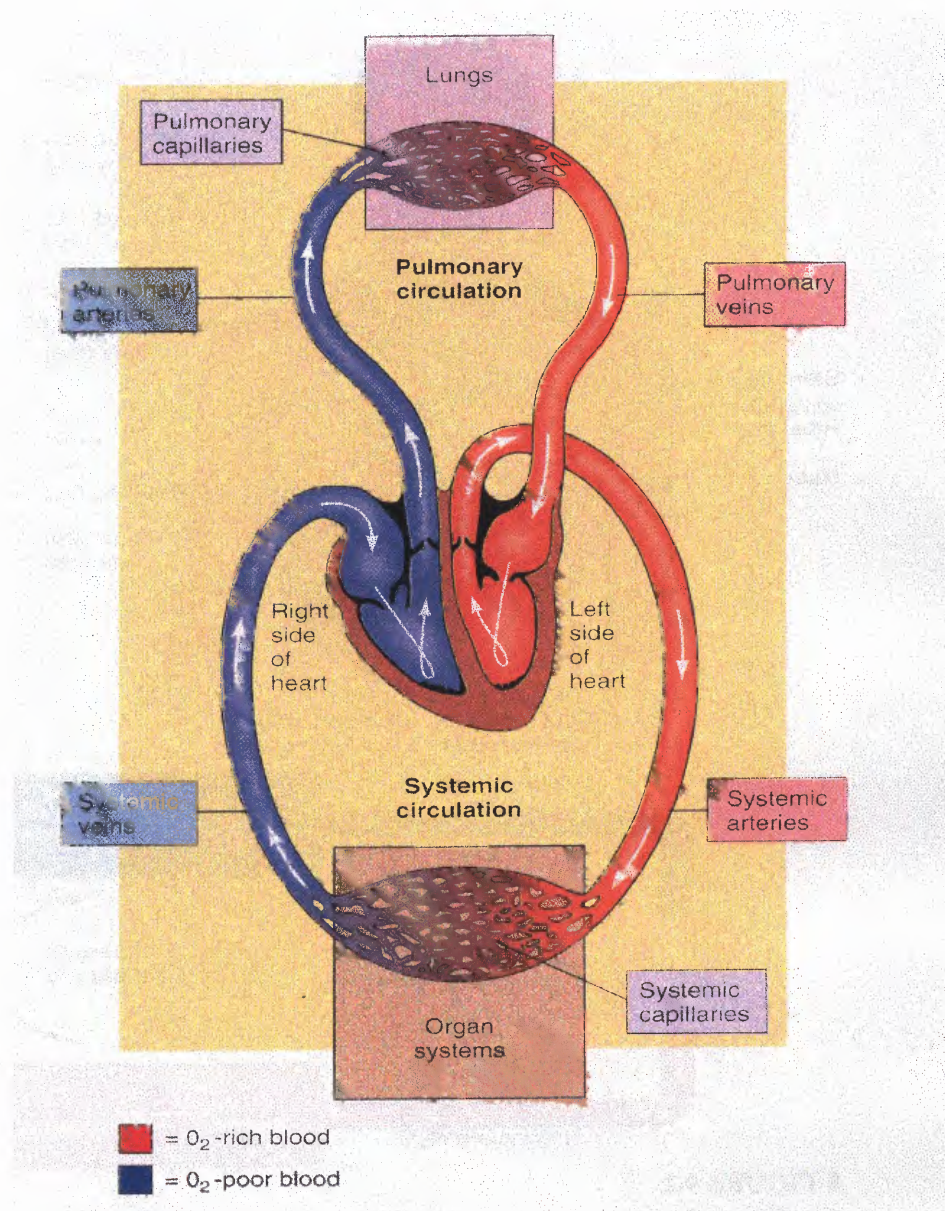


Figure 2.2 The Systemic and Pulmonary Circulations. (From Lauralee Sherwood, Human Anatomy and Physiology, 4th Ed. California: The Brooks/Cole Publishing Company, Inc., 2001.)

In both circuits, the vessels carrying blood away from the heart are called arteries and those carrying blood from either the lung or all other parts of the body back to the heart are called veins. Figure 2.2 illustrates the heart with the systemic and pulmonary circulations.

The heart, located in the chest, is a muscular organ, which is enclosed, in a fibrous sac called the pericardium. The walls of the heart are primarily composed of cardiac-muscle cells called the myocardium. Cardiac-muscle cells combine properties of both skeletal muscle and smooth muscle. However, even more important, approximately one percent of the cardiac-muscle fibers has specialized features that are essential for normal heart excitation. They constitute a network known as the conducting system of the heart and are connected to other cardiac-muscle fibers by gap junctions. The gap junctions allow action potentials to spread from one cardiac-muscle cell to another [2, 29].

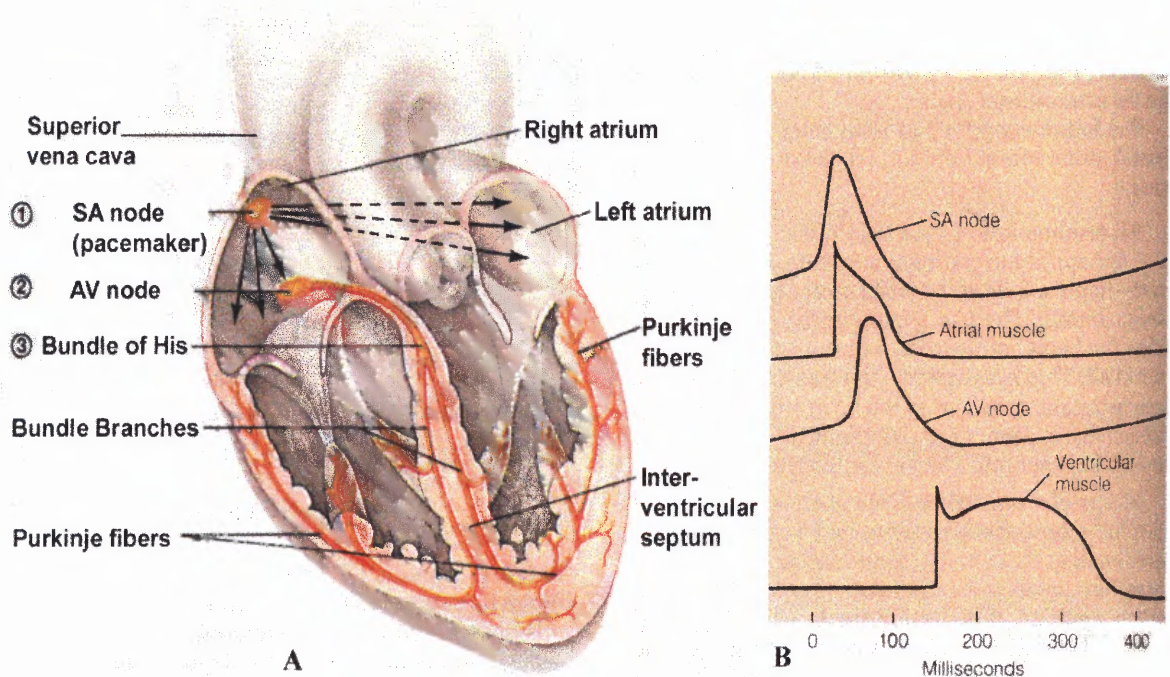


Figure 2.3 The intrinsic conduction system of the heart and succession of the action potential through selected areas of the heart during one heart beat. **B**, The sequence of potentials generated across the heart is shown from top to bottom beginning with the pacemaker potential generated by the SA node and ending with an action potential. (From E. N. Marieb, *Human Anatomy and Physiology*, 3rd ed. New York: The Benjamin/Cummings Publishing Company, Inc., 1995.)

Thus, the initial excitation of one myocardial cell results in excitation of all cells, and as a result, the pumping action of the heart. The conducting system of the heart is illustrated in Figure 2.3. The initial depolarization normally arises in a small group of conducting-system cells called the sinoatrial (SA) node. The SA node is located in the right atrium near the entrance of the superior vena cava (the vein returning from the body tissues that are above the heart). The SA node has the fastest inherent discharge rate of any of the myocardial cells with pacemaker activity. Therefore, the SA node is the normal pacemaker for the entire heart. The action potential initiated in the SA node spreads throughout the myocardium, passing from cell to cell by way of gap junctions. The spread throughout the right atrium and the left atrium does not depend on fibers of the conducting system. The spread is rapid enough that the two atria are depolarized and contract at essentially the same time.

The spread of the action potential from the atria to the ventricles involves a portion of the conducting system called the atrioventricular (AV) node. The AV node is located at the base of the right atrium. The AV node has an important characteristic that makes the cardiac cycle more efficient. For several reasons related to the electrical properties of the cells that make up the AV node, the propagation of action potentials through the AV node results in a delay of approximately 0.1 seconds. This delay allows the atria to finish contracting and, therefore, completely emptying their contents of blood into their respective ventricles before ventricular excitation occurs [2,21].

Upon leaving the AV node, the action potential then travels to the septum, the area between the two ventricles, by the conducting-system fibers called the bundle of His. The bundle of His then divides into the left and right bundle branches, which

eventually leave the septum and enter the walls of their respective ventricles. These fibers then make contact with the Purkinje fibers, which are large conducting cells that rapidly distribute the action potential throughout most of the ventricles. The rapid conduction along the Purkinje fibers and the distribution of these fibers cause the depolarization of the left and right ventricular cells approximately simultaneously, thus resulting in a single coordinated contraction. Figure 2.4 illustrates the sequence of cardiac excitation.

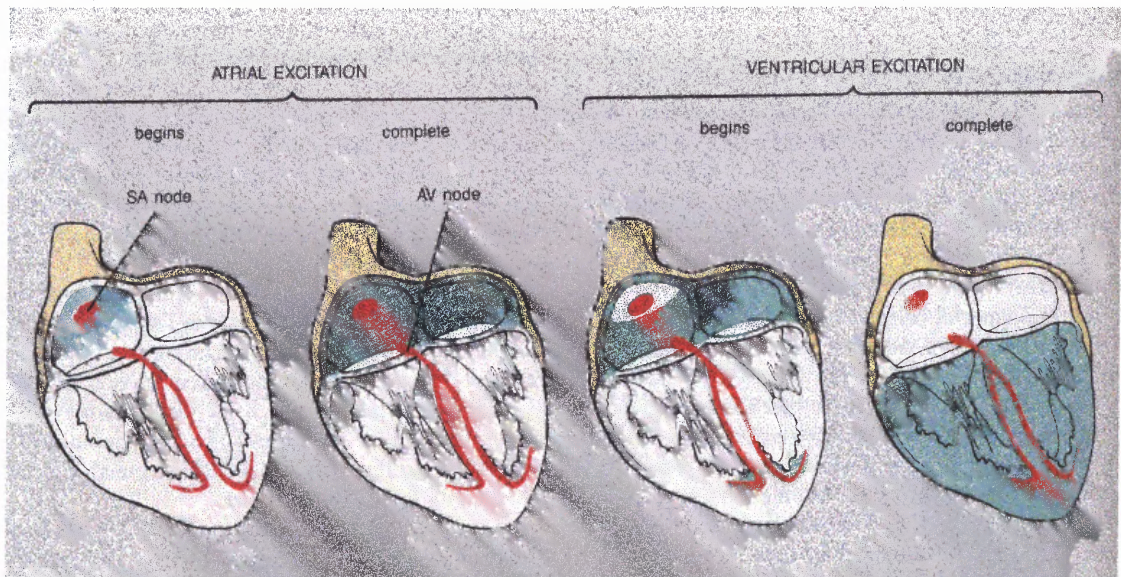


Figure 2.4. The Sequence of Cardiac Excitation (from A.J. Vander, J.H. Sherman, and D.S. Luciano, Human Physiology, 1994)

2.2 Blood Pressure

The force that blood exerts against the walls of a vessel is called blood pressure. Normally, some amount of blood is present in every blood vessel of the body, including all arteries, arterioles, capillaries, venules and veins.

Blood volume is greatest in the veins. Venous blood pressure, however, is quite low because of the large-radius and low resistance of the vein. Skeletal movement, mechanical movement from respiration and one-way valves, facilitates return of deoxygenated blood to the heart.

Less than fifteen percent of the blood volume is present in the arteries. Mean arterial pressure, however, is approximately 100 mm Hg. Mean arterial pressure (MAP) depends upon overall arterial resistance (TPR) and cardiac output (CO) [2]. Specifically:

$$\text{MAP}=\text{TPR}*\text{CO} [\text{mmHg}]. \quad (2.1)$$

The resistance of a particular arteriole depends upon the associated organ's requirements. Under different conditions, an arteriole radius will be varied by control mechanisms to accommodate the need of the associated organ. If the overall radius of all arterioles decreases, then the TPR is increased, which may cause arterial blood pressure to increase, depending upon the CO value.

When blood flows into arteries and arterioles, stretching occurs due to the pressure that blood exerts on the arterial walls. The maximum pressure, which is reached when the ventricles eject blood, is called the systolic pressure. The minimum arterial pressure occurs just before ventricular ejection begins and is called diastolic pressure.

2.3. Metabolic Function/Respiration

In the human respiration serves to provide cells with oxygen, eliminate carbon dioxide and regulate pH of the blood. In order to provide cells with oxygen, air from the environment enters the body during inhalation. Carbon dioxide and other unwanted substances are removed from the body during exhalation. Upon inhalation, air enters the body via the trachea, and then flows into the bronchi. The air then reaches the alveoli. The properties of the alveoli allow rapid and efficient exchange of gasses between the blood within the capillaries and the alveoli. The volume of oxygen per unit time (VO_2) that is transported from the capillaries to the body cells is equal to the volume of the inspired oxygen that is diffused from the alveoli into the blood at any given instant. Analogously, the volume of CO_2 produced by the body cells per unit time (VCO_2) is equal to the amount of CO_2 that diffuses from the blood to the alveoli. The total amount of air entering and leaving the body per unit time is the called ventilation (VE) [2].

In HRV studies, one important equation that links the circulatory system to the respiratory system is the calculation of volume of blood ejected from a ventricle during systole known as stroke volume (SV), which can be derived once VO_2 is known [2, 16]:

$$SV = VO_2 / HR \quad (2.2)$$

The physiologic mechanism of heart rate variability is mediated through respiratory afferents synapsing in the medulla oblongata and entraining the central regulatory oscillator. Similarly, the mechanism of blood pressure variability (BPV) is entrained to respiration, and is a combination of the effects of the changes of stroke volume and the increase in vagal tone with inspiration [2].

2.4 The Nervous System

Human behavior is controlled and regulated by two major communication systems, the endocrine system and the nervous system. The nervous system can be divided into two separate, but interconnected, parts. The first part consists of the brain and spinal cord and is called the central nervous system. The second part, which consists of nerves, which extend from the brain and the spinal cord out to all points of the body, is called the peripheral nervous system.

The peripheral nervous system consists of both an afferent division and efferent division. The afferent division conveys information from primary receptors to the central nervous system. The efferent division carries signals from the central nervous system out to effector cells such as muscles and organs. The efferent division is subdivided into a somatic nervous system and an autonomic nervous system. The somatic nervous system consists of all the nerve fibers going from the central nervous system to skeletal-muscle cells. The efferent innervation of all tissues other than skeletal muscle is done by the autonomic nervous system. Table 2.1 illustrates the organization of the human nervous system [1, 2].

Table 2.1 The Nervous System

I. Central Nervous System	II. Peripheral Nervous System
A. Brain B. Spinal Cord	A. Afferent Division B. Efferent Division <ol style="list-style-type: none"> 1. Somatic Nervous System 2. Autonomic Nervous System <ol style="list-style-type: none"> a. Sympathetic Nervous System b. Parasympathetic Nervous System

2.4.1 The Autonomic Nervous System

Cardiac muscle cells, smooth muscle cells, and glands are innervated by the autonomic nervous system. Although it is not entirely true, the autonomic nervous system controls bodily functions that one often assumes to be automatically controlled. Such functions include heart rate, blood pressure, and body temperature. For example, when one is placed under a lot of physical stress such as climbing three flights of stairs, the person's heart rate and respiration rate automatically increase to supply the body with the energy needed on demand. Likewise, when a person is resting, the heart rate and respiration rate slow down due to the decrease in energy expenditure. Therefore, one can assume that the body automatically controls heart rate and respiration rate. However, it is possible to override the autonomic nervous system and consciously control some of its functions. A good example of this is that under certain meditation techniques, it has been shown that some people can actually lower their heart rate substantially below their resting rate, or even stop their heart from beating for a brief period of time. In addition, some people can slow their breathing rate to only one breath for every few minutes during deep meditation.

As shown in Table 2.1, the autonomic nervous system is divided into two anatomically and physiologically different systems. These two systems are termed the sympathetic nervous system and the parasympathetic nervous system. Anatomically, the sympathetic and parasympathetic nervous systems differ for two reasons. One difference is that the nerve fibers of each system leave the central nervous system at different levels [1, 2].

The sympathetic nerve fibers leave the central nervous system from the thoracic and lumbar sections of the spinal cord. The parasympathetic nerve fibers leave the central nervous system from the brain through cranial nerves III, V, VII, IX, and X and the second and third sacral spinal nerves. Cranial nerve X is also called the vagus nerve. The parasympathetic innervation of much of the thorax and abdomen, and especially the heart, is done by the nerve fibers, which leave from the brain through cranial nerve X. Therefore, parasympathetic activity related to the heart is often called vagal activity. Figure 2.5 illustrates the anatomic difference between the sympathetic nervous system and parasympathetic nervous system as well as some of their respective effector organs [2].

The second anatomical difference between the sympathetic and parasympathetic nervous systems has to do with the location of the ganglia. Each connection of the autonomic nervous system between the central nervous system and the effector cell consists of two-neuron chains connected by a synapse. Most, but not all, of the sympathetic ganglia are located close to the spinal cord and form two chains of ganglia, one on each side of the spinal cord, called the sympathetic trunk. Conversely, the parasympathetic ganglia lie within the organs innervated by the postganglionic neurons.

Physiologically, the sympathetic and parasympathetic nervous systems are also different. One common physiological characteristic is that the major neurotransmitter released between the pre- and post-ganglionic fibers is acetylcholine. However, in the sympathetic division, the major neurotransmitter between the postganglionic fiber and the target cell is usually norepinephrine, a neurotransmitter that activates excitatory receptors, but in some cases can inhibit certain organs. In the parasympathetic division,

the major neurotransmitter between the postganglionic fiber and the target cell is the same as the pre- and post- ganglionic neurotransmitter, acetylcholine. Although acetylcholine generally has an excitatory effect, it is also known to have inhibitory effects as well, such as the slowing of the heart by the vagus nerve. In Figure 2.5, it is important to realize that some organs, such as the heart, eyes, and stomach, receive autonomic activity from both the sympathetic and parasympathetic nervous systems. This is often called "dual innervation". Usually, but not always, whatever effect the sympathetic nervous system has on the effector cells, the parasympathetic nervous system has the opposite effect.

In general, the sympathetic nervous system increases its response under conditions of stress. It is responsible for what is known as the fight-or-flight response. On the other hand, activity of the parasympathetic nervous system is associated with relaxing and the storing of energy. For example, heart rate increases with sympathetic activity and decreases with parasympathetic activity. Table 2.2 (Page # 21) summarizes the effects of the autonomic nervous system on selected organs.

Dual innervation by nerve fibers that cause opposite responses provides a very fine degree of control over the effector organ- it is like equipping a car with both an accelerator and a brake. One can slow the car simply by decreasing the pressure on the accelerator; however, the combined effects of releasing the accelerator and applying the brake provide faster and more accurate control. Analogously, the sympathetic and parasympathetic divisions are usually activated reciprocally; that is, as the activity of one division is increased, the activity of the other is decreased [1, 2].

In addition to dual innervation, another important physiological characteristic is that the sympathetic and parasympathetic nervous systems are continually active.

Without these sympathetic and parasympathetic tones, each nervous system would only be able to produce one desired output, such as increasing heart rate. For instance, when sympathetic tone increases, heart rate increases. Conversely, when sympathetic tone decreases below its basal rate, the heart rate will decrease because of less sympathetic influence.

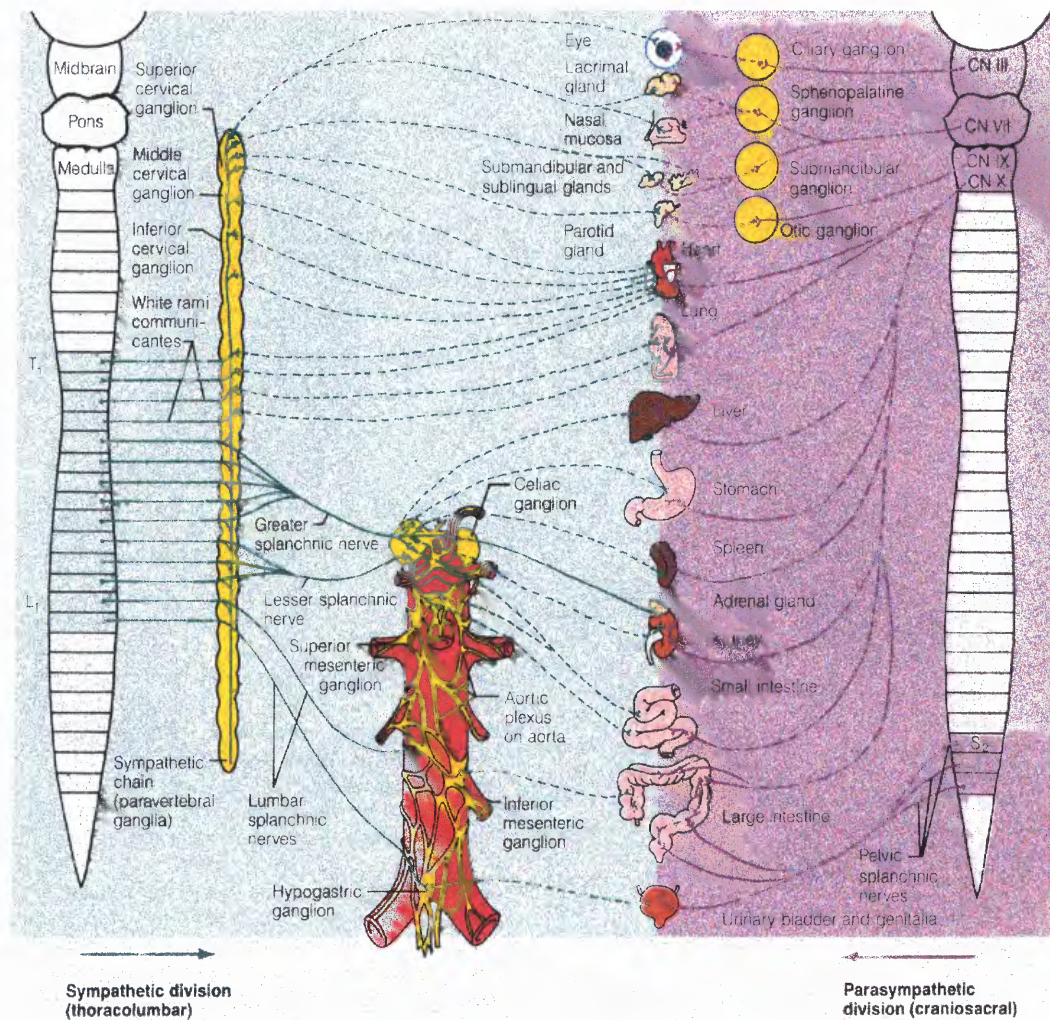


Figure 2.5 The Sympathetic Nervous System and Parasympathetic Nervous System. (From E. N. Marieb, *Human Anatomy and Physiology*, 3rd ed. New York: The Benjamin/Cummings Publishing Company, Inc., 1995.)

Table 2.2 Autonomic Effects on Selected Organs of the Body. (From A.J. Vander, J.H. Sherman, and D.S. Luciano, Human Physiology, 1994)

Effector Organ	Effect of Sympathetic Stimulation	Effect of Parasympathetic Stimulation
Eyes Iris muscles Ciliary muscle	contracts (dilates pupil) Relaxes (flattens lens)	relaxes (constricts pupil) Contracts
Heart SA node Atria AV node Ventricles	Increases heart rate Increases contractility Increases conduction velocity Increases contractility	Decreases heart rate Decreases contractility Decreases conduction velocity Decreases contractility slightly
Arterioles Coronary Skin Skeletal muscle Abdominal viscera Salivary glands	Dilates (β_2); constricts (α) Constricts Dilates (β_2); constricts (α) Dilates (β_2); constricts (α) Constricts	Dilates None None None Dilates
Lungs Bronchial Muscle	Relaxes	Contracts
Stomach Motility, tone Sphincters Secretion	Decreases Contracts Inhibits (?)	Increases Relaxes Stimulates

2.4.2 Autonomic Nervous System and Sleep

The parasympathetic and sympathetic nervous system have been regarded as antagonistic. This behavior is exemplified in end organ responses such as the heart where an increase in sympathetic activity increases the heart rate while increases in parasympathetic activity decrease the heart rate. This has resulted in a depiction of the autonomic nervous system as a balance swinging around a fulcrum.

Sleep is a state of reduced consciousness that offers potential for the assessment of autonomic regulation in an environment relatively devoid of physical activity and higher cortical activity. The efferent and afferent systems that may be involved in ANS regulation in the SAHS are primarily related to the pulmonary and cardiovascular systems [1].

The normal average heart beat in a resting teen is 70-80 beats per minute, during sleep it goes down to 50-60 beats per minute, and it accelerates to above 100 with emotional excitement. During sleep the parasympathetic nervous system is in control and the sympathetic nervous system is suppressed so that the heart rate becomes low. During fear the sympathetic nervous system takes command and the parasympathetic nervous system is suppressed so the heart rate will be higher [1, 2, 29].

2.5 Heart Rate and Heart Rate Variability

2.5.1 Physiology of Changes in Heart Rate

Change in heart rate is sensitive to changes in body temperature, plasma electrolyte concentrations and hormone concentrations. However, the most important influence of beat-to-beat variations of heart rate comes from the autonomic nervous system. More specifically, sympathetic activity increases heart rate, whereas activity in the parasympathetic (vagus) nerves causes the heart rate to decrease. Due to considerably more parasympathetic activity to the heart than sympathetic activity in the resting state, the normal resting heart rate is below the inherent rate of 100 beats/minute.

The autonomic nervous system innervates the heart in a number of places. The sympathetic nervous system terminates at the SA node, the conduction system, atrial and ventricular myocardium, and coronary vessels. The parasympathetic fibers terminate in the SA and AV nodes, atrial and ventricular musculature, and coronary vessels. Interplay between the two systems will cause the heart to speed up or slow down, depending on which system is more active. Figure 2.6 illustrates the autonomic innervation of the heart [1, 2].

Perhaps the most important site of innervation of the autonomic nervous system on the heart occurs at the SA node. The SA node possesses an inherent discharge rate, often referred to as the pacemaker potential. The pacemaker potential is a slow depolarization of the cells of the SA node. The innervation of the sympathetic and parasympathetic nervous system on the SA node changes the characteristics of

depolarization within the SA node cells, thus changing heart rate. Figure 2.7 illustrates these changes due to autonomic innervation.

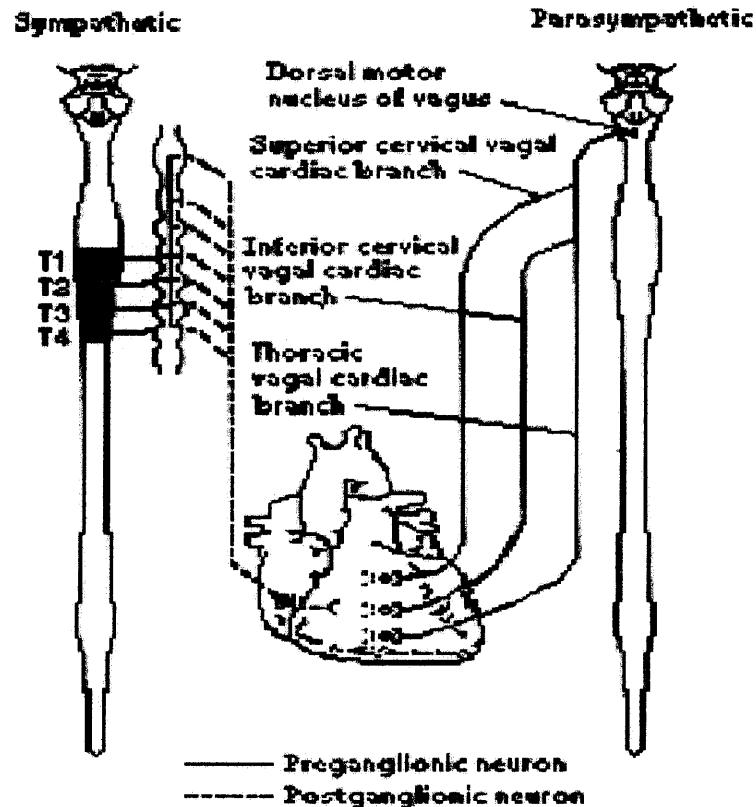


Figure 2.6 Autonomic Innervation of the Heart (From M.D. Kamath and E.L. Fallen, "Power spectral analysis of heart rate variability," *Crit. Rev. in Biomed. Eng.*, 1993)

For comparative purposes, the pacemaker potential labeled "Normal" is the control. From the figure, one can observe that sympathetic stimulation increases the slope of the pacemaker potential. As a result, the SA node cells reach the threshold more rapidly, thus increasing the heart rate. Conversely, parasympathetic stimulation decreases the slope of the pacemaker potential. Consequently, the SA node cells reach the threshold more slowly, and heart rate decreases. In addition to decreasing the slope of the pacemaker potential, parasympathetic stimulation also hyperpolarizes the plasma

membrane of the SA node cells so that the pacemaker potential starts from a more negative membrane potential. As a result, the time it takes the SA node cells to reach the threshold increases, which decreases heart rate [2].

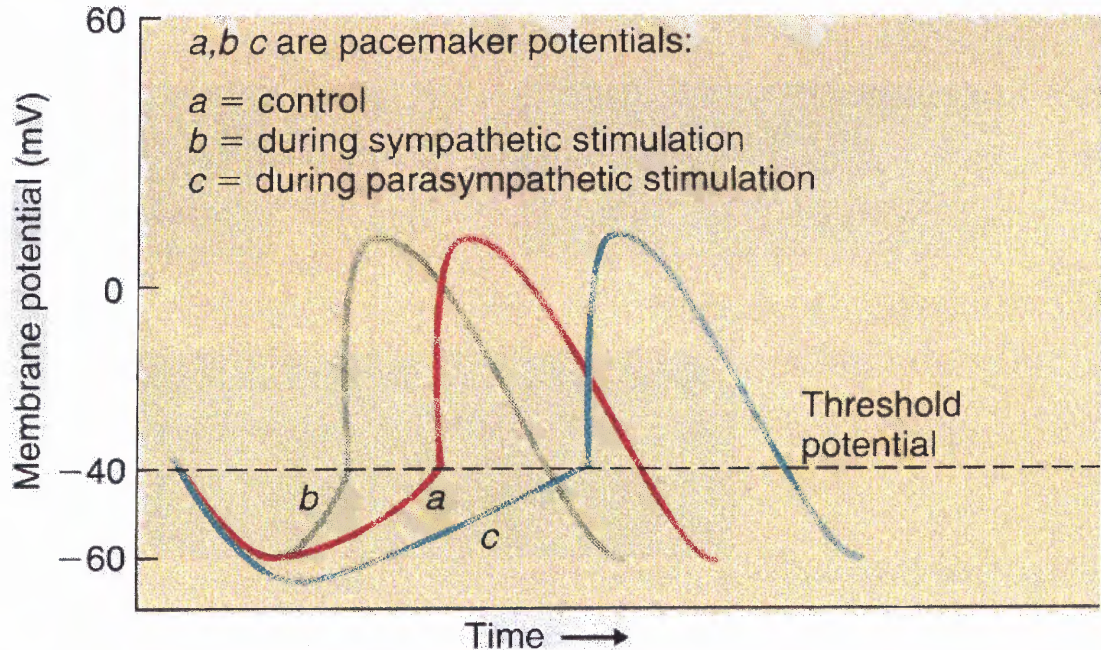


Figure 2.7 Effect of Autonomic Stimulation on the Slope of the Pacemaker Potential (from A.J. Vander, J.H. Sherman, and D.S. Luciano, Human Physiology, 1994)

2.5.2 Heart Rate Variability as a Measure of Autonomic Function

Changes in heart rate usually involve the reciprocal action of the two divisions of the autonomic nervous system. An increased heart rate is the result of reduced parasympathetic tone and a concomitant increase in sympathetic activity. A decrease in heart rate is usually the result of increased parasympathetic tone and a simultaneous decrease in sympathetic tone. Therefore, changes in heart rate reflect the action of the sympathetic and parasympathetic nervous systems on the heart. However, under certain conditions (emergency or stressful situations), it is possible for heart rate to change by activity of only one division of the autonomic nervous system, independent of the other

division, rather than reciprocal changes in both [1, 2]. This response is typically referred to as a fight-or-flight response.

Initially, the effect of the autonomic nervous system on the heart was estimated by utilizing the traditional technique of average heart rate. As a reference, the average heart rate was measured under normal resting conditions. Then the average heart rate was measured under the administration of drugs. The drugs used were atropine, which blocks the effects of the parasympathetic nervous system, and propranolol, which masks the effects of the sympathetic nervous system. A qualitative assessment can then be made of the autonomic nervous system by comparing the reference heart rate to the heart rate while under the administration of the drugs. This method looks at the average over time of heart rate. However, when the ECG is looked at on a beat-to-beat basis, rather than over a period of time, fluctuations in the heart rate are observed. Recent research indicates that fluctuations in heart rate are a healthy sign. In fact, one hypothesis is that the larger variations in the heart rate correlate to a healthier autonomic nervous system. By contrast a number of physiologic and disease states produce alterations in autonomic function, which reduce the variability in heart rate.

The direct quantification of vagal activity in humans is difficult as recording directly from the nerve is highly invasive. The degree of RSA provides a quantitative measure of the vagal outflow to the myocardium. That is, the phasic inhibition of cardiac vagal activity associated with inspiration produced by the CNS introduces a heart rhythm at the respiratory frequency, typically 0.25Hz [1, 18]. The amplitude of this rhythm (i.e. the degree of slowing down and speeding up) of the heart rate determines the tonic level of the vagal outflow. Spectral analysis techniques have been applied to the heart rate

variability (HRV) in order to estimate the frequency component centered about the respiratory frequency, termed the high frequency band (HF). This evaluation of RSA has provided a useful method for the non-invasive measurement vagal input to the myocardium.

The heart rate demonstrates a frequency component at a lower frequency (LF) centered at about 0.1Hz (i.e. one cycle per 10 seconds). These slower cycles, related to sympathetic activity, have been associated with Mayer waves and baroreceptors [18]. There is a certain amount of disagreement as to the physiological significance of the LF component of HRV, because pharmacological interventions blocking the vagus also produce a reduction in LF power in HRV studies. Thus, the LF variability is thought to have both a sympathetic and vagal component and is not a pure measure of sympathetic activity. The sympathetic nervous system modulates blood pressure Mayer waves. The cyclical increases in blood pressure most likely modulate the heart rate via baroreceptor feedback mechanisms. A better concept that is used to isolate the sympathetic activity is that of "sympatho-vagal balance" which recognizes both reciprocal and non-reciprocal parasympathetic and sympathetic influences on heart rate by computing the low frequency to high frequency ratio. An increase in the low frequency to high frequency ratio indicates either an increase of sympathetic activity, a decrease in parasympathetic activity, or a reciprocal change in both.

Power spectrum analysis of short segments of beat-to-beat heart rate variability (PS/HRV) reveals three distinct peaks. In human PS/HRV, the high frequency (HF) band (0.15 to 0.4 Hz) is correlated with respiratory driven vagal efferent input to the sinus node. The low frequency band (LF) 0.06 to 0.15 Hz is believed to be due to baroreceptor

mediated blood pressure control. Therefore, PS/HRV represents a noninvasive signature of the balance between sympathetic and parasympathetic components of the autonomic nervous system.

2.6 The Electrocardiogram

The electrocardiogram (ECG) is primarily a tool for evaluating the electrical events within the heart. The action potentials of cardiac muscles can be viewed as batteries that cause charge to move throughout the body fluids. These moving charges, or currents, represent the sum of the action potentials occurring simultaneously in many individual cells and can be detected by recording electrodes at the surface of the skin. Figure 2.8 illustrates a typical normal ECG recorded between the right and left wrists for one heartbeat [2, 29].

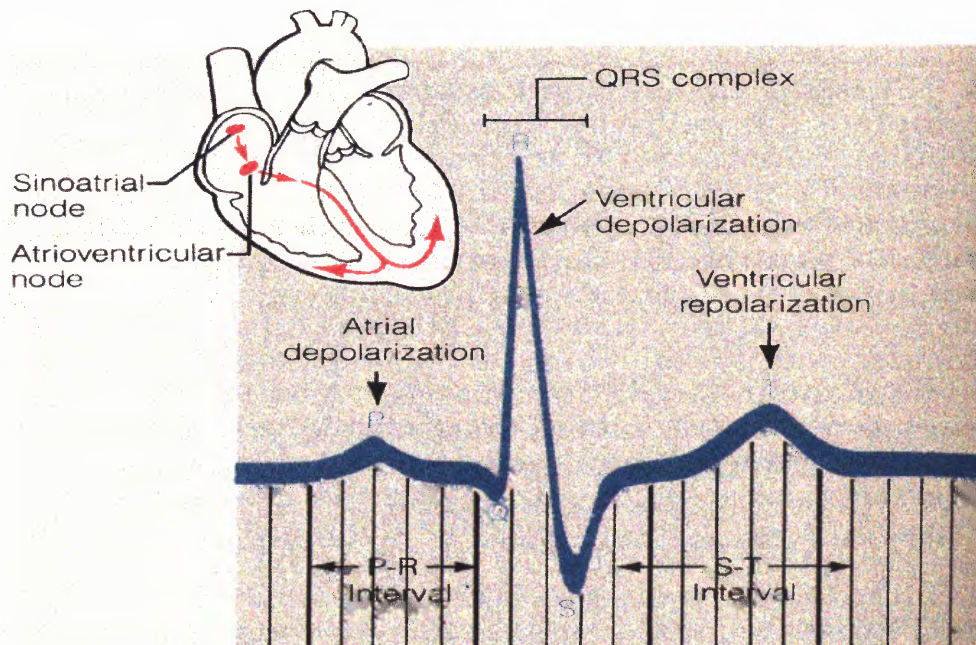


Figure 2.8 An electrocardiogram tracing (lead I) illustrating the three normally recognizable deflection waves and the important intervals. (From E. N. Marieb, *Human Anatomy and Physiology*, 3rd ed., 1995.)

The first deflection, the P wave, corresponds to the current flow during atrial depolarization (contraction). The second deflection, the QRS complex, is a result of ventricular depolarization. The third and final deflection is the T wave. The T wave is a result of ventricular repolarization (relaxation). It should be noted that atrial repolarization is usually not evident in the ECG because it occurs at the same time as the QRS complex.

As mentioned earlier, the ECG is a measure of the electrical activity of the heart measured on the skin. In order to measure the ECG, bipolar leads are required. The bipolar method of acquiring ECG detects electrical variations at two different locations on the skin and displays the difference to obtain one waveform. Figure 2.9 is an illustration of the standard limb lead connections that form the Einthoven's triangle. In addition, the diagram also shows the names of the respective leads. To record lead I, the negative terminal of the ECG monitor is connected to the right arm (RA) and the positive terminal is connected to the left arm (LA). To record lead II, the negative terminal of the ECG monitor is connected to the right arm and the positive terminal is connected to the left leg. To record lead III, the negative terminal of the ECG monitor is connected to the left arm and the positive terminal is connected to the left leg (LL). The reference point or ground is connected to the right leg (RL) [2, 29].

It is important to realize that depending on where the electrodes are attached, a different waveshape will be obtained for the same electrical events occurring in the heart. In other words, leads I, II, and III all have a different waveform shape. In addition to obtaining different waveforms depending on the location of the electrodes, each individual has a unique ECG.

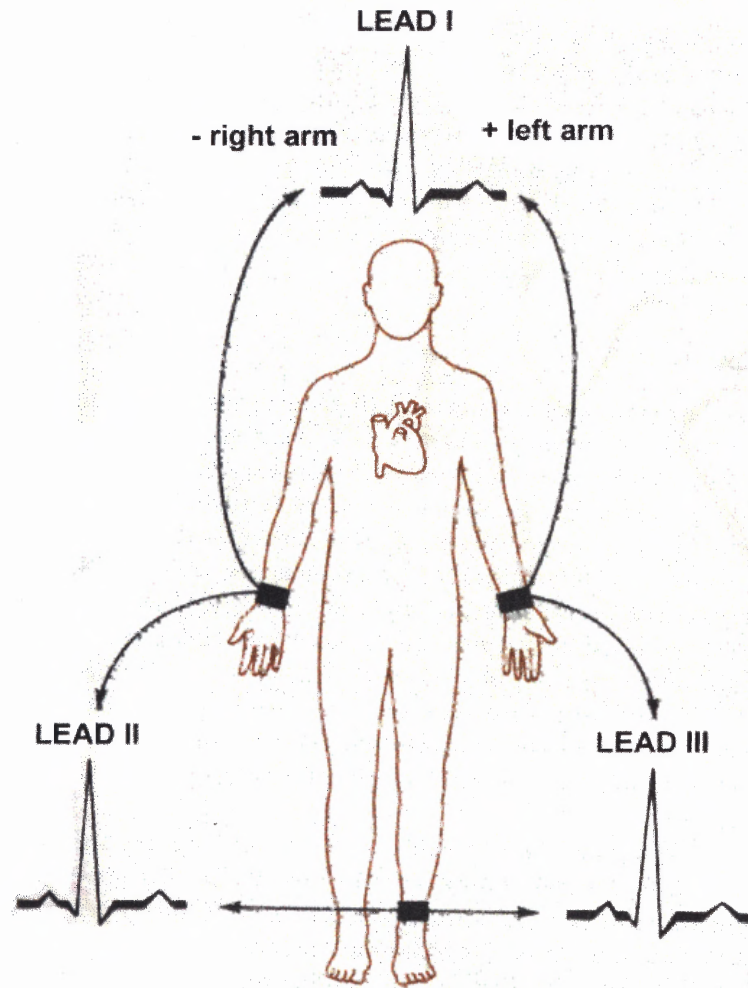


Figure 2.9 The placement of the positive and negative electrodes for three commonly used leads, as shown. (From J. G. Creager, *Human Anatomy and Physiology*. Belmont, CA: Wadsworth Inc., 1983.)

2.7 Electroencephalogram (EEG)

2.7.1 Brain Waves

The gross electrical activity of different parts of the brain can be recorded electrographically. Extracellular current flow arising from electrical activity within the cerebral cortex can be detected by placing recording electrode on the scalp to produce a graphical record known as an Electroencephalogram or EEG. These “brain waves” for the most part are not due to action potentials but instead represent the momentary collective postsynaptic potentials activity in the cell bodies and dendrites located in the cortical layer under the recording electrode [2, 8, 29].

As mentioned briefly in the previous section, electrodes placed on the scalp measure continuing oscillations due to the electrical activity of the brain. These variations in potential are called brain waves, and when they are recorded, the record is termed an electroencephalogram. The amplitude of these waves when measured through the scalp is about 10-100microVolt, and their frequency can vary from 0.5Hz to 100Hz. The character of the brain waves is highly dependent on the degree of activity in the cortex. Much of the time, especially during alert activity, the brain waves are small in amplitude and quite asynchronous. However, at other times the brain will exhibit very rhythmic activity that is almost sinusoidal in nature.

2.7.2 Brain Wave During Sleep

The brain wave patterns are divided into four different types of waves: alpha, beta, theta and delta waves [1, 2].

Alpha waves consist of high-amplitude, well-synchronized sinusoidal waves having a frequency of between 8 and 12 Hz. They occur in almost all adults, particularly in the thalamocortical region of the brain, when they are awake but in a quiet, resting state with eye closed. Alpha waves will disappear during sleep and when an awake person focuses attention on a specific mental activity.

Beta waves are desynchronized, and lower-amplitude than alpha waves. Desynchronization is not only characteristic of the transition between the closing and the opening of the eyes, but also of the most alert, attentive, or excited states. Beta waves normally occur at frequencies above 13 Hz; sometimes they can be as high as 50Hz. These mostly appear in the parietal and frontal lobes during intense mental activity.

Theta waves oscillate at frequencies between 4 and 7Hz. These waves occur mainly in the parietal and temporal lobes of children, but they can also appear during emotional stress in adults, especially during disappointment and frustration.

Delta waves include all frequencies below 4Hz. These occur in very deep sleep, in infants, and in serious organic brain disease. They also have occurred in animals whose cerebral cortex has been transected from the thalamus, indicating the waves can occur in the cortex independent of other brain areas.

2.8 Sleep Physiology

Currently there can be no absolute definition of sleep. In the human, sleep and sleep type is identified by electroencephalographic (EEG) frequency. This does not extend to all organisms as the simplest single cell organisms demonstrate rest-activity cycles [1].

The exact function of sleep is still to be definitively elucidated. Many theories have abounded as to the function of sleep [1]. These are include but are not limited to

1. Energy conservation (save energy, stop expenditure)
2. Wakefulness (being awake)
3. Immune function
4. Growth (in children, repair work in adults)
5. Data storage (reverse learning)

2.8.1 Sleep

In the human being sleep is differentiated into two main types namely:

1. Rapid Eye Movement (REM) and
2. Non-Rapid Eye Movement (NREM).

REM sleep has been divided into two principal classes namely phasic (high amplitude, low frequency) and tonic (low amplitude, high frequency) REM. NREM

sleep is characterized by four main sleep stages ranging from light sleep: stages 1 and 2 sleep to deep sleep: stages 3 and 4 sleep. In humans the temporal arrangement of sleep type is described graphically by a hypnogram (Fig: 2.9.1)

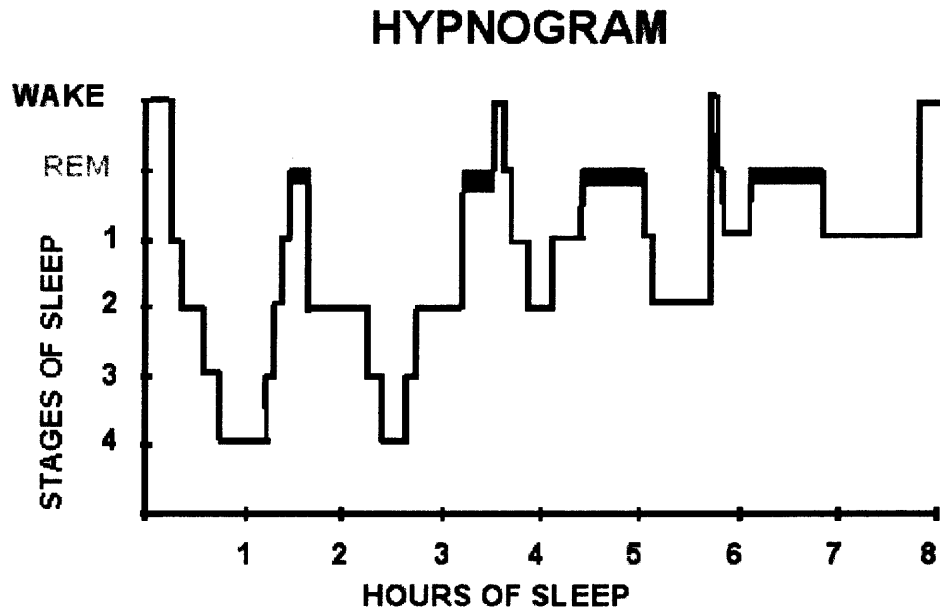


(Fig: 2.9.1) Typical Hypnogram from a healthy young subject.

Typically humans transition from quiet wakefulness into stage 1 sleep that lasts for 1 to 7 minutes, followed by a rapid progression taking between 10 and 25 minutes, through sequential NREM sleep stages to stage 4 sleep. REM sleep then follows deep sleep. This NREM-REM sleep cycle has an ultradian rhythm of approximately 90 minutes. As the sleep episode progresses this 90-minute cycle repeats; however the density of each sleep type alters across the course of time into sleep. Deep sleep (stage 3 and 4) is most prominent in the early part of the night and is related to homeostatic sleep pressure influences. Thus, as the sleep drive is progressively

satisfied across the course of the night, the time spent in deep sleep decreases. REM sleep exhibits the reverse pattern. The first episode of REM sleep may be as short as a couple of minutes lengthening to approximately 20-30 minutes by the end of the sleep episode [1, 2].

2.8.2 Types of Sleep – Sleep Stages

A methodology for the identification of human sleep stages uses their recognizable electroencephalograph (EEG) characteristics.

Wakefulness

The first stage is wakefulness which is characterized by low amplitude desynchronized EEG in the eyes open state. Relaxed wakefulness with the eyes closed may contain alpha rhythm.

Stage 1 Sleep

Stage 1 sleep is generally low amplitude EEG with some theta rhythms and vertex waves (sharp negative waves). Transitions into sleep are identified by alpha-theta transitions. There may also be slow rolling eye movements in stage 1 sleep.

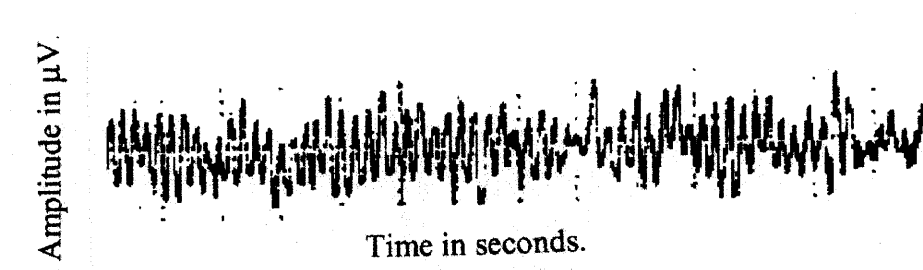


(Fig: 2.9.2) Stage 1 sleep – Alpha.

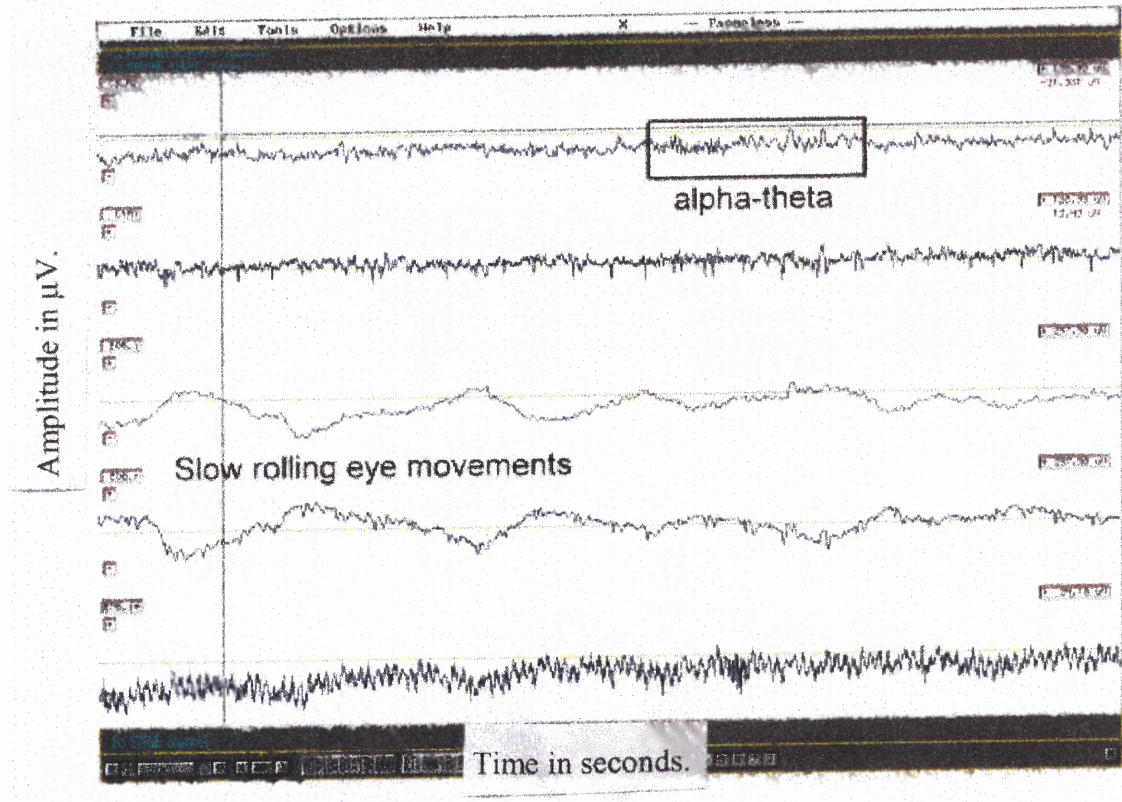


(Fig: 2.9.3) EEG during sleep stage 1.

Stage 2 Sleep

During stage 2 sleep the EEG becomes more synchronized and is characterized by the appearance of K-complexes (a sharp negative wave followed by a slower positive component) and sleep spindles (short rhythmic waveform clusters of 12 – 14Hz). If a K-complex or spindle is present then it is stage 2 sleep. However stage 2 sleep can be scored in the absence of K-complexes and spindles if it is surrounded with other episodes of stage 2 sleep and has the characteristics frequency components. There may also be slow rolling eye movement.

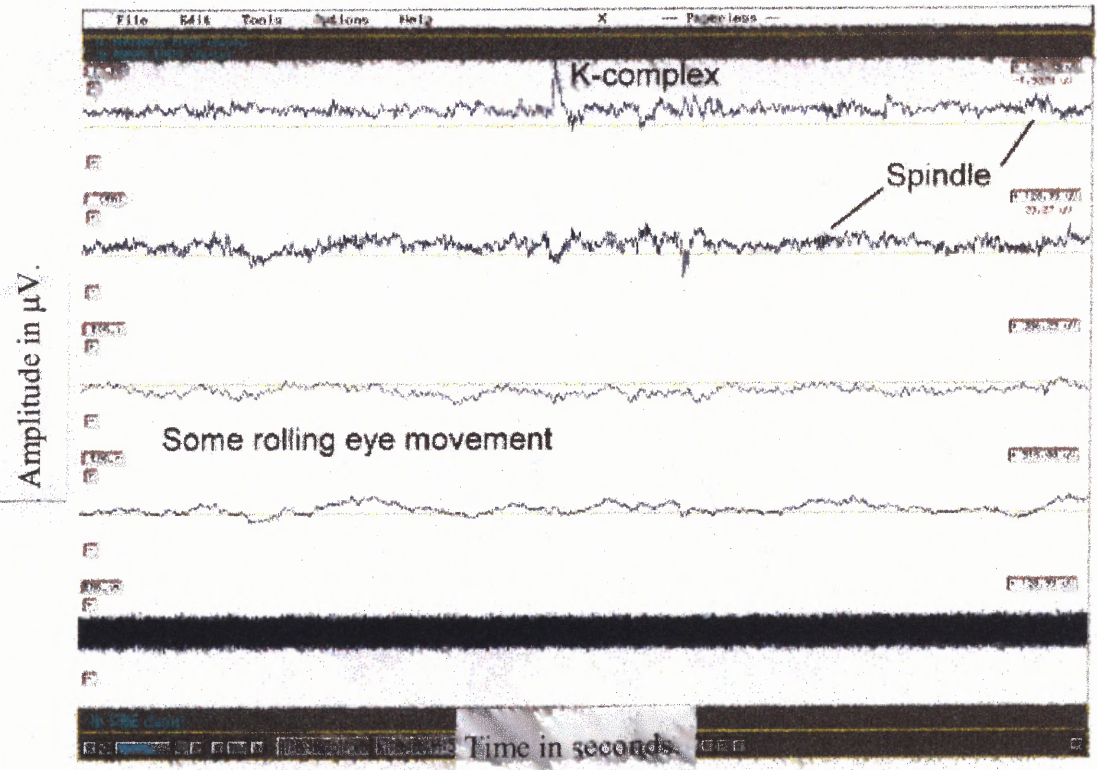


(Fig: 2.9.4) EEG sleep stage 2.

Slow Wave Sleep

Both stage 3 and 4 sleep are characterized by EEG delta wave activity. Delta waves are large amplitude waves at a frequency of $< 4\text{Hz}$. Stage 3 has $>20\%$ and $<50\%$ delta waves, stage 4 has $>50\%$ delta waves. There is usually little to no eye movement present in deep sleep.

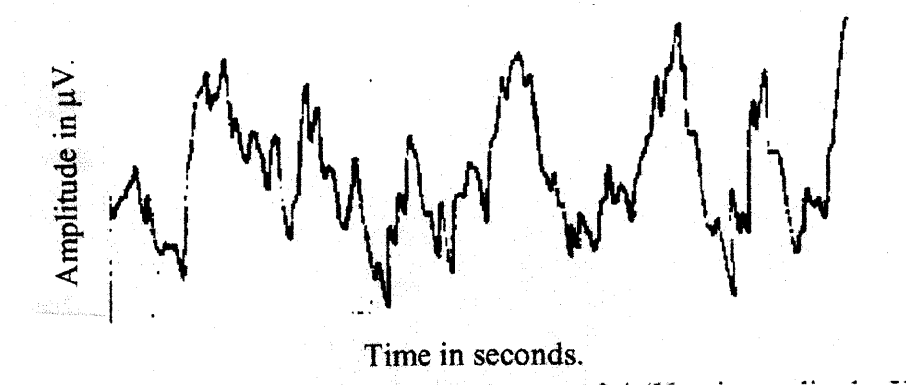


(Fig: 2.9.5) EEG slow wave sleep during stage 3&4.

Rapid Eye Movement Sleep (REM)

REM sleep exhibits some of the characteristic traits from both sleep and wakefulness EEG recordings. The EEG in REM is low amplitude and desynchronized. It may exhibit a saw tooth pattern [1, 2].

REM can also be broadly classified in to two types namely phasic and tonic REM. During phasic REM there are rapid eye movements and brief bursts of EMG, while during tonic REM eye movement are not present.

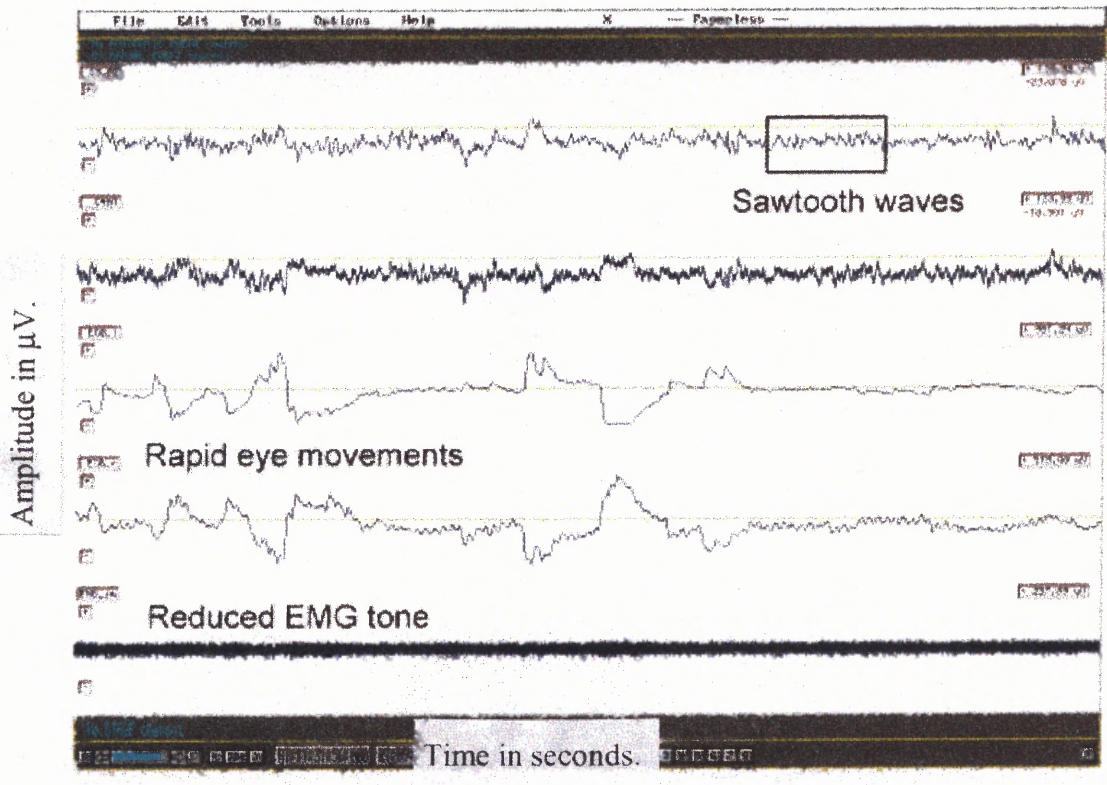


(Fig. 2.9.6) EEG - REM sleep.

2.9 Sleep Apnea Disease (SA)

Apnea has been described as a total cessation in airflow for a period of greater than 10 seconds. As the apnea continues to progress there is an absence or reduction of alveolar ventilation. Hypopnea is a reduction in airflow of greater than 50% for a period of 10 seconds or greater with apnea being the extreme case of hypopnea. The sleep apnea / hypopnea syndrome (SAHS) is characterized by repetitive pauses in respiration during sleep. The literal Greek meaning of “Apnea” is “want to breath”. A syndrome is defined by “ a group of concurrent symptoms of a disease”. Conservative prevalence studies estimate that 4% of males and 2% of females have the SAHS in American population. It is considered a major health problem having been reported as a more serious public

health problem than smoking and asthma. It has also been reported that the SAHS contributes to road traffic accidents, memory impairment and personality changes [1].

2.9.1 Symptoms

Interruptions of the normal respiratory cycle, due to apnea or hypopnea, typically end with an arousal, which fragments the normal sleep architecture. This arousal-arousal cycle potentially causes a daytime neurological disorder of excessive daytime sleepiness, impaired cognitive function, short-term memory impairment and mood swings. Other associated symptoms include snoring, nocturnal enuresis, nocturnal choking, unrefreshing sleep, morning headaches, impaired sexual function, spouse reports of arousal and restless sleep. Typically, but by no means always, a patient with the SAHS is an obese, middle-aged male presenting with excessive snoring and excessive daytime sleep (EDS) [1, 20].

2.9.2 Severity of Sleep Apnea

The severity of sleep apnea is classified according to the number of times per hour that a person stops breathing (apnea) or has slowed breathing (hypoapnea). Periods of apnea must result in at least a 4% drop in blood oxygen levels. The classification is referred to as the apnea-hypoapnea index (AHI) [1, 20].

- **Mild Apnea.** Mild apnea is 5 to 15 episodes of apnea or slowed breathing per hour with 86% or more oxygen saturation in the blood. Symptoms may include drowsiness or falling asleep during activities that do not require

much attention, such as watching TV or reading. These symptoms may cause only minor problems with work or social function.

- **Moderate Apnea.** Moderate apnea is 15 to 30 episodes of apnea or hypoapnea per hour with 80% to 85% oxygen saturation in the blood. Symptoms may include drowsiness or falling asleep during activities that require some attention, such as attending a concert or a meeting. These symptoms may cause moderate problems with work or social function.
- **Severe Apnea.** Severe apnea is more than 30 episodes of apnea or hypoapnea per hour with 79% or less oxygen saturation in the blood. Symptoms may include drowsiness or falling asleep during activities that require active attention, such as eating, talking, driving, or walking. These symptoms may cause severe problems with work or social function.

2.9.3 Types of Apnea

An apnea may arise from different mechanisms. This has led to the sub-classification of apnea types. The most common cause of an apnea event is the result of mechanical obstruction of the upper airway. This is termed an obstructive sleep apnea event. A narrow, floppy upper airway provides the pathophysiological basis for OSA. This may have a congenital or acquired origin. Usually such an airway does not cause problem during wakefulness. However, with sleep the associated loss of skeletal muscle tone increases the collapsibility of the upper airway [15], particularly during rapid eye movement (REM) sleep when muscle relaxation is profound. This has two important consequences as gas is accelerated through it. First, the structures will tend to vibrate as

turbulent flow patterns are produced, with snoring the result. Second, the pharynx will tend to collapse due to the Bernoulli effect, with resultant partial or complete obstruction. Obstruction will persist until sleep is interrupted and muscle tone is restored. Usually these interruptions are momentary arousals lasting less than 15 s and the sufferer is unaware of them. Occasionally, the obstructive event will result in an awakening, and the sufferer may complain of waking suddenly or with a snort or a snore. With arousal, breathing is restored and after a few breaths deeper sleep will resume with recurrence of the problem as the muscles again relax. In the more severe cases of OSA, this cycle of apnea and arousal may occur hundreds of times a night. In the more subtle cases, it may only occur in certain sleep stages (particularly REM sleep) and postures (particularly supine) or after alcohol consumption. The result of this constant sleep disruption is lethargy and somnolence during wakefulness [1, 2, 15, 20].

(Figure: 2.9.7) illustrates an obstructive apnea where airflow is discontinued however; intrathoracic movement indicates the presence of a respiratory effort.

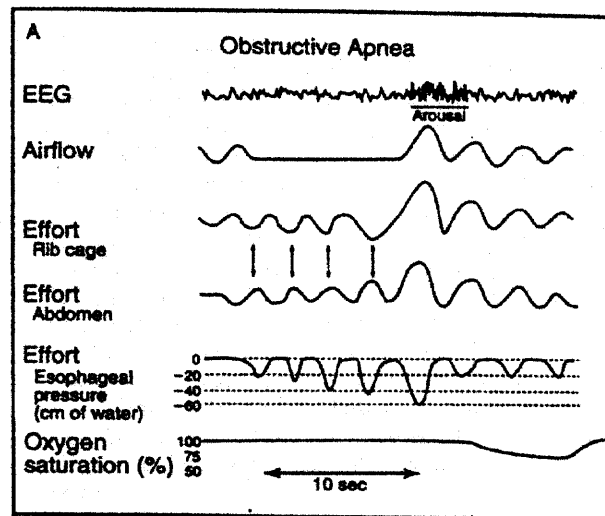


(Fig: 2.9.7) Obstructive Sleep Apnea.

An apnea that results from loss of central respiratory drive is termed a central apnea. During a central apnea there is little to no chest or abdominal wall expansion; therefore, no negative intrathoracic pressure developed during the apnea. A central apnea resulting from Cheyne-Stokes respiration (periodic breathing) in a heart failure patient, is illustrated in (Fig: 2.9.8) [1, 16, 19, 20].

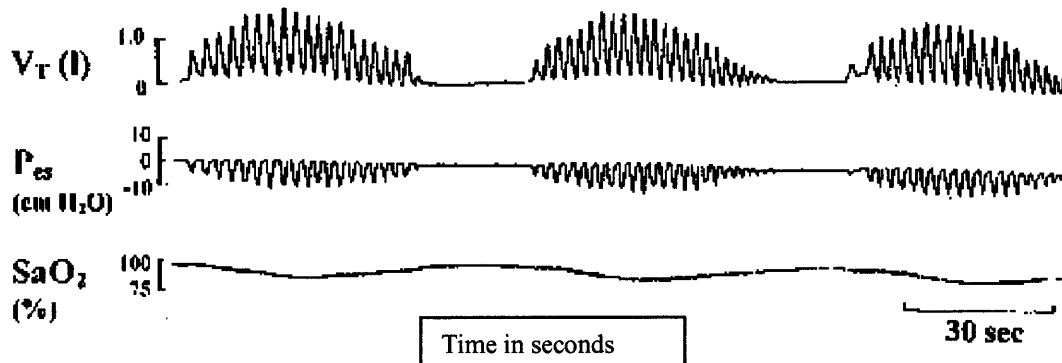


(Fig: 2.9.8) Central Sleep Apnea example. The top tracing illustrates tidal volume (V_T); the middle trace in the intrathoracic pressure recording (P_{es}) and the bottom trace illustrate the corresponding arterial oxyhaemoglobin saturation (SaO_2).

There is also a hybrid type of apnea termed a mixed apnea. Mixed apneas begin centrally and the upper airway collapses. Then respiratory efforts begin against the occluded airway, turning it into an obstructive event. Hypopneas are not usually sub-classified through they result from the same combination of mechanisms as apneas.

Table: 2.3 Symptoms Associated with Sleep Apnea

Adults	Children
Heavy snoring	Snoring
Excessive daytime sleepiness	Restless sleeping
Witnessed apneas	Somnolence
Sudden awakenings with “choking”	Aggression / behavioural problems
Accidents related to sleepiness	Hyperactivity
Poor memory/concentration	Odd sleeping postures
Gastro- oesophageal reflux	Frequent coughs/colds
Mood/personality changes	
Nocturnal sweating	
Restlessness during sleep	
Dry mouth on awakening	
Nocturnal or morning headache	

2.9.4 Physiological Changes during an Apnea

Hemoglobin Saturation

The reduction in alveolar ventilation resulting from either an apnea or hypoapnea event may, but not always, produce a decline in arterial oxyhaemoglobin saturation (SaO_2). Apneas are more likely to produce an arterial desaturation than hypoapneas [1].

Arousals

Respiratory disturbances typically end with cortical arousals. Arousals are characterized by an increase in EEG frequency. Brief arousals, lasting less than 15 seconds, are termed micro arousals. Definitions of EEG arousal classification vary. The most widely applied criteria for arousal are those reported by the American Sleep Disorders Association (ASDA). The ASDA criteria define a duration of 3-seconds for an arousal to be scored. Several reports have noted that not all respiratory events are terminated with a visually identifiable cortical arousal. Davies et al [33]. have shown that auditory stimuli provoke heart rate and blood pressure alterations without noticeable EEG changes. Conclusions drawn from this work have generated the concept of subcortical or autonomic arousals. These may provide a quantifiable method for measurement of sleep disruption.

Heart Rate

Inspiratory efforts against an occluded upper airway produce large negative intrathoracic pressure swings (Fig: 2.9.9). This is akin to performing the Mueller manoeuvre (voluntary negative intra-thoracic pressure), which is known to cause vagal activation. This is illustrated in the bottom trace of (Fig: 2.9.7) where a lengthening of the R-R intervals in the ECG trace is witnessed during the apnea. Supporting evidence for vagal involvement producing the apnea related bradycardia is that atropine sulphate inhibits

this reflex. Hedner et al [1]. report that, during an apnea, there is increasing muscle sympathetic nerve activity, peaking immediately prior to apnea cessation. The effect of increased sympathetic stimulus during an apnea, usually increasing the heart rate, may be swamped by the concurrent increase in vagal activity.

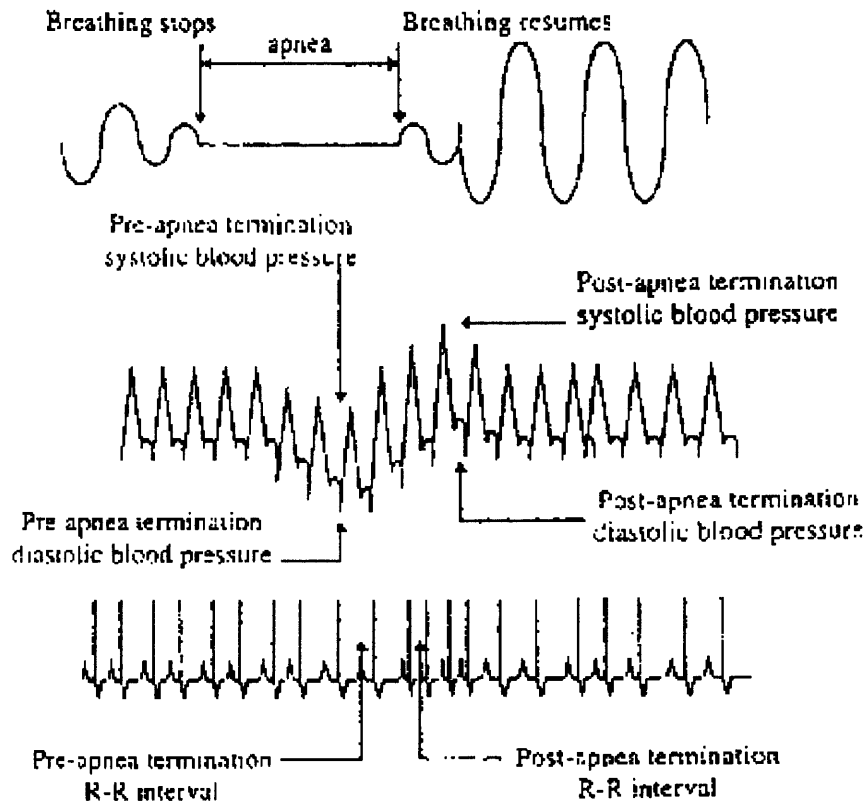


(Figure: 2.9.9) Transient heart rate and blood pressure consequences of an apnea.

The arousal at the termination of an apnea initiates a burst of sympathetic activity. In the SAHS, transient sympathetic increases have been demonstrated by blood pressure, heart rate (Figure: 2.9.9), catecholamine and MSNA recordings. The resulting tachycardia at arousal is not completely abolished by pharmacological Beta-blockade suggesting that there may be vagal inhibition in addition to sympathetic activation. In addition, at arousal there is reported carotid body activation and baroreceptor inhibition. After the

arousal heart rate and sympathetic activity fall to near resting levels [1, 15, 16], which can be seen in our data (Fig: 2.9.9.1). The first waveform shows the airflow of a 10 second apnea period. The following two graphs are electrocardiograph with the lengthening of the R-R intervals and simultaneous increase in blood pressure during the apnea. After the arousal the heart rate and blood pressure fall to near resting levels.

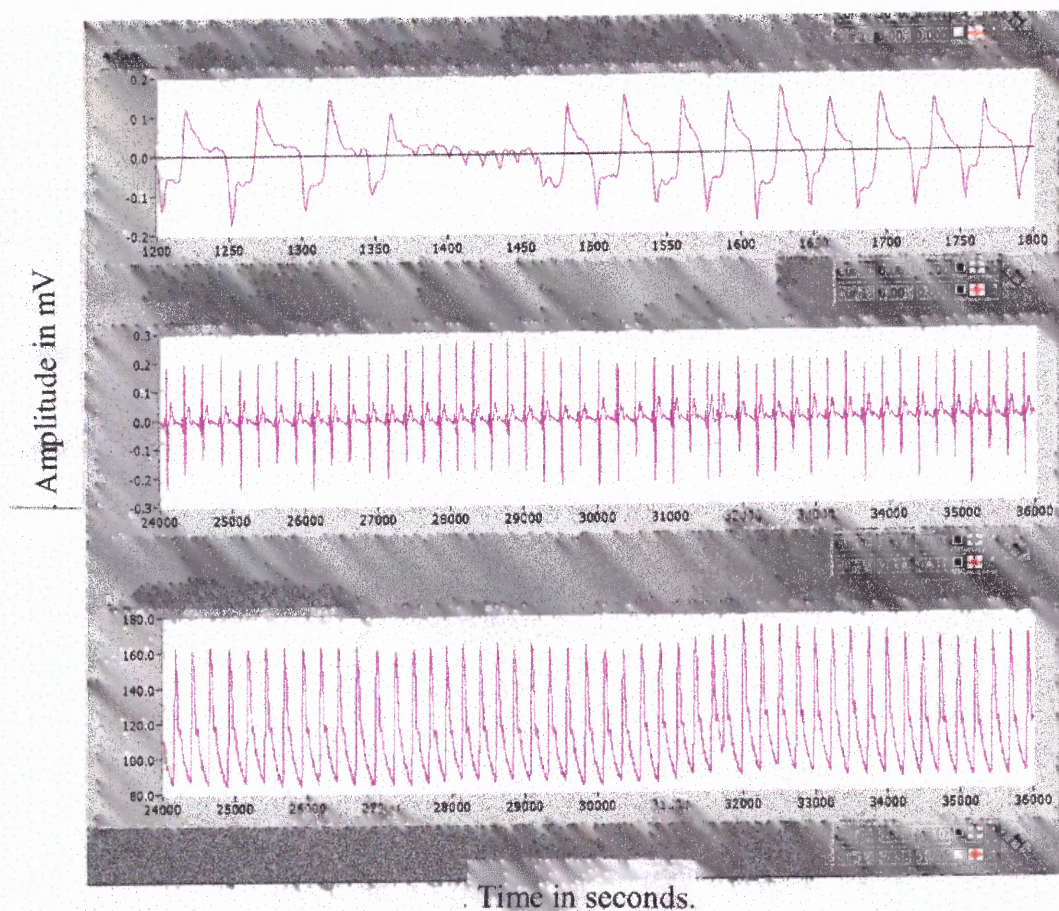


(Fig: 2.9.9.1) Airflow, heart rate and blood pressure consequences of an apnea

Blood Pressure

Systemic and pulmonary arterial pressure increase during an apnea. By the termination of an apnea, blood pressure can increase, with an associated decrease in stroke volume

suggesting an increase in peripheral resistance [1]. Following an apnea, blood pressures return to normal.

Haemodynamics Effects

It has been suggested that the negative intrapleural pressures developed during apnea induces hemodynamic changes in the myocardium and shifts in thoracic blood volume. It is unlikely that the blood pressure alterations are due to mechanical hemodynamic changes as studies have demonstrated that central apnea events, where no respiratory effort is produced, elicit blood pressure increases and bursts of muscles sympathetic nerve activity. Non-apnea arousals, i.e. those produced by nocturnal myoclonus (shock-like muscle contraction) and auditory stimuli also yield increases in systemic blood pressure and heart rate [1, 2, 20].

CHAPTER 3

ENGINEERING BACKGROUND

The purpose of this chapter is to introduce a brief background of signal-processing methods used in this study. One major component of this thesis is the investigation of heart rate variability using wavelets. The rest of this chapter will present the reason for using time-frequency analysis, the background on wavelets and the general approach to computing time-frequency distributions.

3.1 The Need for Time-Frequency Distributions

The distribution of signal energy in time and the distribution of signal energy in frequency are very straightforward. The distribution in time is defined as the squared magnitude of the signal, $|x(t)|^2$, and the distribution in frequency is defined as the squared magnitude of the Fourier transform, $|X(\omega)|^2$. Neither the signal nor its Fourier transform indicate how the energy of the signal is distributed simultaneously in time and frequency [17, 18].

3.2 The Uncertainty Principle

The uncertainty principle in time-frequency analysis provides us with a lower limit on the spread of signal energy in time and frequency. To define the spread of a signal in time and frequency, we first need to define the average time μ_t and average frequency μ_ω of a signal:

$$\mu_t = \int t |x(t)|^2 dt \quad (3.1)$$

$$\mu_\omega = \int \omega |X(\omega)|^2 d\omega \quad (3.2)$$

The spread of the signal in time σ_t^2 (duration) and frequency σ_ω^2 (bandwidth) is defined as:

$$\sigma_t^2 = \int (t - \mu_t)^2 |x(t)|^2 dt \quad (3.3)$$

$$\sigma_\omega^2 = \int (\omega - \mu_\omega)^2 |X(\omega)|^2 d\omega \quad (3.4)$$

The uncertainty principle states that [35]:

$$\sigma_t \sigma_\omega \geq \frac{1}{2} \quad (3.5)$$

Therefore a signal cannot have an arbitrarily small duration and bandwidth. A Gaussian signal:

$$x(t) = \left(\frac{\alpha}{\pi}\right)^{1/4} e^{-\alpha t^2/2} \quad (3.6)$$

meets this bound with equality where α is an arbitrary constant.

3.2.1 The Analytic Signal and Instantaneous Frequency

Most signals are real valued functions of time. Since the Fourier transform of a real signal will be even, there is an unnecessary redundancy in a real signal. To eliminate the redundancy, one can compute what is called the "analytic signal" from the real valued signal. The analytic signal, $x_a(t)$, is of the form:

$$x_a(t) = x(t) + jH[x(t)] \quad (3.7)$$

where $H[]$ is the Hilbert transform operator . The Fourier transform of the analytic

signal will satisfy:

$$X_a(\omega) = \begin{cases} 2X(\omega) & \text{for } \omega > 0 \\ 0 & \text{otherwise} \end{cases} \quad (3.8)$$

One advantage of the analytic signal is that it can be sampled at half the rate of the real signal. Another advantage of the analytic signal, which will be discussed later, is that there are fewer cross terms in the time-frequency distribution of an analytic signal.

In computing examples of time-frequency distributions, we will often use narrow band signals of the form:

$$x(t) = A(t)e^{j\phi(t)} \quad (3.9)$$

The above is the analytic signal corresponding to $A(t)\cos(\phi(t))$. The frequency of a signal at a given time is denoted as the instantaneous frequency, and for the signal in equation 3.1 it is defined as [13, 17, 18]:

$$\omega_x(t) = \frac{d}{dt} \arg\{x(t)\} = \frac{d}{dt} \phi(t) \quad (3.10)$$

where $\arg\{x(t)\} = \tan^{-1} \frac{\text{Im}\{x(t)\}}{\text{Re}\{x(t)\}} = \phi(t)$

Thus for a signal, the “ideal” time-frequency distribution should be similar to:

$$W_x(t, \omega) = A(t)^2 \delta(\omega - \omega_x(t)) \quad (3.11)$$

where $\delta(\cdot)$ is a Dirac delta function. The above equation implies that the energy of the time-frequency distribution is concentrated along the instantaneous frequency of the signal. A dual quantity is the average time of a signal at a given frequency. This quantity is called the group delay. For a signal of the form:

$$X(\omega) = A(\omega)e^{j\phi(\omega)} \quad (3.12)$$

the group delay is defined as:

$$W_x(\omega) = \frac{d}{d\omega} \arg\{X(\omega)\} = \frac{d}{d\omega} \phi(\omega) \quad (3.13)$$

where $\arg\{X(\omega)\} = \tan^{-1} \frac{\text{Im}\{X(\omega)\}}{\text{Re}\{X(\omega)\}} = \phi(\omega)$

3.2.2 Properties of Time-Frequency Distributions

There are many methods for constructing time-frequency distributions. To provide guidelines for constructing time-frequency distributions, authors have proposed many "desirable" properties that time-frequency distributions should satisfy. For example, since time-frequency distributions are usually considered to be energy distributions, they should be real and positive functions. Also, the time marginal of a time-frequency distribution is the integral of the time-frequency distribution over frequency, and the time marginal should be identical to the distribution of signal energy over time.

3.3 Power Spectral Analysis of Heart Rate Variability

Power spectral analysis of heart rate variability is a potentially powerful tool for evaluating the activity of the autonomic nervous system non-invasively. Power spectral analysis is a technique, which transforms a signal from the time domain to the frequency domain. It is based on the theory proposed by Fourier who states that all periodic functions can be represented as a sum of sines and cosines at a fundamental frequency and its harmonics. This sum is referred to as a Fourier series. Since heart rate variability is not periodic, a similar technique called the Fourier transform is applied. The time domain signal used for computing the heart rate variability power spectrum is known as the interbeat interval (IBI)[17, 18].

The ECG and BP signals are converted from analog to digital form and stored in .TXT format on the data acquisition computer. The data is then transferred over to a signal-processing computer. A LabVIEW program is used to identify the channel and obtain the HRV power spectrum. The following is a description of the necessary steps to obtain the power spectrum of HRV.

The first step to obtain the power spectrum of HRV is to detect every R-wave in the ECG. Because the R-wave complex is more pronounced in the ECG the LabVIEW detection program can easily detect these R-waves.

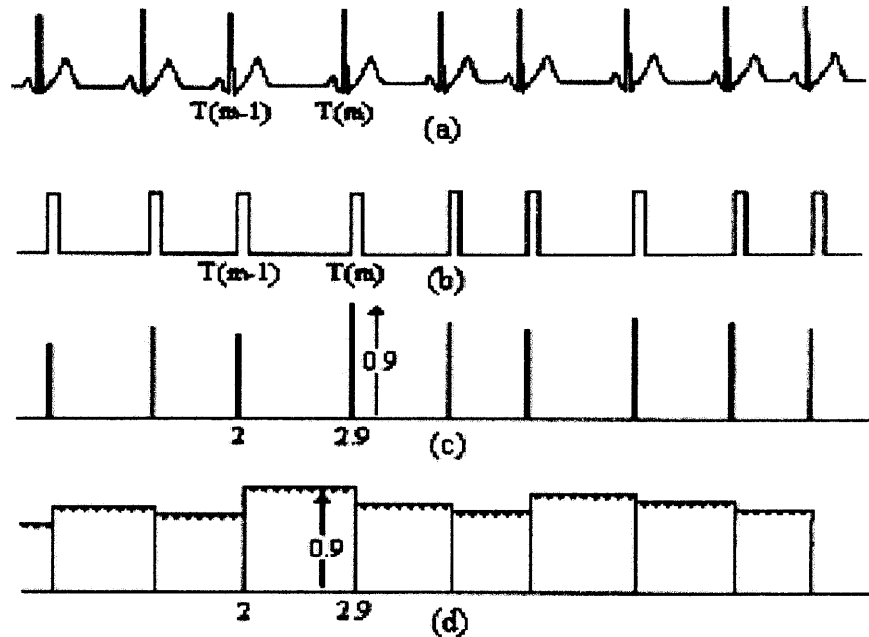


Figure 3.1 Figure Depicting the Construction of the IBI Signal (from S.J. Shin, W.N. Tapp, S.S. Reisman, and B.H. Natelson, "Assessment of autonomic regulation of heart rate variability by the method of complex demodulation," 1989)

Before trying to detect the R-waves, the ECG signals are detrended using a locally weighted robust regression algorithm built in LabVIEW. To help detect each R-wave, a vertical threshold (which the R-wave must exceed) and a horizontal threshold (to prevent detecting an R-wave for a period of time after one was detected) can be varied. If an error occurs during the R-wave detection, the analyst can use existing software to manually detect or the mis-detected R-waves.

Once the R-waves are properly detected, an interbeat interval (IBI) signal can be constructed. To obtain the IBI signal, the distance in time between a specific beat (T_m) and the beat previous in time (T_{m-1}) is calculated. This value of time difference then becomes the amplitude of the IBI signal at that specific beat. Mathematically, the IBI

signal is computed by the formula $IBI_m = T_m - T_{m-1}$. See Figure 3.1 for a graphical representation.

Although the IBI represents the heart period at discrete points, the IBI signal is not suitable for FFT analysis because the discrete points, located at each R-wave, are not evenly spaced. In order to produce equidistant IBI samples suitable for analysis, the IBI signal must be interpolated. The interpolation method used was that of a backward step function. This method assumes no new information about the direction of the time series is available until the next heartbeat occurs. Therefore, the amplitude of all of the interpolated values between a beat at time T_{m-1} , and the beat at T_m , were set equal to the time difference between T_m and T_{m-1} . The interpolated interbeat interval (IIBI) is then sampled to produce an IIBI with evenly spaced samples. For example, in Figure 3.1(c) if a beat occurs at a time equal to 2 seconds and the next beat occurs at a time equal to 2.9 seconds, then the interpolated values between time 2 seconds and 2.9 seconds are all 0.9 as shown in Figure 3.1(d). After the IIBI signal is obtained, it is detrended using a locally weighted robust regression algorithm (available in LabVIEW), which acts like a filter. Essentially, this removes low frequency components below .05 Hz. If these low frequency components are not removed, they can dominate the power spectrum and decrease the detail of the components in the frequencies above 0.05 Hz. Another example of an IBI signal and an IIBI signal is shown in Figure 3.2.

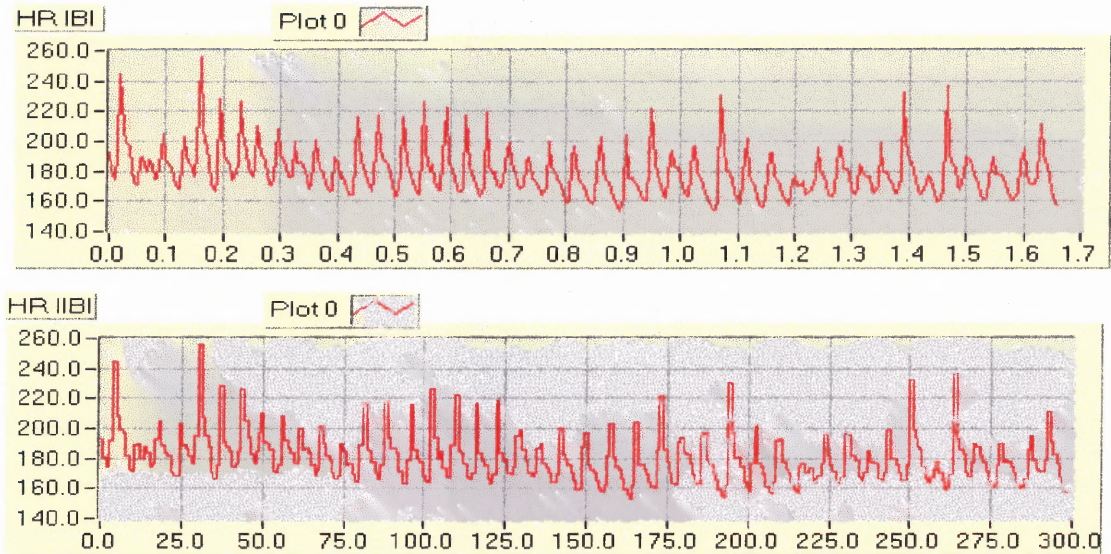


Figure 3.2 IBI and IIBI Signals of heart rate.

The final step to obtain the power spectrum of HRV is to take the FFT of the detrended IIBI signal. In the existing software, this is done by decimating the IIBI signal by a factor of ten (the ECG is sampled at 200 Hz) and taking an 8192 point FFT of the decimated IIBI signal. When the signal is decimated by a factor of ten, every tenth point of the original signal is kept, and the nine points in between every tenth point are not used. In a time series of samples, every tenth point occurs at the same time as in the undecimated signal, except that there are no samples in between. In effect, decimating is similar to down-sampling. Because the length of the IIBI signal is approximately the same length of the sampled ECG, which is acquired using a sampling frequency of 200 Hz, decimating the IIBI by a factor of 10, is similar to sampling the IIBI at 20 Hz. This can be done because the IIBI signal contains no frequency components above 6 Hz.

The software is programmed to take an 8192-point FFT by default regardless of the input signal length. In our experiments, ~300 seconds of ECG were collected. At a sampling frequency of 200 Hz, this corresponds to 60,000 samples. Recall that the IIBI is approximately the same length as the ECG. If an 8192-point FFT were taken, only the first one-eighth of the IIBI would be represented in the spectrum. In addition, the frequency resolution would be $200/8192 = 0.0244$ Hz and the spectrum would be between 0 Hz and 100 Hz. However, the spectrum of the IIBI, the heart rate variability spectrum, consists of low frequencies less than 6 Hz; therefore, the spectrum does not need to be calculated up to 100 Hz. As a result, the IIBI is decimated by a factor of ten. In this case, the IIBI signal would then be 6,000 samples long for a 300-sec long ECG signal. For example the length of the IIBI signal is 6,000 points long. The length of the IBI signal depends on the number of heartbeats. Now, in order to take an 8192-point FFT of a signal that has only 6,000 samples, a technique called zero padding must be used. Essentially all samples from 6001 to 8192 are given the value of zero. The only effect this has on the spectrum is that it increases the frequency resolution. When the FFT is calculated, we limited our spectrum from 0 Hz up to 10 Hz. The frequency resolution is now $20/8192 = 0.00244$ Hz. Once the power spectrum is obtained, it is smoothed twice by applying a modified Daniell Rectangular smoothing algorithm. Figure 3.3 illustrates the power spectrum of the IIBI signal in Figure 3.2.

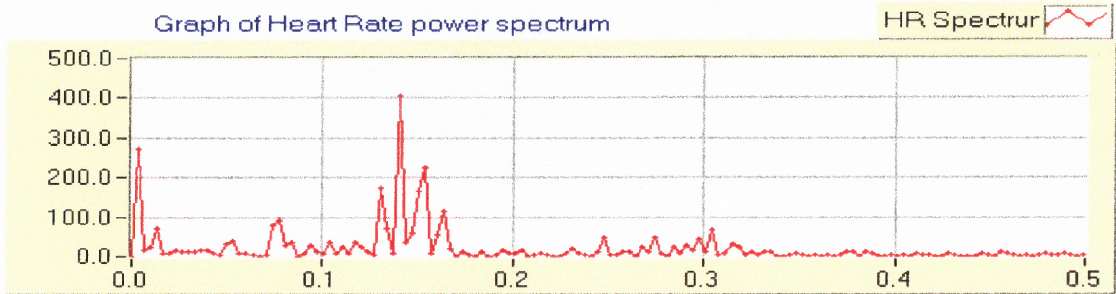


Figure 3.3 Power Spectrum of IIBI Signal in Figure 3.2.

It should also be noted that when performing the FFT, the IIBI signal is windowed by applying a split cosine bell taper. The taper begins at 20 percent from each end of the time signal. The application of the split cosine bell taper is done before the zero padding takes place so as to provide a smooth transition to zero rather than the window's abrupt changes from one to zero.

It should be noted that if the window were a simple rectangular function, the sharp one to zero changes are the cause of the side lobes in the FFT output sinc function ($\sin(x)/x$). To minimize the spectral leakage caused by those sidelobes, we have to reduce the sidelobe amplitudes by using window functions other than the rectangular window. The purpose of the split cosine bell taper window is to reduce any additional spectral components that result from the shape of the window. Multiplying the time signal by the window function does the windowing. The split cosine bell taper for a 6,000-point long signal is shown in Figure 3.4.

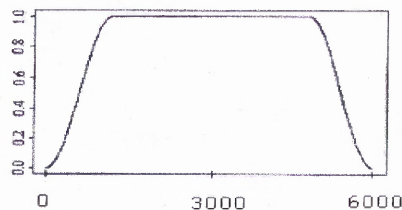


Figure 3.4 Plot of the Split Cosine Bell Taper used as a Window in the FFT Calculation

Past research in power spectral analysis of heart rate variability correlates the three distinct peaks with certain physiological parameters as illustrated by a more classical power spectrum of the IIBI signal in Figure 3.5. The very low frequency band is associated with vasomotor control and temperature control. The low frequency band is associated with baroreceptor-mediated blood pressure control. The high frequency band is associated with baroreceptor-mediated blood pressure control. The high frequency band has been linked with respiration [18].

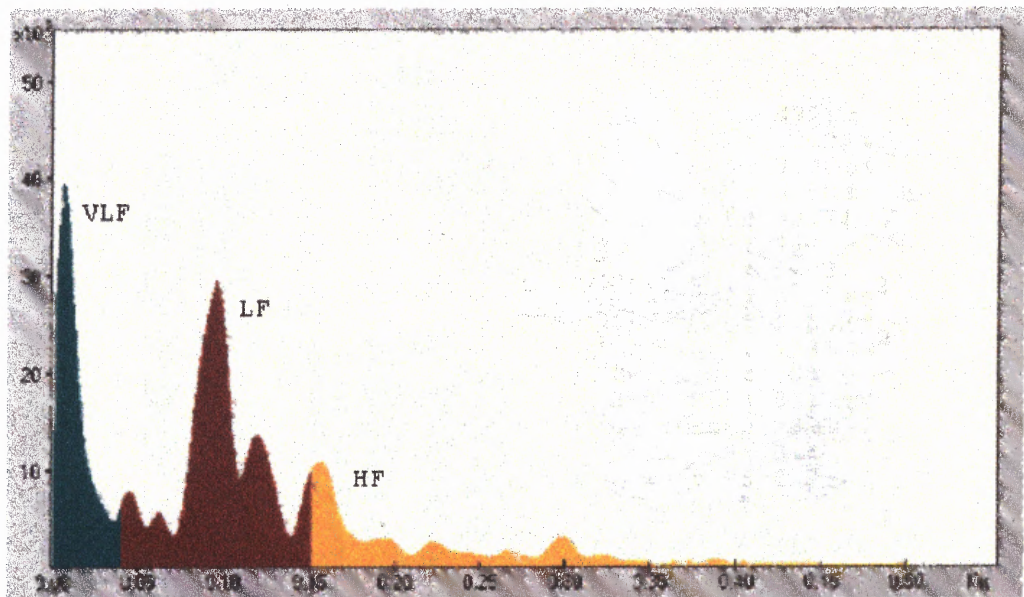


Figure 3.5 Example of power spectral density of HRV. Blue: power of spectrum of RR interval in VLF range, red: power in LF range and yellow: power in HF range. (From www.skyaid.org/Skyaid%20Org/Medical/HRV_Courses.htm, 2001)

To date, the best-known and best-defined peak in power spectral analysis of heart rate variability is the high frequency peak. The high frequency peak reflects changes in the interbeat interval that cycles up and down at the same frequency as respiration. This influence of respiration on heart rate has been known for more than one century and is called respiratory sinus arrhythmia (RSA). Properly defined, RSA is

a rhythmical fluctuation in heart periods at the respiratory frequency that is characterized by a shortening and lengthening of heart periods in a phase relationship with inspiration and expiration, respectively. RSA is being used increasingly as a measure of vagal control of the heart. As a result, the high frequency peak, which often occurs at the same frequency as the respiration peak, corresponds approximately to the RSA and it is purely parasympathetic in origin. From experience, one might contest that the frequency of respiration is not limited to within the narrow band of 0.15 Hz to 0.4 Hz. The normal respiration rate can be as low as only a few breaths per minute at rest and as high as up to 40 breaths per minute during intense exercise. This stresses the fact that, when doing research on heart rate variability to determine parasympathetic activity, the frequency of respiration must be known. More specifically, the power spectrum of the respiration waveform should be computed. [13, 17, 18].

Unlike parasympathetic activity, the sympathetic activity is not easily separated from the power spectrum of heart rate variability. It has been hypothesized that the low frequency peak (0.04 to 0.15 Hz) is a mixture of both parasympathetic activity and sympathetic activity. A better concept that is used to isolate the sympathetic activity is that of "sympatho-vagal balance" which recognizes both reciprocal and non-reciprocal parasympathetic and sympathetic influences on heart rate by computing the low frequency to high frequency ratio. An increase in the low frequency to high frequency ratio indicates either an increase of sympathetic activity, a decrease in parasympathetic activity, or a reciprocal change in both.

3.4 Wavelet Transforms

Analysis of signals using appropriate basis functions is one of the fundamental problems in the signal processing field. Fourier proposed the complex sinusoids as the basis functions for signal decomposition. The Fourier transform of a finite energy continuous time signal $f(t)$, (i.e. $f(t) \in L^2$) is defined as [14, 22]:

$$F(\Omega) = \int_{-\infty}^{\infty} e^{-j\Omega t} f(t) dt \quad (3.14)$$

The strength of the standard Fourier analysis is that it allows the decomposition of a signal into its individual frequency components and establishes the relative intensity of each frequency component. Because of the infinite durations of these basis functions, any time-local information (e.g. an abrupt change in the signal) is spread over the whole frequency spectrum. Therefore, this transform cannot reflect any time-localized characteristic of $f(t)$ into frequency domain. It only provides the frequency behavior of $f(t)$ in the interval $-\infty < t < \infty$. Gabor addressed this problem by introducing a window function to localize $f(t)$ and calculating the Fourier transform of the windowed signal as

$$F_{SF}(\Omega, \tau) = \int_{-\infty}^{\infty} \omega(t - \tau) e^{-j\Omega t} f(t) dt \quad (3.15)$$

where $\omega(t - \tau)$ is the appropriate time-frequency localized, window function. This transform is called the Windowed or Short-Time Fourier Transform (STFT) (also referred to the Gabor transform when the window function used in the STFT is Gaussian) [13, 14, 22].

The major advantage of Short-Time Fourier Transform is that if a signal has

most of its energy in the given time interval $[-T, T]$ and in the frequency interval $[-\Omega, \Omega]$, then its STFT will be localized in the region $[-T, T] \times [-\Omega, \Omega]$ of the time-frequency plane. Of course, the uncertainty principle prevents the possibility of having arbitrary high resolution in both time and frequency domains, since it lower-bounds the time bandwidth product of any basis function by $\Delta T \Delta \Omega \geq \frac{1}{4\pi}$ where $(\Delta T)^2$ and $(\Delta \Omega)^2$ are the variances of time function and its Fourier transform respectively.

An important parameter of a window function is its size (or scale). The selection of an appropriate window size poses a fundamental problem in signal analysis. Thus, by varying the window function used, one can trade the resolution in time for the resolution in frequency. An intuitive way to achieve this is to have short time duration high frequency basis functions, and long time duration low frequency ones. Fortunately, the wavelet transform provides for this desired feature and is defined as,

$$W_f(a, b) = \frac{1}{\sqrt{a}} \int \psi\left(\frac{t-b}{a}\right) f(t) dt \quad (3.16)$$

where $a \in R^+, b \in R$. Here a , and b are the scale and shift variables respectively, and they are continuous variables. Depending on the scaling parameter a , the wavelet function $\psi(t)$ dilates or contracts in time and causing the corresponding contraction or dilation in the frequency domain. Therefore a flexible time-frequency resolution is achievable with the wavelet transforms. Another significant difference of these transforms is that, the STFT is never a real function on the time-frequency plane regardless of the choice of $\omega(t)$, but the wavelet transform is real if the basic wavelet $\psi(t)$ is chosen to be real.

3.4.1 Continuous Wavelet Transform

The continuous wavelet transform maps a function $f(t)$ onto time-scale space as

$$W_f(a,b) = \frac{1}{\sqrt{a}} \int \psi\left(\frac{t-b}{a}\right) f(t) dt \quad (3.17)$$

This operation can be expressed in a simpler inner product notation as

$$W_f(a,b) = \langle \psi_{ab}(t), f(t) \rangle \quad (3.18)$$

$\psi_{ab}(t)$ represents a family of functions obtained from a single wavelet function $\psi(t)$ and the dilation and translation parameters a and b as

$$\psi_{ab}(t) = \frac{1}{\sqrt{a}} \psi\left(\frac{t-b}{a}\right) \quad (3.19)$$

where a and b are continuous.

The wavelet function $\psi(t)$ is a band-pass function. It is desired that this function have a good time and frequency localization so that $f(t)$ is decomposed into elementary building blocks which are jointly well localized in time and frequency. The wavelet function has to satisfy the “admissibility” condition that makes it an isometry (reflection or a half turn rotation) of $L^2(R)$ onto $L^2(R \times R)$. This requirement limits the wavelet functions which must satisfy

$$C_h = \int_{-\infty}^{\infty} \frac{|\Psi(\Omega)|^2}{|\Omega|} d\Omega < \infty \quad (3.20)$$

where $\Psi(\Omega)$ is the Fourier transform of the wavelet function $\psi(t)$. The admissibility condition is directly related to the decay of the wavelet function $\psi(t)$ which is required

to have good localization. The admissibility condition for a continuous $\Psi(\Omega)$ is equivalent to a zero-mean wavelet function in time

$$\Psi(0) = \int_{-\infty}^{\infty} \psi(t) dt = 0 \quad (3.21)$$

This condition forces that the wavelet function is a band pass function and decays at least as fast as $|t|^{1-\epsilon}$ in time (in practice we need to have much faster decay of $\psi(t)$, in order to have good time localization).

The admissibility condition assures that the “resolution of the identity” holds. This guarantees that any function $f(t) \in L^2(R^n)$ can be reconstructed from the wavelet space as

$$f(t) = \frac{1}{C_h} \int_{-\infty}^{\infty} \frac{1}{a^2} da \int W_f(a,b) \psi_{a,b} db \quad (3.22)$$

where the wavelet coefficients were defined earlier in Eq. (3.17). Whenever $\psi(t)$ is a real function, the integral limits of C_h expression in Eq. (3.22) are changed from 0 to ∞ .

Resolution of the identity ensures that the Continuous Wavelet Transform (CWT) is complete if $W_f(a,b)$ are known for all a and b . A continuous signal $f(t)$ is represented by a pass band function $\psi(t)$ and its dilated and translated versions. The dilation in time leads to different resolutions in frequency. Fig. 3.6 displays a wavelet function $\psi(t)$ and its dilations for different values of parameter “ a ” along with their Fourier transforms. This figure helps to visualize the time-frequency plane and emphasizes the band pass nature of $\psi(t)$ and its dilations. Fig. 3.3 also displays the time-frequency resolution cells of the wavelet transform compared with the STFT. This

figure indicates the fixed time-frequency resolution of the STFT versus the more flexible resolution of the wavelet transforms.

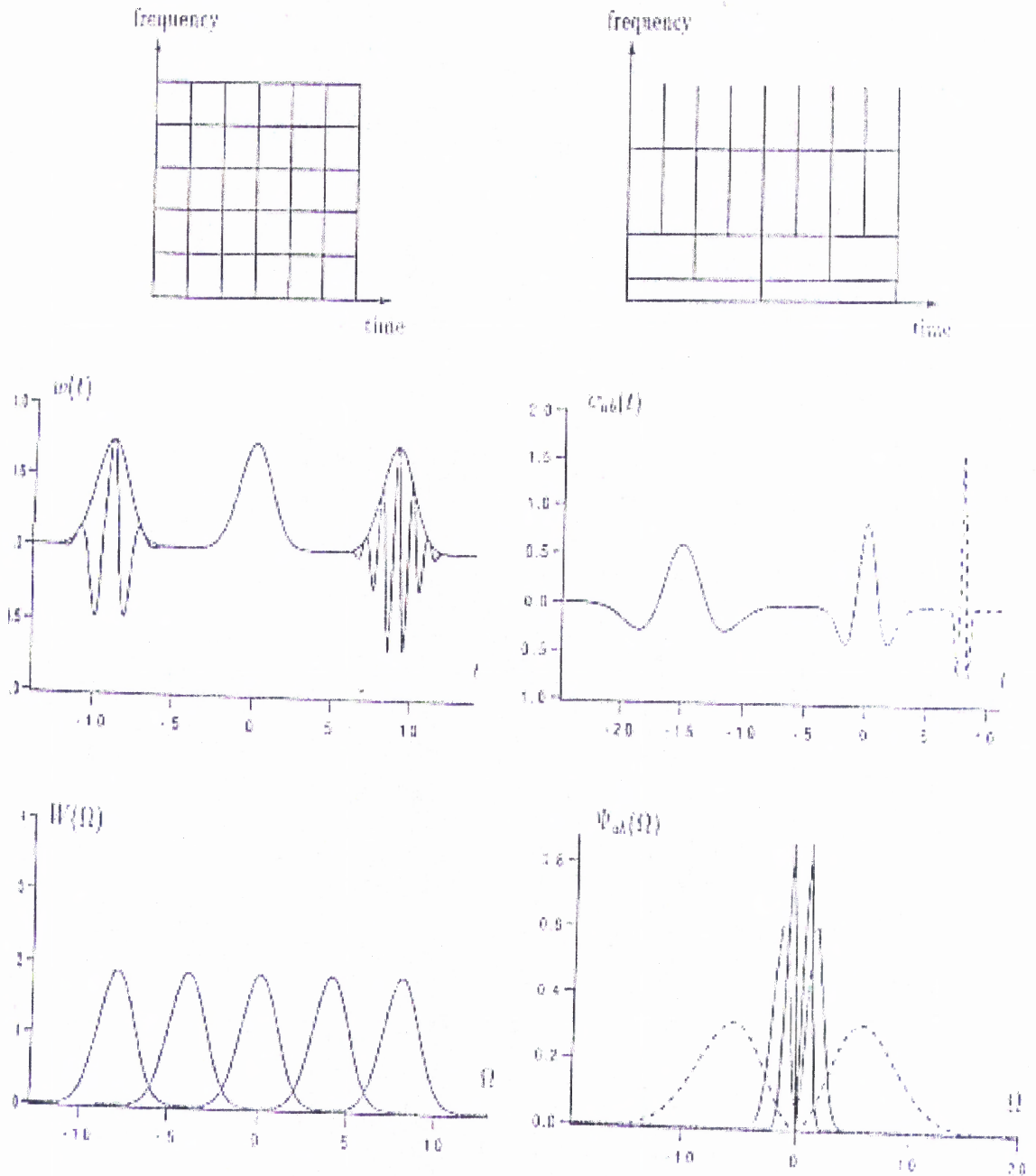


Figure 3.6 The time-frequency plane resolution cells of the STFT vs. Wavelet transform

The STFT yields the deposition of a signal into a set of equal bandwidth functions sweeping the entire frequency spectrum. On the other hand the wavelet transform provides the decomposition of a signal by a set of constant Q (or equal bandwidth on a logarithmic scale) band pass functions. The constant bandwidth condition on a logarithmic scale can be easily seen by the following relation,

$$\psi_{ab}(t) = \frac{1}{\sqrt{a}} \psi\left(\frac{t-b}{a}\right) \Leftrightarrow \Psi_{a,b}(\Omega) = \sqrt{a} \Psi(a\Omega) e^{-j\Omega b} \quad (3.23)$$

The roles played by the transform parameters are different for STFT and wavelet transforms. The time parameter τ in the STFT refers to actual time instant, while the parameter b in the continuous wavelet transform refers to the time instant $\frac{1}{a}b$.

There is a time-frequency resolution trade-off in the wavelet transform. To quantify how the continuous wavelet transform spans the time-frequency plane, the measures of time and frequency resolutions are defined. Let σ_t and σ_Ω be the standard deviations of the mother wavelet function $\psi(t)$ in the time and frequency domains respectively and the corresponding variances are defined as

$$\sigma_t^2 = \int (t - t_0)^2 |\psi(t)|^2 dt \quad (3.24)$$

and

$$\sigma_\Omega^2 = \int (\Omega - \Omega_0)^2 |\Psi(\Omega)|^2 d\Omega \quad (3.25)$$

Let the wavelet function $\psi(t)$ be centered at (t_0, Ω_0) in the time-frequency plane. Hence

$\psi\left(\frac{t-b}{a}\right)$ is centered at $(t_0, \frac{\Omega_0}{a})$ with the variances

$$\sigma_{ab_t}^2 = \int_{-\infty}^{\infty} (t - t_0)^2 |\psi_{ab}(t)|^2 dt = a^2 \sigma_t^2 \quad (3.26)$$

and

$$\sigma_{ab_\Omega}^2 = \int_{-\infty}^{\infty} \left(\Omega - \frac{\Omega_0}{a}\right)^2 |\psi_{ab}(\Omega)|^2 d\Omega = \frac{1}{a^2} \sigma_\Omega^2 \quad (3.27)$$

These results explain the role of scaling parameter a in the wavelet transform. Fig. 3.7 displays time-frequency resolutions of the wavelet and scaling functions for different values of a .

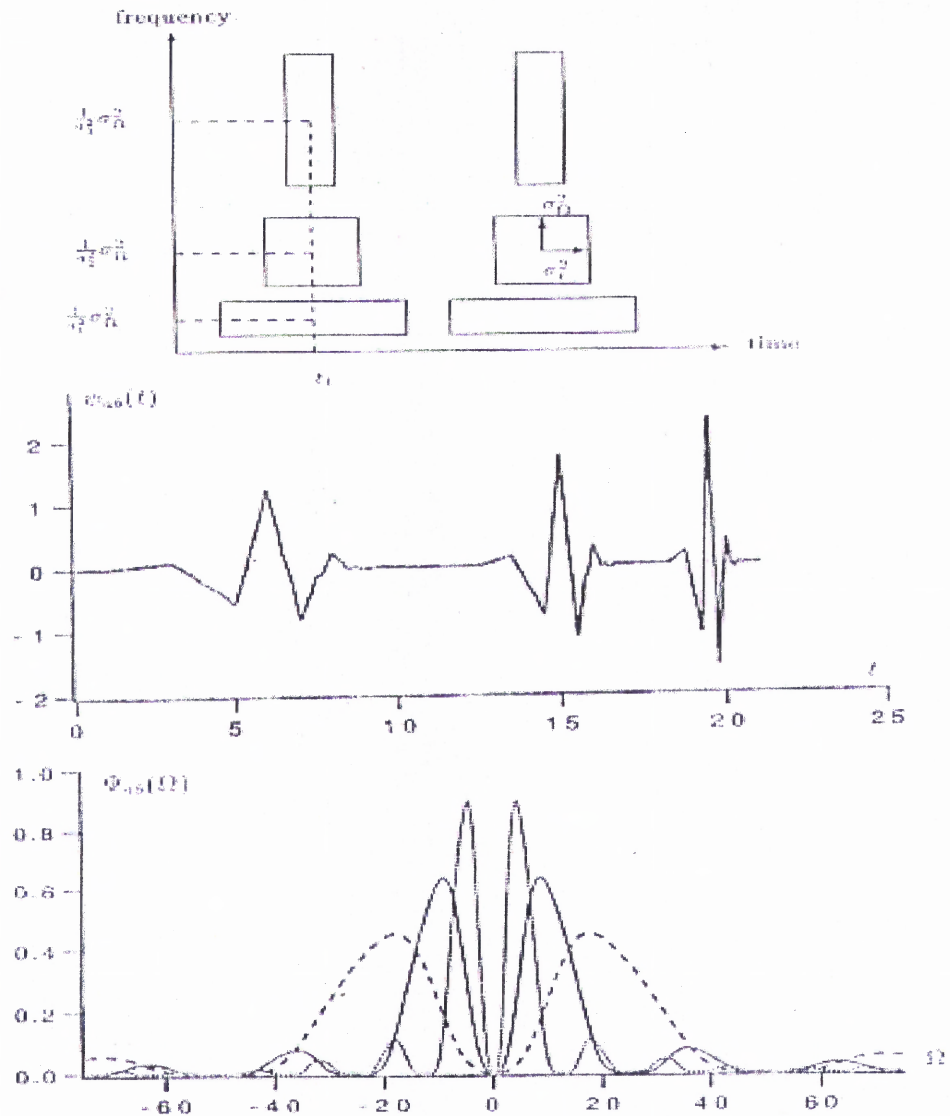


Figure 3.7 The role of scaling parameter in wavelet transform

3.4.2 Parseval Relation of Wavelet Transforms (Energy Preservation Property)

We will now show that the Parseval relation in the wavelet transform

$$E = \int_{-\infty}^{\infty} \int_{-\infty}^{\infty} |W_f(a,b)|^2 \frac{dadb}{a^2} = C_h \int_{-\infty}^{\infty} |f(t)|^2 dt \quad (3.28)$$

holds for any signal $f(t)$ which is squared-integrable. Its proof requires the

admissibility condition, which was defined in Eq. (3.20). By using the dual relation of wavelet transform in the time-frequency domain

$$W_f(a, b) = f(t) * \psi_{ab}(-t)|_{t=b} \Leftrightarrow F(\Omega) \frac{1}{\sqrt{a}} \overline{\Psi(a\Omega)} e^{j\Omega b} \quad (3.29)$$

one can get

$$\begin{aligned} \int_{-\infty}^{\infty} \int_{-\infty}^{\infty} |W_f(a, b)|^2 \frac{dad b}{a^2} &= \frac{1}{2\pi} \int_{-\infty}^{\infty} |F(\Omega)|^2 \underbrace{\int \frac{|\Psi(a\Omega)|^2}{|a|} dad}_{C_h} d\Omega \\ &= C_h \int_{-\infty}^{\infty} |f(t)|^2 dt \end{aligned} \quad (3.30)$$

It is worth noting that the wavelet transform energy between the different scales also preserves such that

$$\int_{-\infty}^{\infty} |\psi(t)|^2 dt = \int_{-\infty}^{\infty} \frac{1}{a} |\psi_{ab}(t)|^2 dt \quad (3.31)$$

3.4.3 Discrete Wavelet Transform

Although the admissibility condition assures the complete representation of $f(t)$ with its wavelet transform coefficients $W_f(a, b)$, it requires the wavelet transform operation to be performed for all values of a and b which are continuous parameters. This transform representation is not practical. One would prefer to perform the wavelet transform operation as few times as possible. Therefore these scaling or dilation, and translation or shift parameters, a and b respectively, are discretized. This discretization provides a transform grid or frame on the time-scale plane for the representation of signal $f(t)$. It is intuitive that this grid or frame should be defined properly such that the complete

representation of $f(t)$ is still possible. This is called the Discrete Wavelet Transform (DWT). This version of the wavelet transform reduces the redundancies of the wavelet space $W_f(a,b)$ significantly. The mathematical reasoning on the choice of frames or grids is perfectly treated in the literature [22].

Now we can define the basis functions of a Discrete Wavelet Transform as the subset of continuous wavelet function

$$\psi_{ab}(t) = \frac{1}{\sqrt{a}} \psi\left(\frac{t-b}{a}\right) \quad (3.32)$$

with the corresponding discrete transform lattices or grids

$$a = a_0^m \quad b = nb_0 a_0^m \quad (3.33)$$

Hence, the discrete wavelet transform basis functions can be expressed as

$$\psi_{mn}(t) = a_0^{-\frac{m}{2}} \psi(a_0^{-m}t - nb_0) \quad (3.34)$$

Here m and n are integers. It is intuitively seen that this discrete wavelet family approaches to a continuous wavelet family when $a_0 \rightarrow 1$ and $b_0 \rightarrow 0$

It can be shown that the functions of a discrete wavelet transform basis $\psi_{mn}(t)$ can form a frame or the sets of m and n parameters are proper for the completeness if the wavelet function $\psi(t)$ satisfies the admissibility condition. Then the frame bounds are constrained by the inequalities $0 < A < B < \infty$

$$A \leq \frac{\pi}{b_0 \log a_0} \int \frac{|\Psi(\Omega)|^2}{|\Omega|} d\Omega \leq B \quad (3.35)$$

These inequalities hold for any choice of a_0 and b_0 . These bounds diverge for non-

admissible wavelet functions.

The discrete wavelet transform is defined on the grid points or in the frame of time-scale plane as

$$W_f(m, n) = \langle \psi_{m, n}, f \rangle = a_0^{-\frac{m}{2}} \int \psi(a_0^{-m}t - nb_0) f(t) dt \quad (3.36)$$

and the wavelet transform representation of the signal

$$f(t) = \sum_m \sum_n W_f(m, n) \psi_{mn}(t) \quad (3.37)$$

There is a particular interest on binary or dyadic grid where $a_0 = 2$ and $b_0 = 1$, which leads to the conventional multiresolution concept and the orthogonal discrete wavelet transforms.

CHAPTER 4

METHODS

4.1 Subjects

The sleep apnea data were acquired from the Pulmonary Function Test (PFT) Lab at the New York Presbyterian Hospital (Columbia Presbyterian Medical Center) and the normal subjects data were acquired from the NJIT Biomedical Engineering Signal Processing Research Lab. A total of 22 subjects (18 males and 4 females, 49 ± 20 years) experiencing both OSA and CSA in whom sleep-disordered breathing were diagnosed, were used for this thesis. The inclusion criterion was the presence of at least five OSA per hour of sleep. The severity of the disorder, from moderate to severe, was based on the apnea / hypopnea index (the number of apneas / hypopneas per hour of sleep). Chronic hypertension was present in 14 subjects and none of them were treated for hypertension. Three subjects were current smokers.

The gold standard for a definitive diagnosis of the sleep apnea / hypoapnea syndrome is polysomnography (PSG) [9]. Polysomnography is a scientific evaluation of sleep. A polysomnograph is a machine that converts physiological signals (Ex. Oxygen saturation, Airflow, EEG, ECG, blood pressure, thoracic and abdominal movement) in the body to a graphical representation, which can help determine what is occurring during sleep. The subjects were chosen from the patients who came with the complaint of the following: snoring, poor sleep quality, excessive daytime sleep, some degree of fatigue and high blood pressure [11].

4.2 Protocol

Each subject underwent overnight polysomnography (PSG). PSG measures included thoracic and abdominal wall expansion, oro-nasal airflow, oximetry, body position, ECG, blood pressure and two-channel electroencephalography. EEG arousal was defined as an abrupt and discrete change in EEG frequency. Sleep stage analysis was performed by a sleep specialist. All subjects reported to the Sleep Laboratory at 20:00 and underwent standard nocturnal polysomnography until 06:00 the following morning. Typically a full night's sleep is observed before a diagnosis is reached, and in some patients a second night's recording is required. Because of the number and variety of measurement made, this test is somewhat uncomfortable for the patient [3].

4.3 Sleep Recordings

Sleep was recorded using standard polysomnographic measurements including electroencephalography (EEG), Electrocardiography (ECG) with precordial surface electrodes, oxyhemoglobin saturation O₂ with finger pulse oximeter (Embla, type XN), blood pressure, nasal and oral airflow measured by thermistors. respiratory movements of the rib cage and abdomen with piezo sensor bands. We recorded two leads of EEG, ECG, nasal airflow, thoracic and abdominal respiratory movements, oxygen saturation, snoring and body position. All sleep recordings were attended by a sleep specialist, which took care of the patients and electrodes during the night. We recorded at least eight continuous hours from 20:00 to 06:00. Data were recorded using the Labview Link 15 program, digital data with 200 Hz sampling rate for the ECG, blood pressure and EEG with 16 bit resolution. Respiration, airflow and oxygen saturation were digitized at

sampling rates of 10 Hz. All signal data were stored in the .TXT format, which allows easy exchange with other programs to display the signals and gives access to many analysis tools.

4.4 Data Analysis

The raw data was analyzed by using the LabVIEW (weighted coherence, Fig: 4.1) program and the output was stored in .asc file format. From this output the time-frequency (Wavelet) analysis was performed to determine the sympathetic and sympatho-vagal activities.

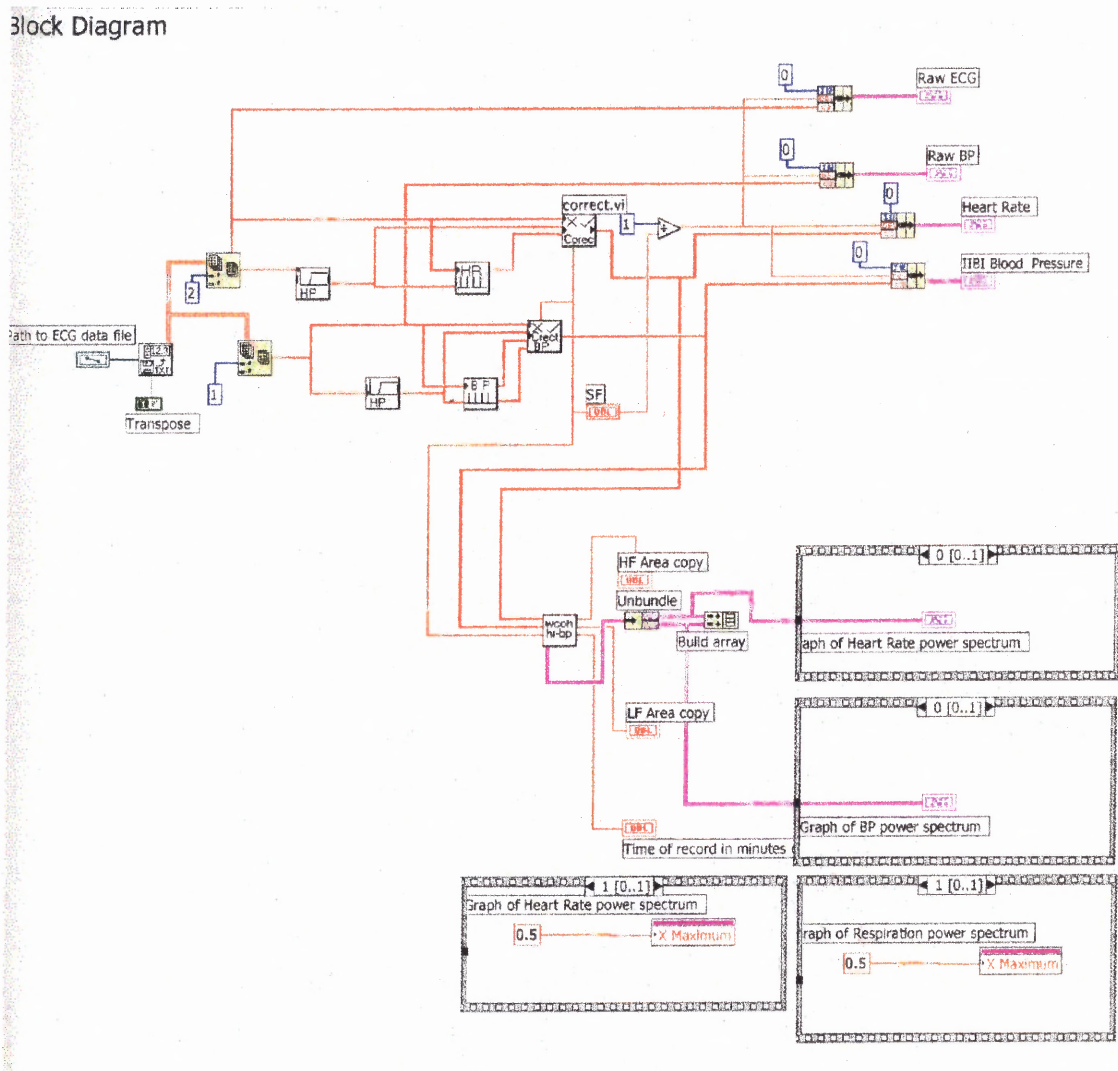


(Fig: 4.1) LabVIEW Program for power spectrum analysis.

4.4.1 Power Spectrum Analysis

The acquired digital data was transferred to a signal-processing computer. The raw data was run with a channel identification program (LabVIEW, Fig: 4.2) to identify the channels and locate the period of apnea.

The following (Fig: 4.3) represents the output of the channel identification program.

1st graph - Oxyhemoglobin saturation (SaO2)

2nd graph - Thoracic movement

3rd graph – Abdominal movement

4th graph – Airflow

5th graph – Electrocardiograph (ECG)

6th graph – Blood pressure (BP)

Block Diagram

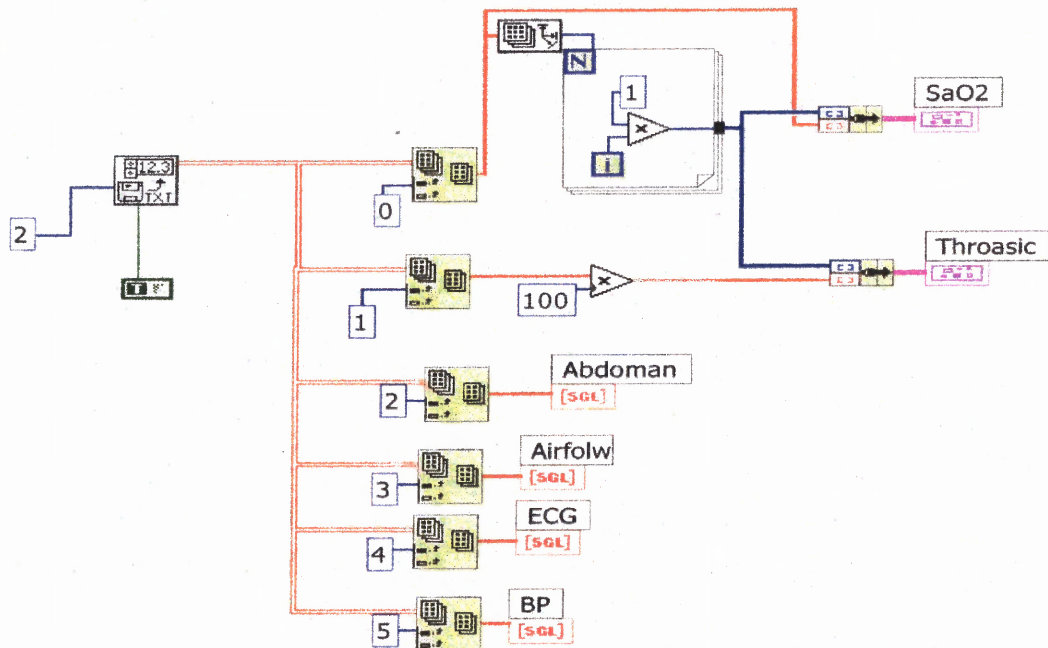


(Fig: 4.2) LabVIEW program for channel identification.

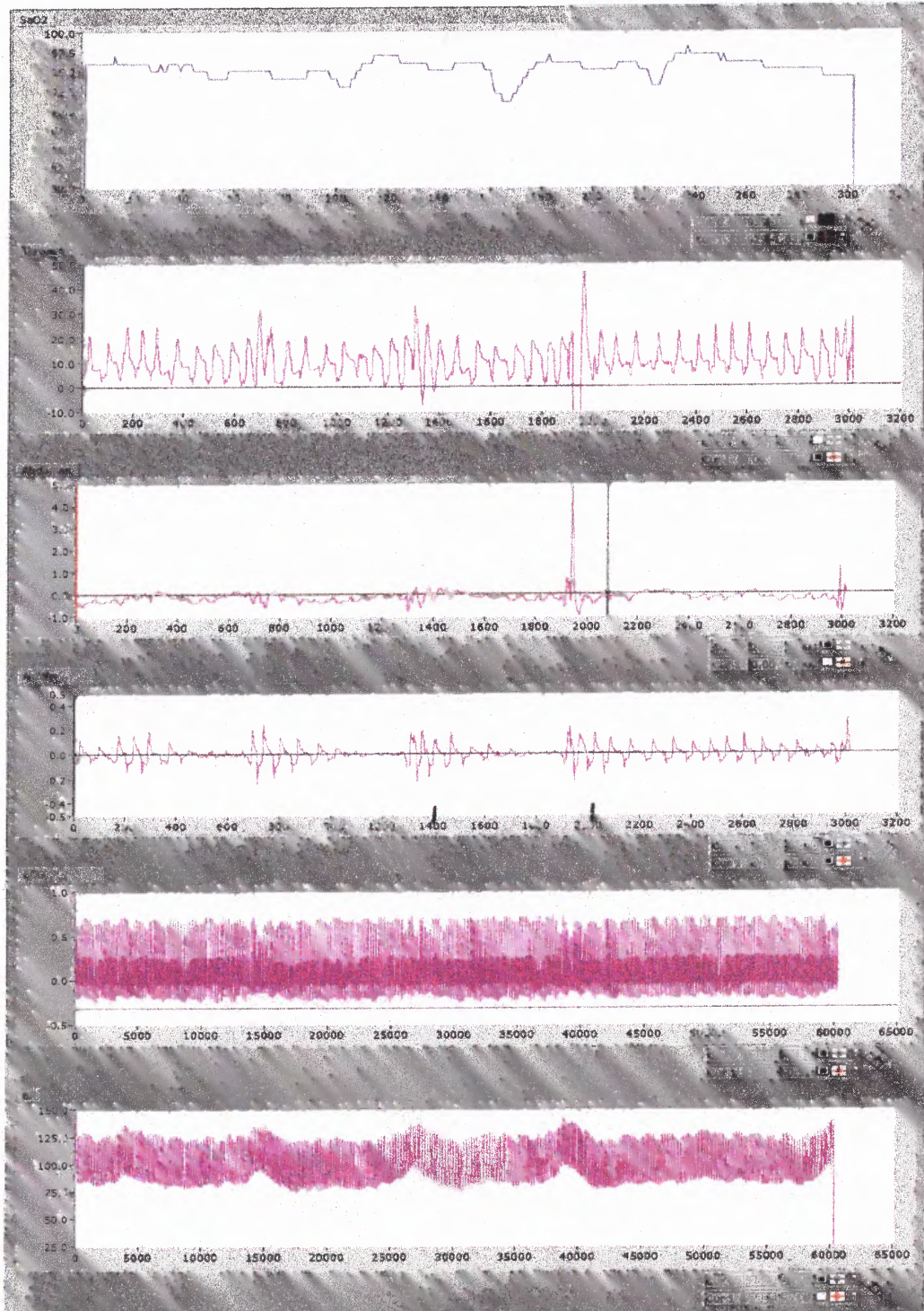


(Fig: 4.3) LabVIEW Program to identify the channels of apnea subject (KT).

Another LabView (weighted coherence, Fig: 4.1) program was used to obtain the HRV power spectrum. The following is a description of the necessary steps to obtain the power spectrum of HRV.

The first step to obtain the power spectrum of HRV is to detect every R-wave in the ECG. Because the R-wave complex is pronounced in the ECG, the LabVIEW detection program can easily detect these R-waves. If an error occurs during the R-wave detection, existing software can be used to manually detect or undetect the incorrectly detected R-waves.

The IBI signal represents the heart period at discrete points. It is not suitable for FFT analysis because the discrete points, located at each R-wave, are not evenly spaced. In order to produce equidistant IBI samples suitable for analysis, the IBI signal must be interpolated. The interpolation method used is that of a backward step function. After the IIBI signal is obtained, it is stored in .asc format to run with the Wavelet program. The IIBI signal is illustrated in Fig: 4.4.

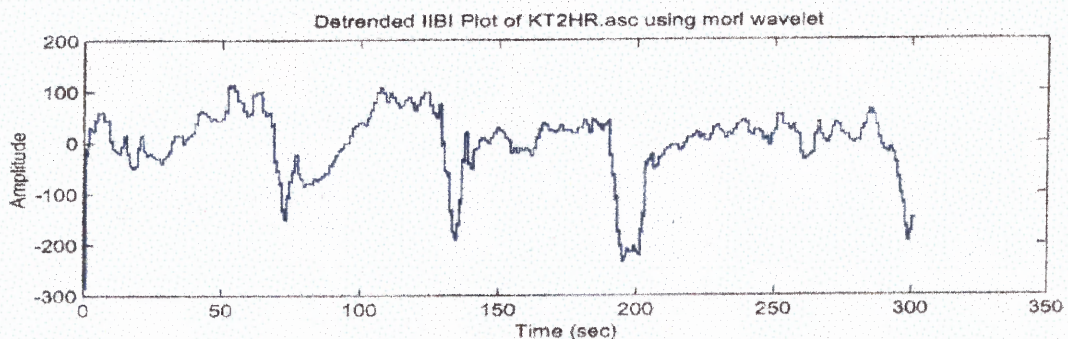


(Fig: 4.4) IIBI Plot of apnea subject (KT) using Morlet Wavelet.

4.4.2 Wavelet Analysis

After opening the Wavelet program (Appendix B) version 6.1, type the root directory file .asc location and then type wl_apnea to access the Wavelet program. The program will ask to enter the sampling frequency, no of windows to open, and the type of wavelet need to use. In our analysis we used Morl Wavelet. It opens up the specified number of windows; the last three windows give us the useful information for the investigation of sleep apnea. (Fig: 4.5) represents the sympathetic and parasympathetic activities of an apnea subject, and (Fig: 4.6) represents the normalized value of sympathetic and parasympathetic activities of an apnea subject.

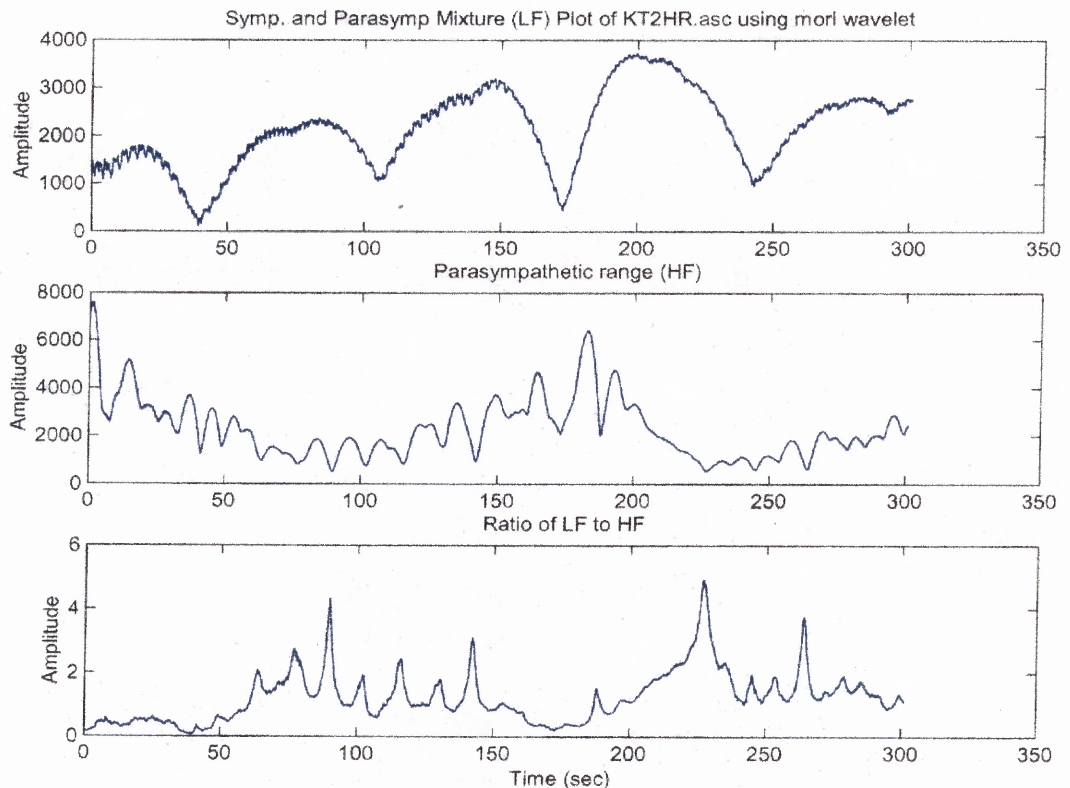


(Fig: 4.5) Sympathetic and Parasympathetic activity of apnea subject (KT).

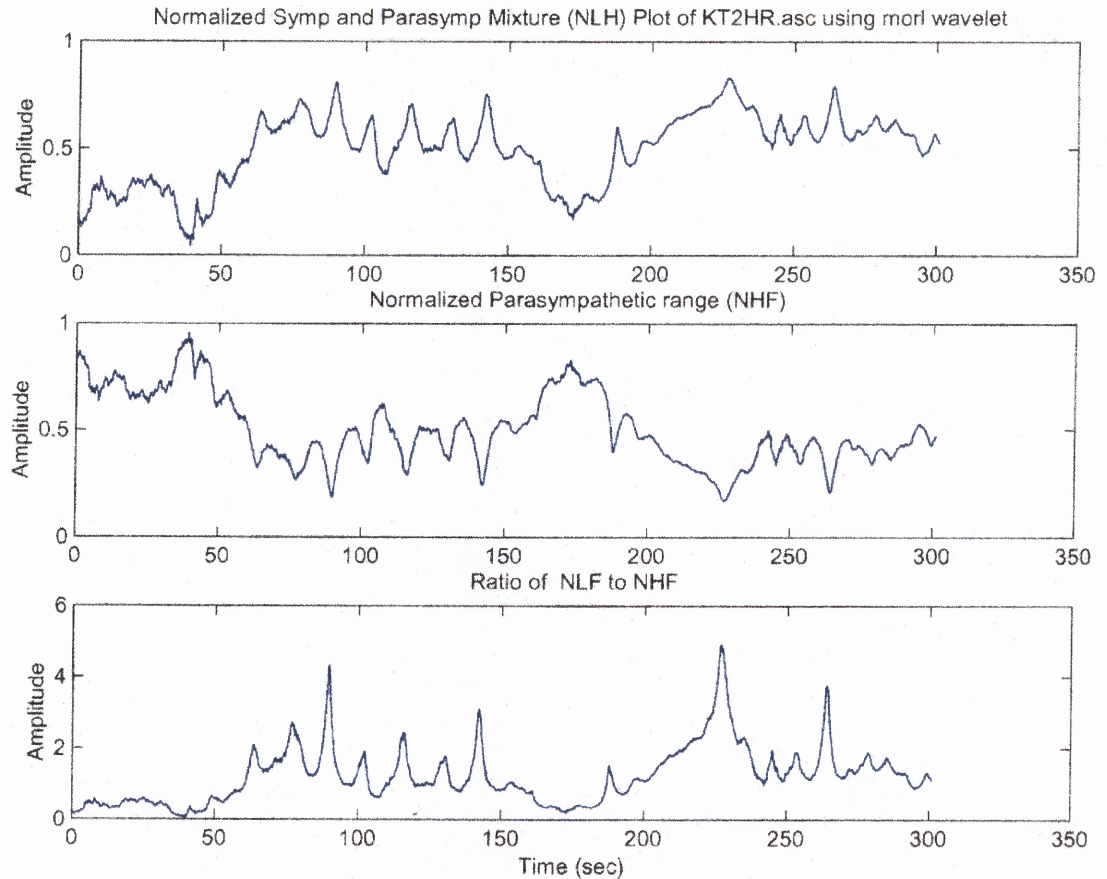


(Fig: 4.6) Normalized Sympathetic and Parasympathetic activity of apnea subject (KT).

4.4.3 Sleep Recording of Control Subjects

In order to compare our results with normal subjects 5 healthy persons participated in the study in the age group of (25 ± 5) . These normal controls had no symptoms of sleepiness and no sleep apnea. The normal subjects data were acquired at the New Jersey Institute of Technology Biomedical Engineering lab. Five channels of physiological signals were acquired from the normal subjects, which include two

channels of EEG, one channel of ECG, continuous Blood Pressure and thoracic respiratory movements.

The EEG signal was acquired with a Grass amplifier (Grass Telefactor W. Warwick, R.I. USA), the ECG signal acquired using Resp-I Impedance Pneumograph (UFI, Morrobay, California), the blood pressure acquired using Colin 7000 continuous blood pressure monitor (Colin Medical Instruments Corp., San Antonio, Texas) and the thoracic respiratory movements were recorded with a chest belt using inductive plethysmography (Respirtrace, Studley Data Systems, Oxford, U.K.).

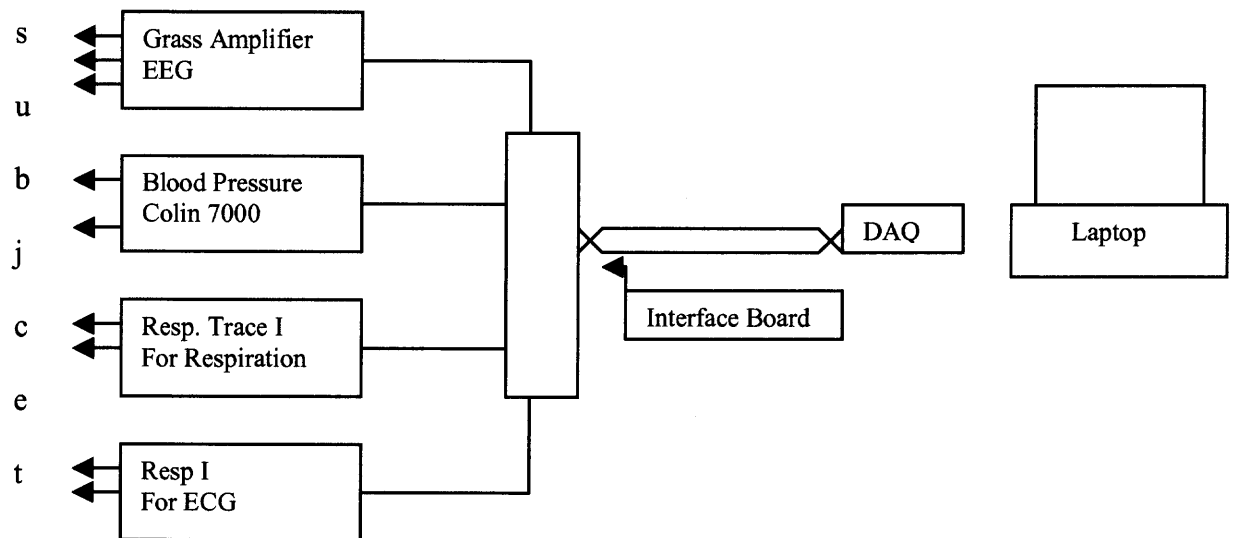


(Fig: 4.7) Equipment setup for the normal subject data acquisition.

The ECG and EEG leads were hooked up to the subject using disposable electrodes and continuous blood pressure monitor cuff kept on the arm. When the subject was ready to sleep the lead connections were checked and the light was turned off. The acquired analogue signals were amplified by the corresponding instrument.

From the data acquisition instrument the amplified signals were transferred to the Laptop through the interface board and DAQ card.

The data were digitized with 200 Hz sampling rate for the ECG, blood pressure, respiration and EEG with 12 bit resolution. The digitized data were recorded in a computer for subsequent analysis using the Labview (Link 15) program. All signal data were stored in the .TXT format, which allows easy exchange with other programs to display the signals and gives access to many analysis tools. Further analysis of normal subject data followed the same technique used above to analysis the data for sleep apnea subjects.

CHAPTER 5

RESULTS

The investigation of the heart rate variability during sleep apnea was performed through power spectral analysis and wavelet analysis. The changes in power spectral components LF, HF & LF/HF have been described by comparing the normal subjects with apnea subjects. From the spectral analysis of each subject, the LF and HF were averaged to 5 minutes. From the average of LF and HF values the mean was calculated. In our study we found that there is a statistically significant difference in sample means of sympatho-vagal balance (LF/HF) between normal and sleep apnea subjects. That is, the sampled subjects from the normal and apnea populations were found to be significantly different in their mean values ($p < 0.05$) by a two-sample t-test (Appendix E). In order to check the difference between the individual groups, t-tests were applied. Statistical significance was stated for $p < 0.05$. In Fig: 5.1 & 5.2 we observed an increase in LF & HF activity in apnea subjects compared to normal subjects, but the difference in sample means were not found to be statistically significant. This increase in LF & HF could be because of the presence of an autonomic dysfunction in sleep apnea patients, or one apnea subject (PW) (Fig: 5.1 and 5.2) having large variation in spectral power compared to the others may cause this variation.

t-test for normal and apnea subjects

DataSet	MEAN (N) (N = 6)	MEAN (A) (N = 7)	t	P
LF	179.87	1024.89	-1.61	0.07
HF	214.5	764.14	-0.82	0.22
LF/HF	1.57	6.52	-2.84	0.01*

*: Significant at 0.05

(with outlier - PW)

(Table: 5.1) The significance levels were given for the group difference between normal and apnea subjects using the t-test.

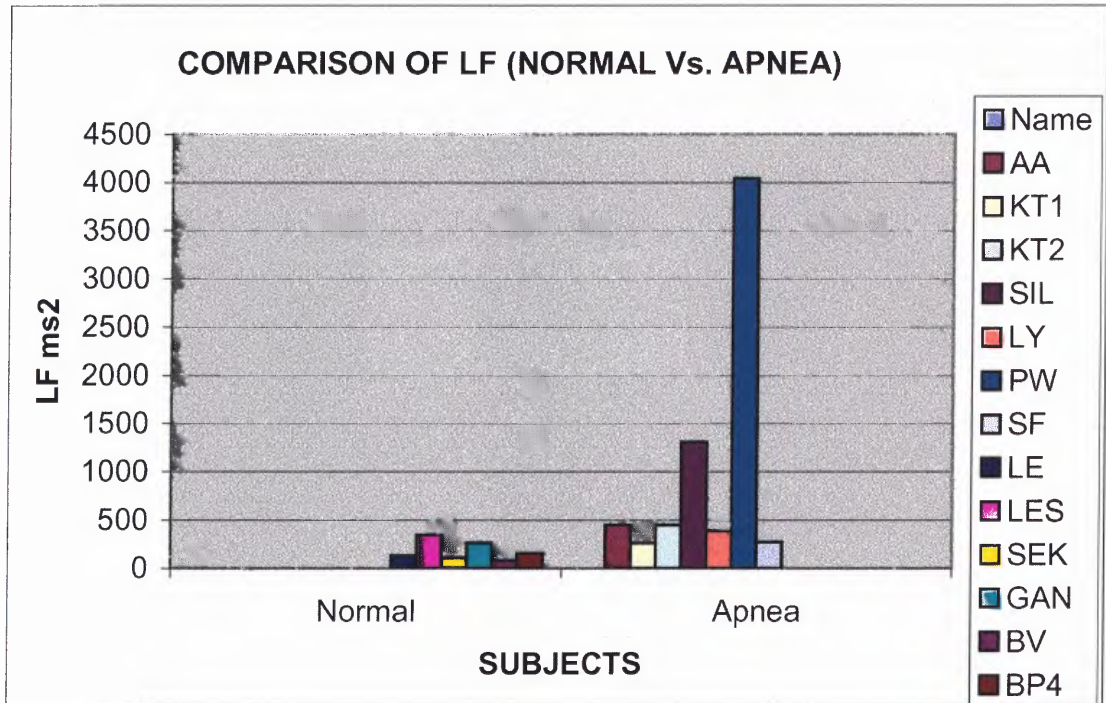


(Fig: 5.1) Comparison of LF (Normal Subjects Vs. Apnea Subjects).

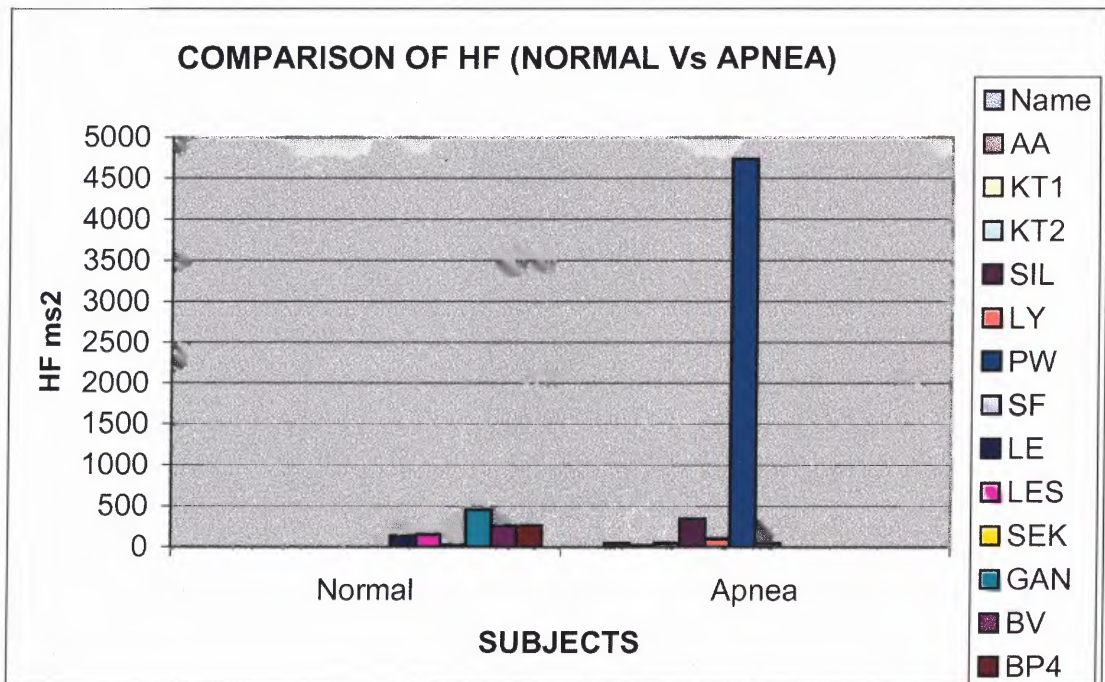


(Fig: 5.2) Comparison of HF (Normal Subjects Vs. Apnea Subjects).

Fig: 5.3. Shows the comparison of LF/HF between the normal and apnea subjects. The mean was investigated during sleep in normal subjects and sleep apnea subjects (Table: 5.1). The LF/HF was significantly higher ($p < 0.01$) in sleep apnea patients as we confirmed in our study (Fig: 5.3). (Table: 5.1) shows a greater decrease of parasympathetic activity (HF) than the decrease of LF activity in sleep apnea patients [8] [35].

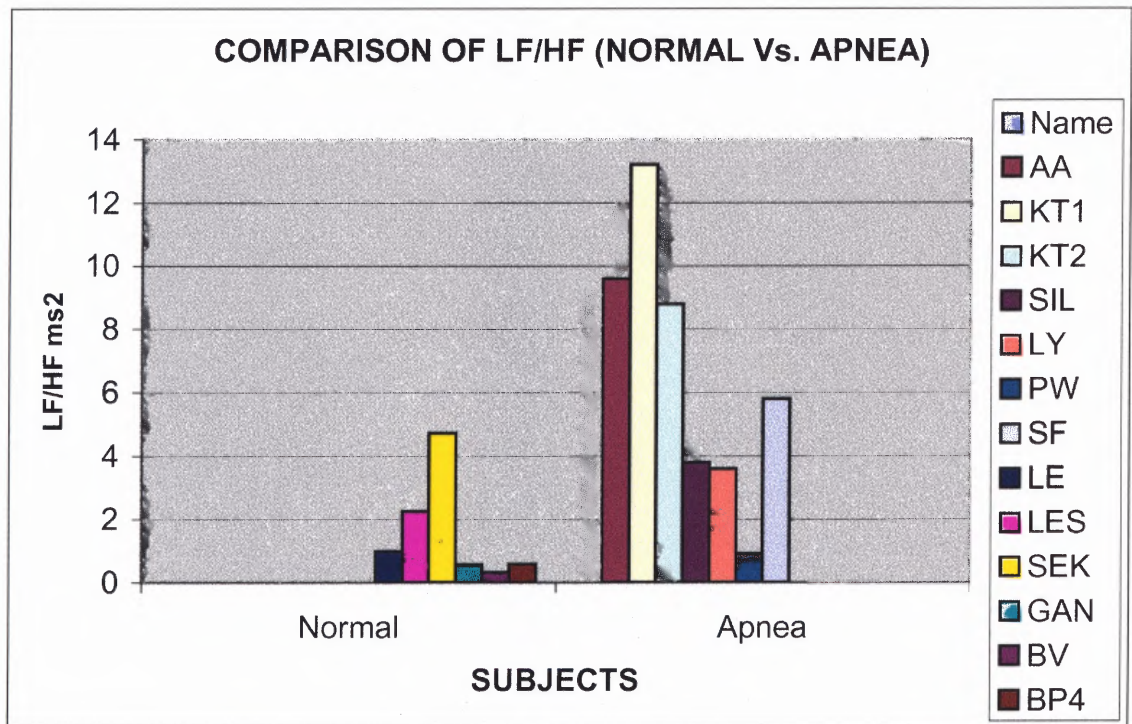


(Fig: 5.3) Comparison of LF/HF (Normal Subjects Vs. Apnea Subjects).

In (Fig: 5.1 & 5.2) one apnea subject has a large variation in LF & HF compared to the rest of the subjects, and therefore could be an outlier. Therefore we did the t-test without that person (PW). We observed (Table: 5.2, Fig: 5.4 & 5.5) increased LF in sleep apnea subjects compared to normal subjects and decreased HF in sleep apnea subjects compared to normal subjects.

t-test for normal and apnea subjects

Data Set	MEAN (N) (N = 6)	MEAN (A) (N = 6)	t	P
LF	179.87	521.51	-2.05	0.03*
HF	214.5	103.5	1.4	0.09
LF/HF	1.57	7.46	-3.5	0.002*

*: Significant at 0.05 (Without outlier - PW)

(Table: 5.2) The significance levels were given for the group difference between normal and apnea subjects using the t-test.

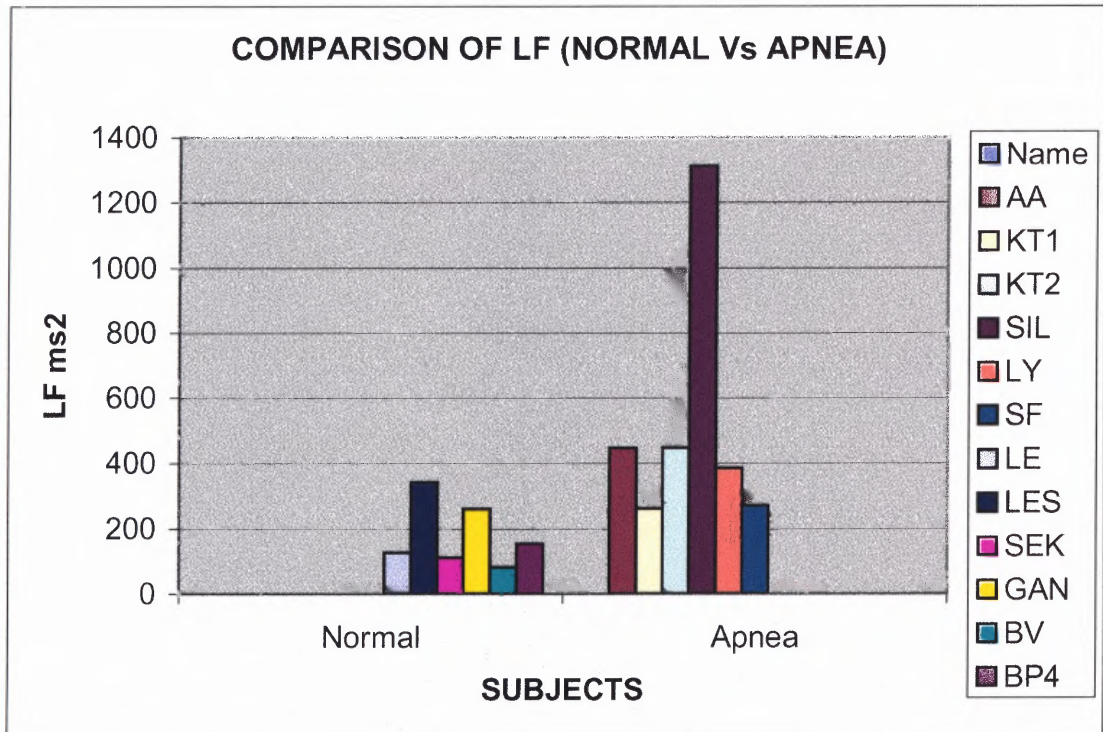


(Fig: 5.4) Comparison of LF (Normal Subjects Vs. Apnea Subjects)

Penzel et al. [35] investigated spectral components in normal and sleep apnea subjects. The LF component decreases in normals compared to sleep apnea subjects and the HF increases in normals compared to sleep apnea subjects. In our data the LF ($p < 0.03$) spectral component is significantly different in normal subjects compared to the sleep apnea subjects and there is no significant difference in the HF component (Table: 5.2).

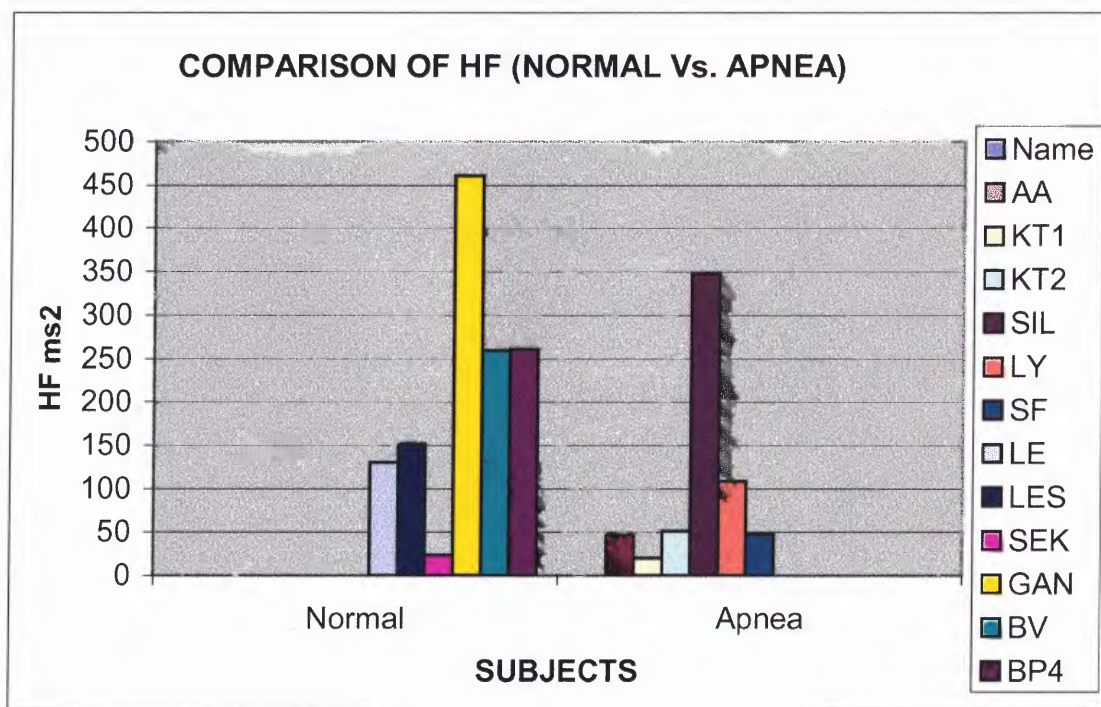


(Fig: 5.5) Comparison of HF (Normal Subjects Vs. Apnea Subjects)

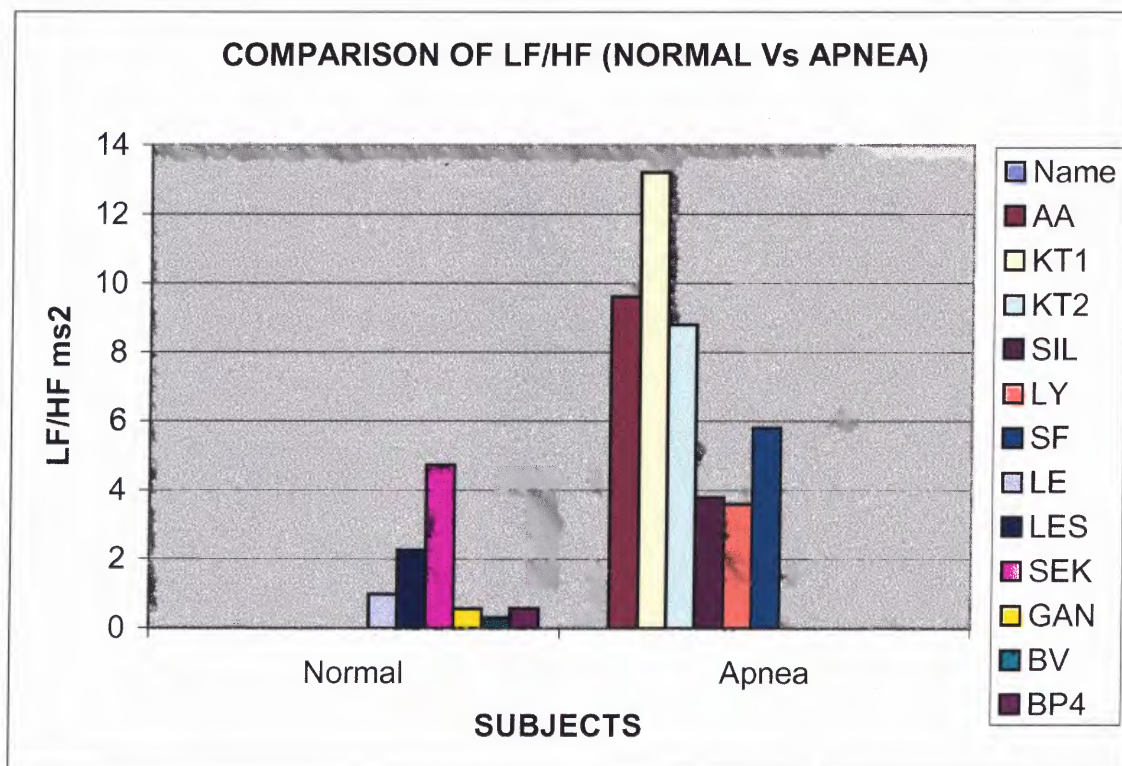


(Fig: 5.6) Comparison of LF/HF (Normal Subjects Vs. Apnea Subjects)

The LF/HF was investigated without the outlier apnea subject (PW); the t-test showed the sample mean to be significantly different ($p < 0.002$) in normal subjects compared to the sleep apnea subjects (Table: 5.2).

We compared the wavelet output of two different sleep apnea subjects, and found that the amplitude changes in the IIBI plot were not the same (Fig: 5.8.b & 5.9.b). This could be because different persons have different disease conditions other than sleep apnea. (Fig: 5.8.a) shows the airflow with multiple apnea and (Fig 5.8.b) shows the IIBI plot of the wavelet output in (Fig: 5.8.a). The airflow (top tracing) illustrates an apnea where the respiratory efforts continue against the obstruction until the patient arouses and respiration is resumed (Fig: 5.7). The wavelet output in Fig: 5.8.b (IIBI-Plot) has an increase and decrease in amplitude corresponding to the apnea period in the airflow graph.

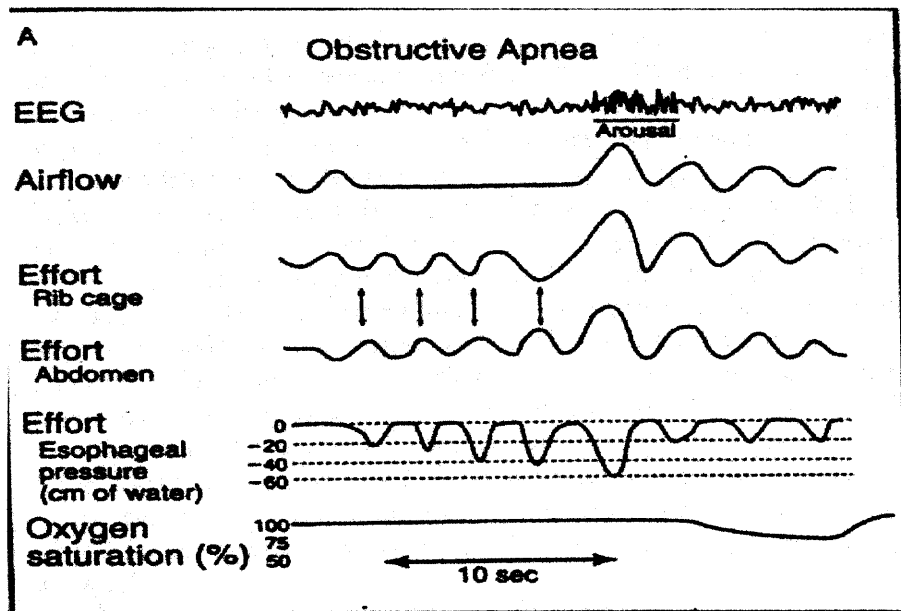


(Fig: 5.7) shows the obstructive apnea for a period of 10 Sec.

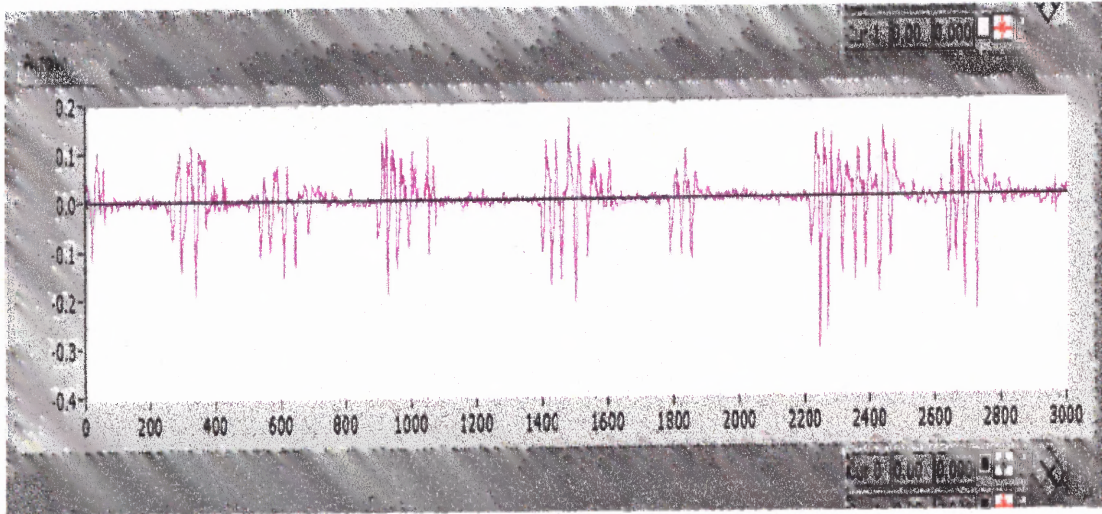


(Fig: 5.8.a) Shows airflow of Apnea subject (HL).

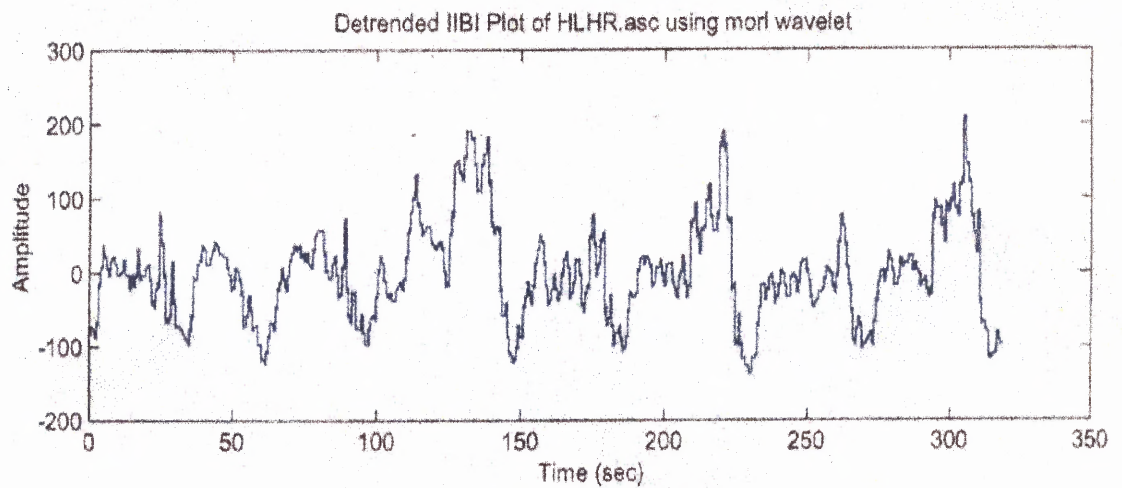


(Fig: 5.8.b) Shows wavelet output of Apnea subject (HL) in (Fig: 5.8.a).

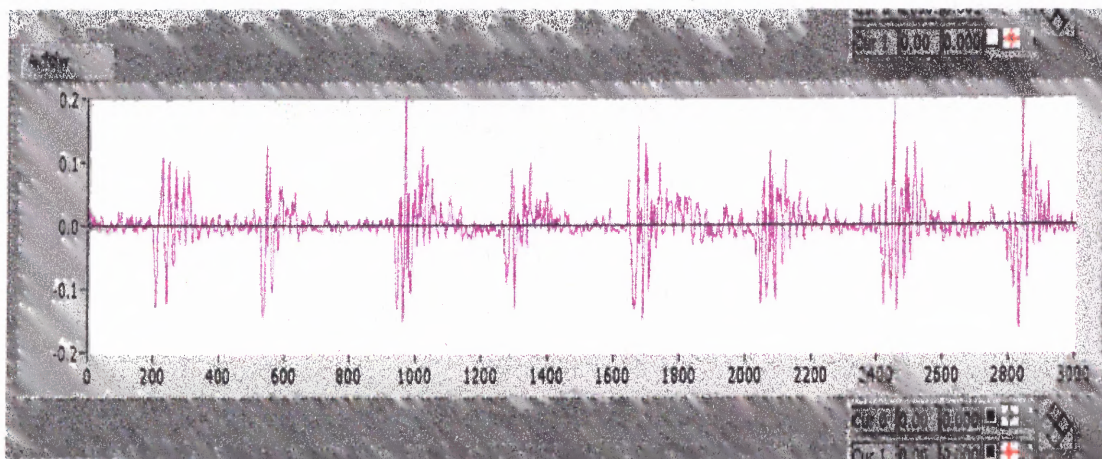


(Fig: 5.9.a) Shows airflow of apnea subject (SE).

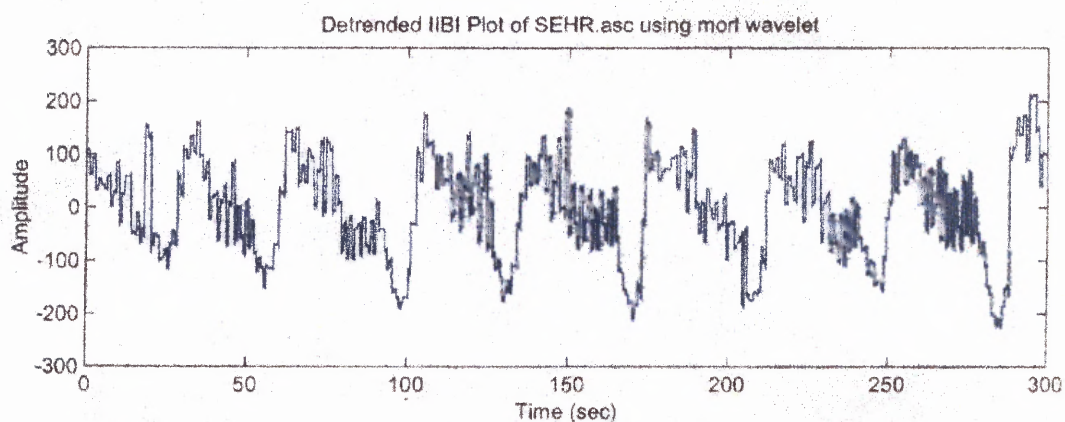


(Fig: 5.9.b) Shows wavelet output of apnea subject (SE) in (Fig: 5.9.a).

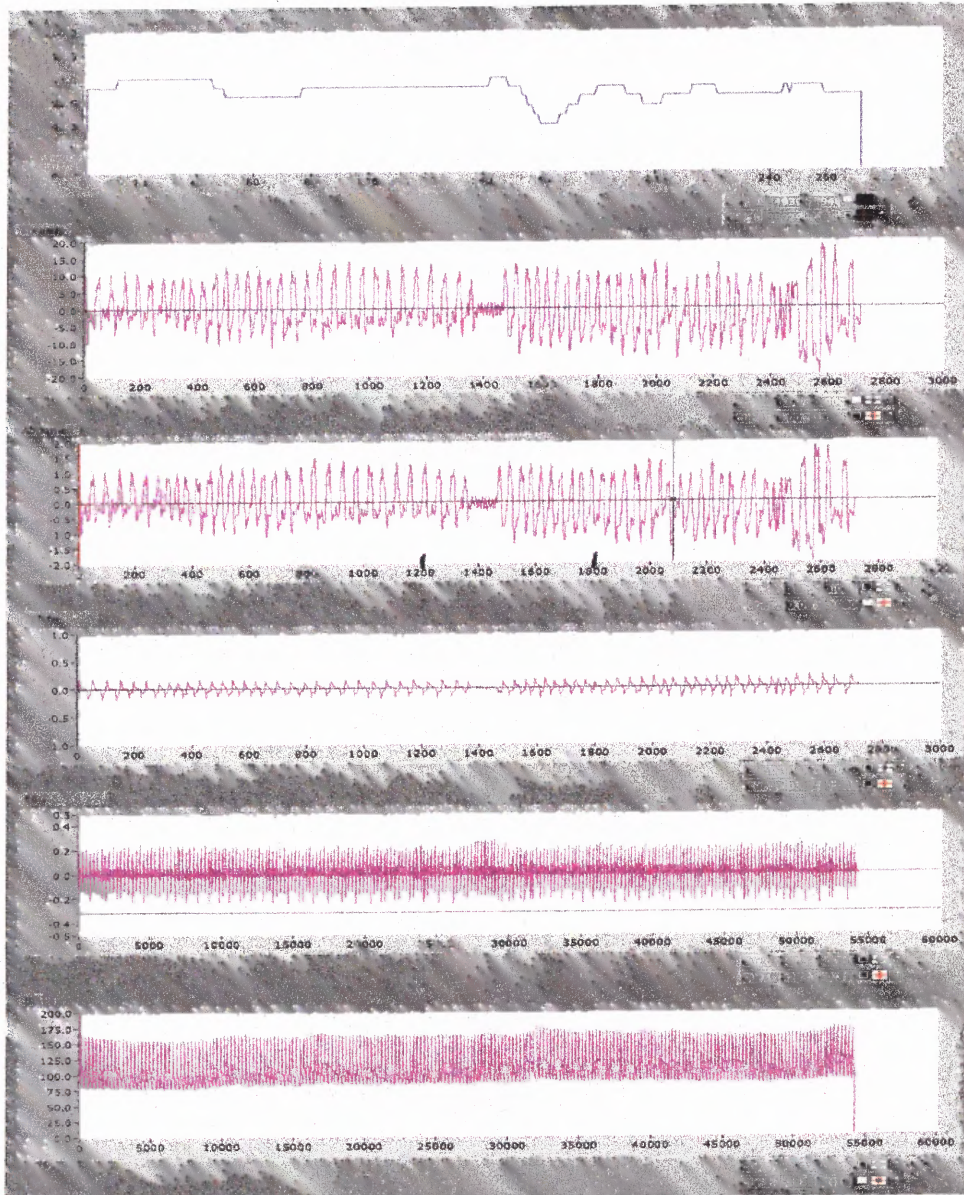
The data contained many spikes/glitches (increase and decrease in waveform amplitude) [32], partially due to repetitive apneas and accompanied by respiratory flow. In this example (Fig: 5.8.b), the apnea is characterized by slow rise in the heart rate followed by a rapid decrease. (Fig: 5.9.b) shows another typical pattern for a different subject in the heart signal during the onset of apnea. Unlike (Fig: 5.8.b), the episodes of apnea in this signal are characterized by a rapid increase in the heart rate followed by a slow decline. When comparing our results with previous studies, we confirmed that the

heart rate variation differs from person to person as every person has different physiological phenomena [32].

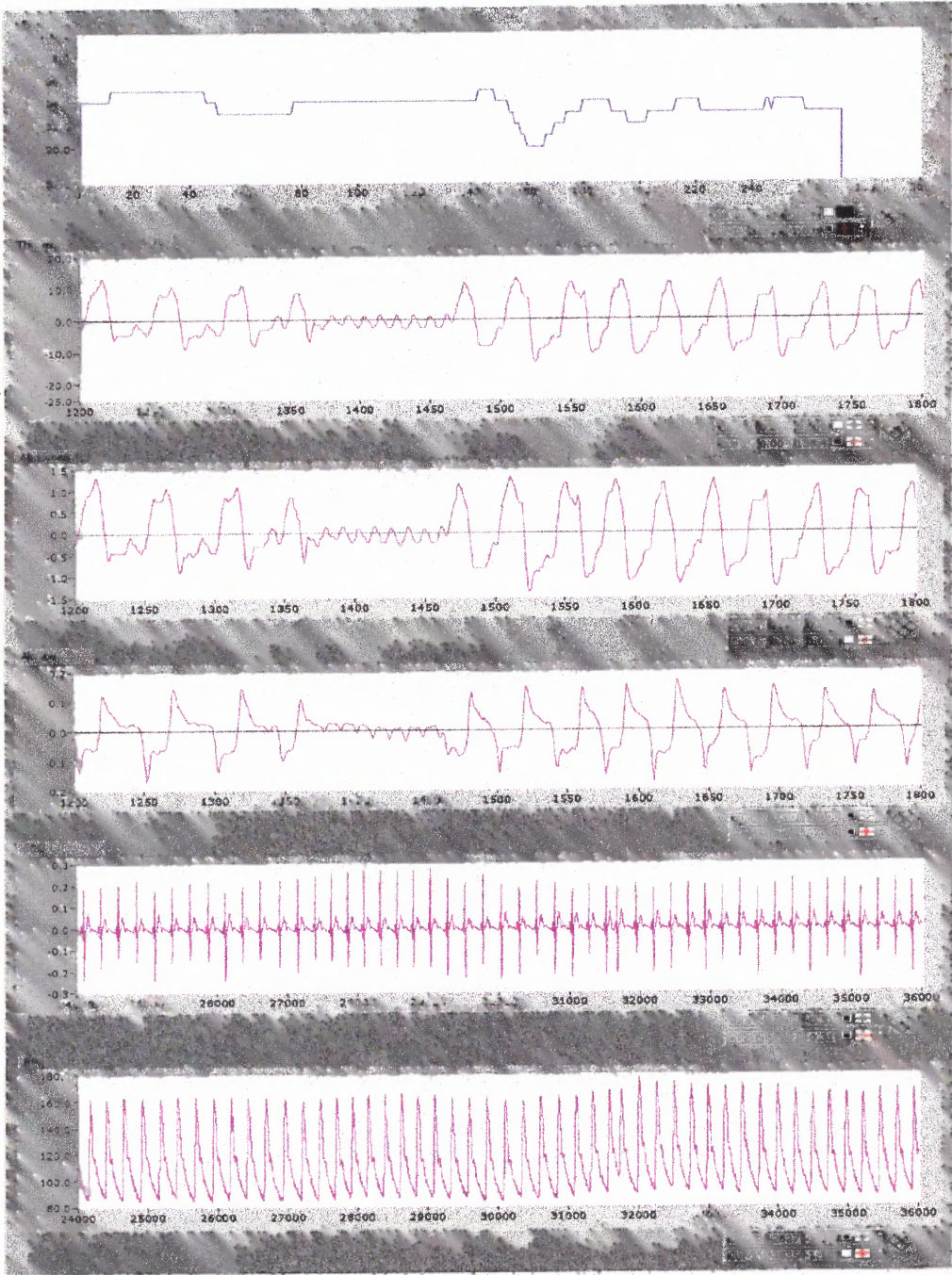
When we compared two different subjects (Fig: 5.8.a & Fig: 5.9.a), both had multiple apneas, but their IIBI plot trends were not the same. Since each subject had multiple apneas, we were unable to identify which apnea effect made an increase and decrease in amplitude in the IIBI plot. Therefore we decided to look at a person who had a normal pattern of sleep with a single apnea over a 5-minute duration. We did not have such data from the sleep apnea data set, so we did the data acquisition in our research lab. In this study six normal subjects were chosen in the age group of 25 ± 3 years. After the data acquisition we did the data analysis and found that all the normal subjects also had an apnea [23]. Such a case is shown in (Fig: 5.10) and (Appendix C).

Fig: 5.10 has six channels; the first channel represents the oxygen saturation (SaO_2), the second channel represents the thoracic movement, the third channel represents the abdominal movement, the fourth channel represents the airflow, the fifth channel represents the electrocardiogram (ECG) and the sixth channel represents the blood pressure (BP). In the graph (Fig: 5.10) we first observed a large oscillation in the oxygen saturation and a single central apnea (no chest or abdominal wall expansion during apnea) for a period of 10 seconds. (Fig: 5.11) shows an expanded version of (Fig: 5.10) in the vicinity of the apnea (135 to 145 seconds) that results from the obstruction period of respiration. During a central apnea there is little to no chest or abdominal wall expansion; therefore no negative intrathoracic pressure developed during the apnea [1]. In addition we observed that the inspiratory efforts against an occluded upper airway produce large negative intrathoracic pressure swings, which is known to cause vagal

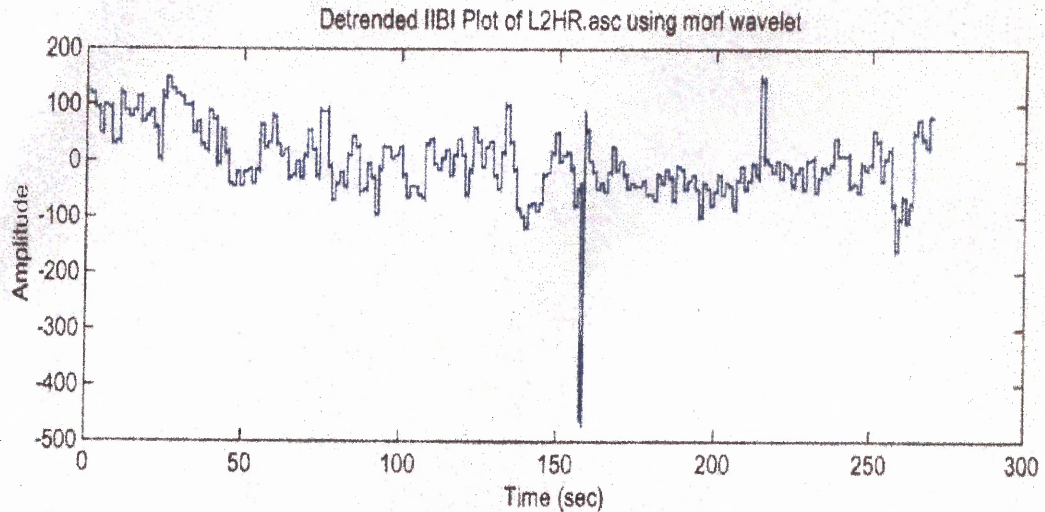
activation. This is illustrated in the fifth channel (ECG) of (Fig: 5.11), where a lengthening of R-R intervals in the ECG trace is witnessed during the apnea [1]. The arousal at the termination of an apnea initiates a burst of sympathetic activity and the transient sympathetic increases have been demonstrated by blood pressure and heart rate (shown in Fig: 5.11 in the fifth and sixth channel (31000 to 32000 seconds)).



(Fig: 5.10) Normal subject (L2) with a single central apnea over 5-minute duration.

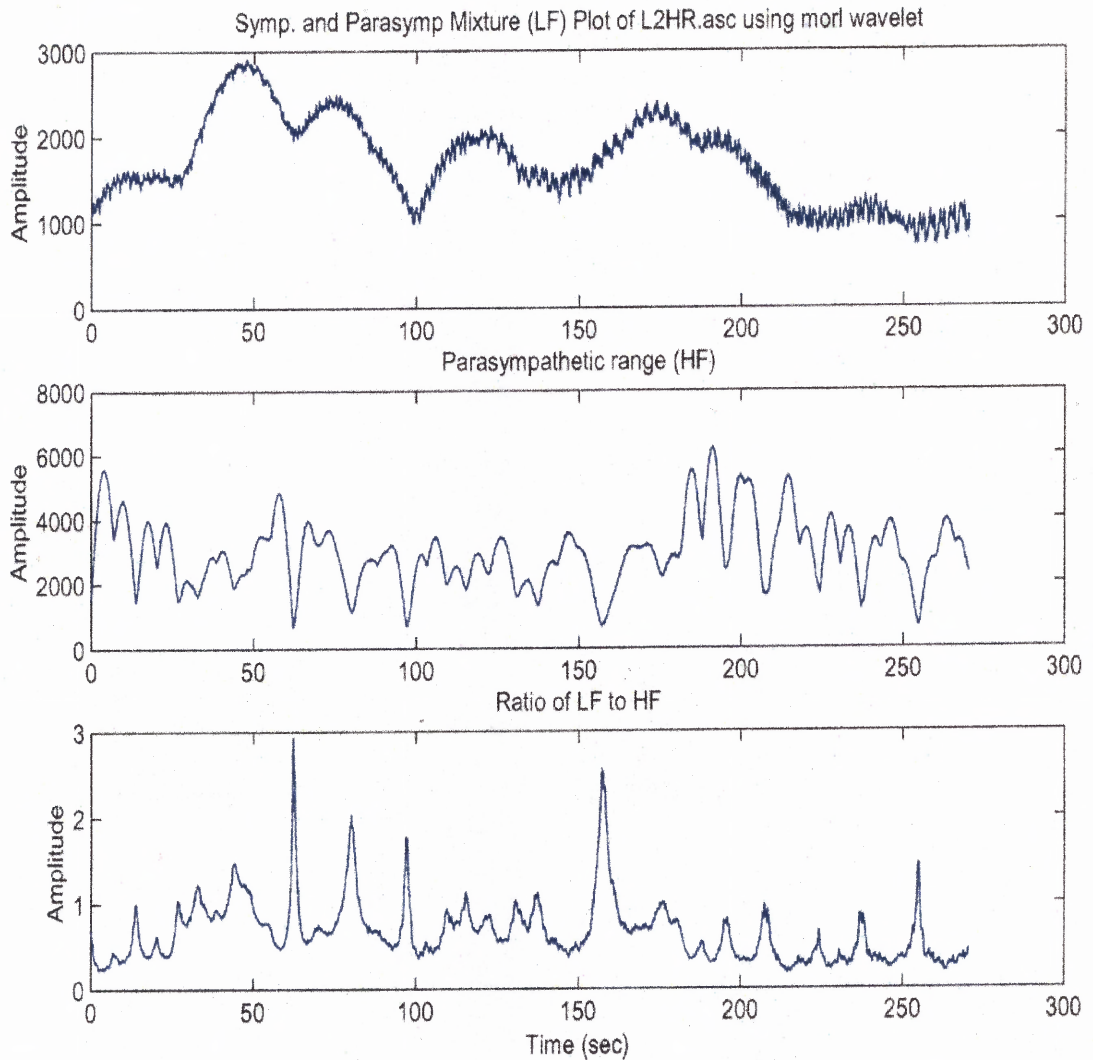


(Fig: 5.11) is an expanded version of (Fig: 5.10) in the vicinity of the apnea (L2) (135 – 145 Seconds).



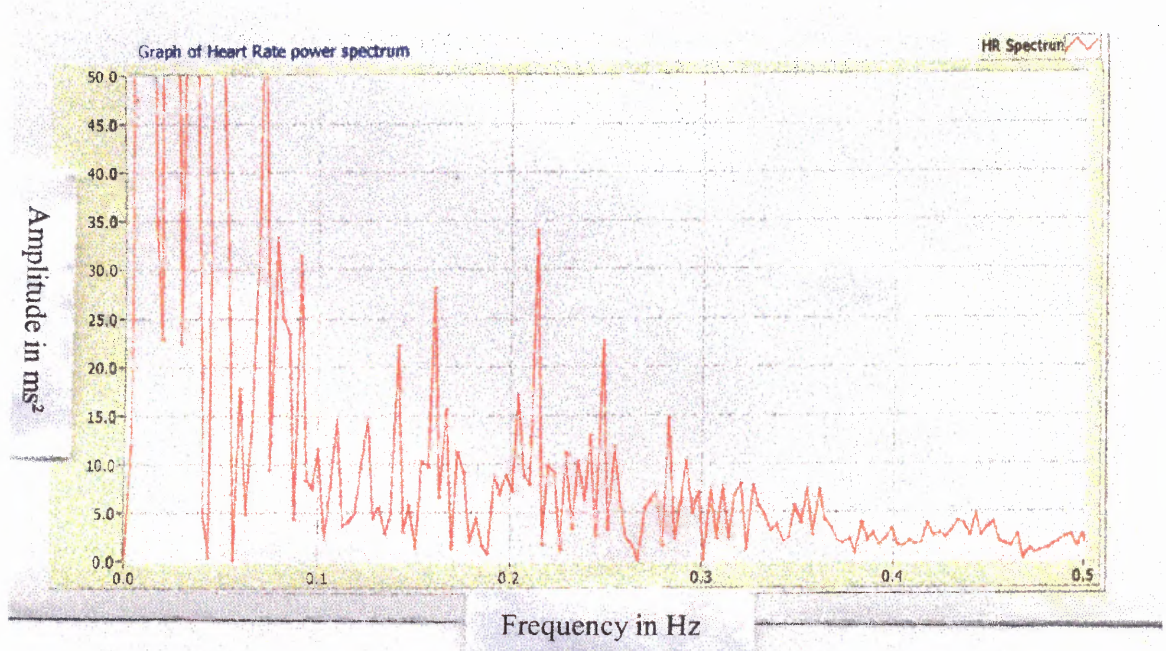
(Fig: 5.12) shows the IIBI Plot of (Fig: 5.11) normal subject (L2) with single apnea over five minute duration.

Fig: 5.12 shows the IIBI plot of Fig: 5.11. The IIBI trend in (Fig: 5.12) shows a sudden increase in HR (after 150 sec) at the end of the apnea to terminate the apnea and resume the normal breathing. In the wavelet output, (Fig: 5.13) there is not much change in the LF/HF ratio during the apnea period compared to the rest of the interval. To get this kind of subject (one apnea over five minutes) is very difficult and this doesn't fulfill the criteria of a sleep apnea subject [1].



(Fig: 5.13) shows the wavelet output of normal subject (L2) with single apnea in 5 min duration in (Fig: 5.11).

Drinnan [28] reported that patients with sleep apnea have significant regular dips in the R-R interval plot, which are not present in the normal subject. Also, Drinnan [28] studies shows that patients with sleep apnea tended to have a spectral peak lying between 0.01 and 0.05 cycles / beat, with the width of the peak indicating variability in the recurrence rate of the apnea, which are not present in the normal subject. When comparing our results of a sleep apnea subject with a normal subject, all the apnea (Appendix D) subjects had spectral peak at 0.01 and 0.05 Hz. [see (Fig: 5.14)], which is not present in the normal subject (Fig: 5.15).



(Fig: 5.14) Spectral output of a sleep apnea subject (HL).

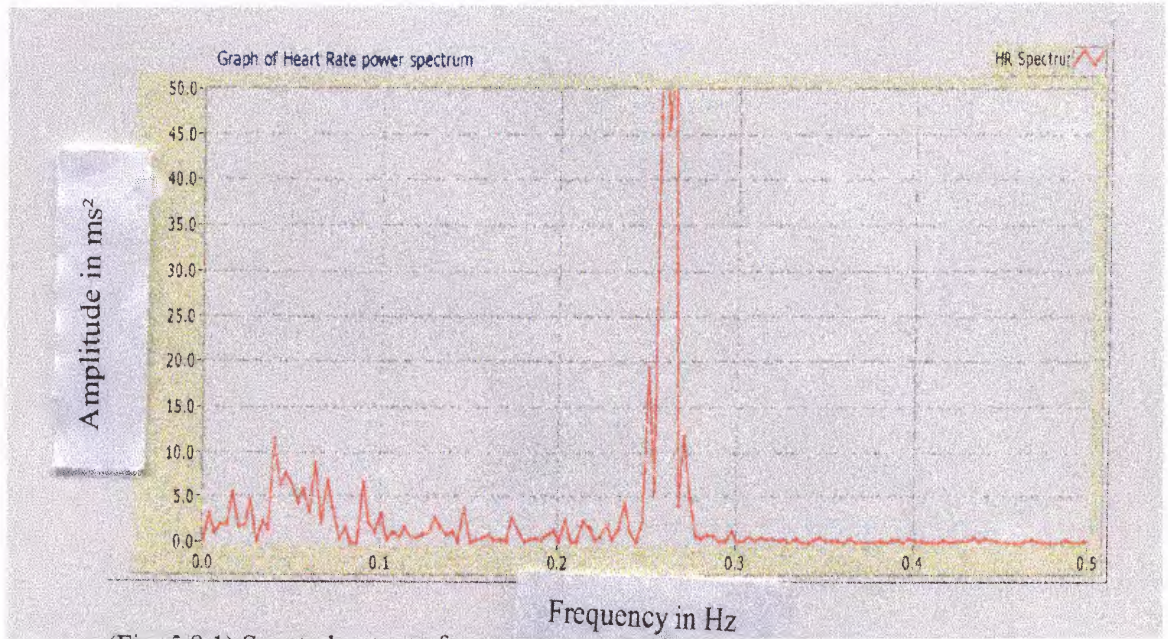


(Fig: 5.15) Spectral output of a normal subject (GN).

In our study, out of five normal subjects, one subject does not have the spectral peak, but rest of the normal subjects had spectral peaks at 0.01 and 0.05 Hz. which can be seen in (Fig: 5.16 and 5.17). This may be because the normal subject had different diseases other than sleep apnea. For the purpose of comparison we kept the arbitrary units of the “power” axis constant for all spectral plots. Drinnan [28], study the X-axis is represented in cycles/beat, but in our study the X-axis is represented in Hz in the spectral output graph, This might be a reason that our result differs from the result of the literature [28].

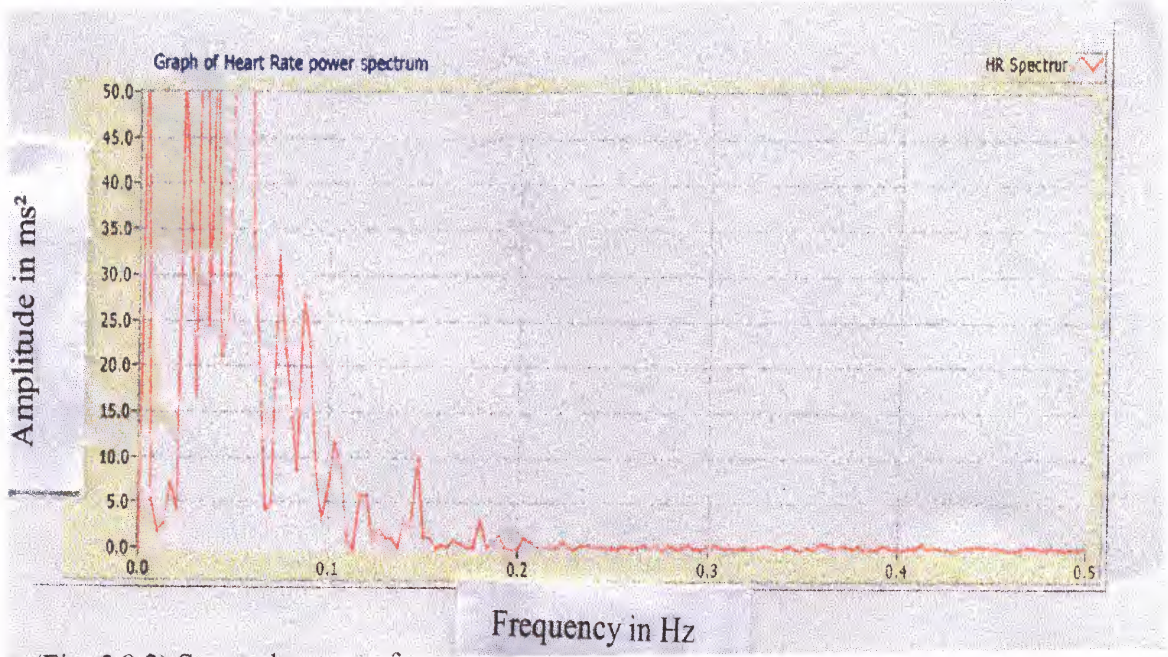


(Fig: 5.16) Spectral output of a normal subject (B).

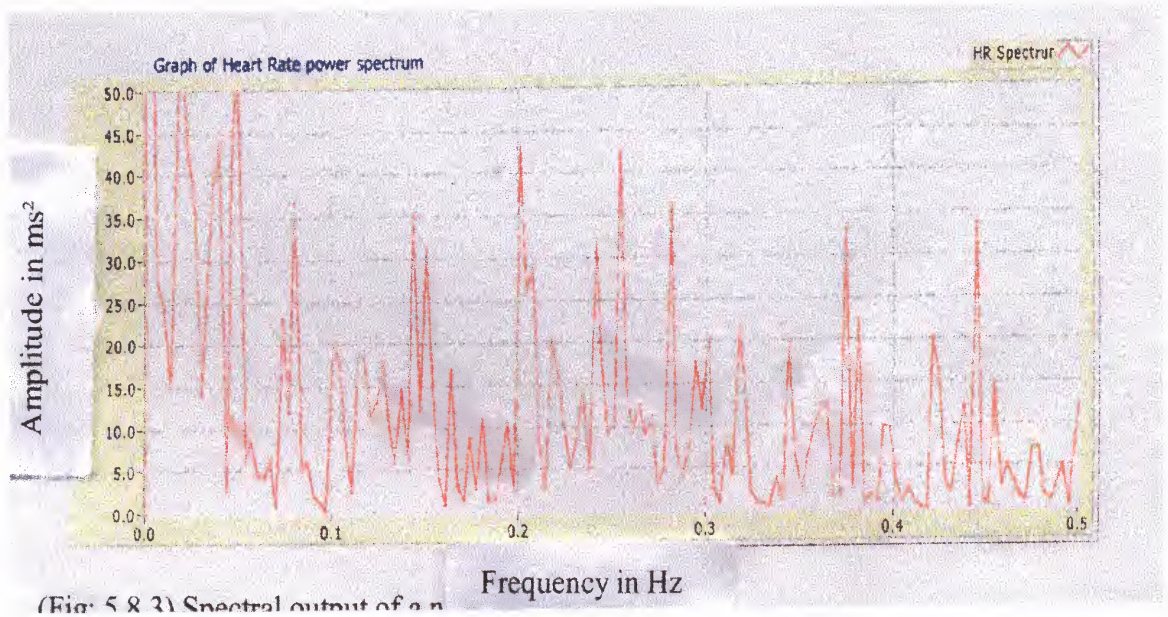


(Fig: 5.17) Spectral output of a normal subject (L).

CHAPTER 6

CONCLUSION

Due to the complexity of the patterns and variations among subjects (Fig: 5.8.a & 5.9.a), we found that the LF: HF ratio oscillated in each case (Appendix E). It is well known, for example, the sympathetic activity is increased during wakefulness and physical activity, whereas parasympathetic activity dominates during sleep [1]. There is also a clear difference in LF and HF spectral power and in their ratios during normal sleep and sleep apnea. Transient physiological phenomena, such as body movements and K-complexes during sleep, also results in altered HRV [5]. The gold standard in diagnosing sleep apnea is polysomnography, an inconvenient, expensive and time-consuming procedure [7]. Screening for SA using the ECG alone would save time, money, and discomfort. When comparing our results with previous studies on HRV during apnea, we can confirm several aspects with existing results.

When comparing two different subjects, the amplitude changes in the IIBI plot were not the same (Fig: 5.8.b & 5.9.b). This could be because different persons have different physiological phenomena other than sleep apnea. The data contained many spikes/glitches (increase/decrease in waveform amplitude), partially due to repetitive apneas and accompanied by respiratory flow. The sleep apnea (Fig: 5.8.b) is characterized a by slow rise in the heart rate followed by a rapid decrease. (Fig: 5.9.a), shows another typical pattern in the heart signal during the onset of apnea. Unlike (Fig: 5.8.b), the episodes of apnea in this signal are characterized by a rapid increase in the heart rate followed by a slow decline.

In a subject with a central apnea there is little to no chest or abdominal wall expansion; therefore no negative intrathoracic pressure developed during the apnea. In addition (Fig: 5.7 – Effort Esophageal pressure) we observed that the inspiratory efforts against an occluded upper airway produce large negative intrathoracic pressure swings because of vagal activation. The lengthening/shortening of R-R intervals in the ECG trace is witnessed during the apnea (Fig: 5.11) [1]. The termination of an apnea initiates a burst of sympathetic activity and the transient sympathetic increases have been demonstrated by blood pressure and heart rate. On the wavelet output, (Fig: 5.13) there is not much change in the LF/HF ratio during the apnea period as compared to the rest of the interval.

With reference to article [28], patients with sleep apnea tended to have a spectral peak lying between 0.01 and 0.05 cycles / beat, with the width of the spectral peak indicating variability in the recurrence rate of the apnea, which are not present in the normal subjects. This statement was not satisfied with our data, since there is no spectral peak at 0.01 and 0.05 Hz in all normal subjects. This might be because the X-axis representations were not same. We represented the X-axis in Hz, but the literature representing the X-axis in cycles/beat.

The changes in power spectral components have been described by LF, HF & LF/HF [35]. We found the LF ($p < 0.03$) spectral component is significantly decreased in normal subjects compared to the sleep apnea subjects and there is no significant difference in the HF ($p < 0.09$) component (Table: 5.2). However there is a trend toward a decrease in the HF component from the mean (N) of normal subjects to the mean (A) of sleep apnea subjects. Since there is a decrease in the HF component (not significant) and

a significant increase in the LF component. We hypothesize that there is an increase in sympathetic activity in sleep apnea subjects compared to normal subjects. The mean (A) of the HF component is lower than the mean (N) of the LF component for the apnea subjects, which is not the case in normal sleep subjects and we concluded that an autonomic dysfunction is present in patients with sleep apnea. The LF/HF investigation (student t-test) showed the sample mean to be statistically significantly lower ($p < 0.002$) in normal subjects compared to the sleep apnea subjects (Table: 5.2) [8][32]. This again shows a significant increase in the sympatho-vagal balance in apnea subjects. Studies show that either weight loss or CPAP (Continuous Positive Airway Pressure) is the best treatment and indicate a significant improvement from the sleep apnea disease in the cardiovascular point of view (To increase the ability of the heart muscle to contract and supply enough blood to the metabolic need) [6]. Considerably more research is needed to understand the effects and clinical relevance on total HRV power and its various components in health and sleep apnea disease.

Future Work

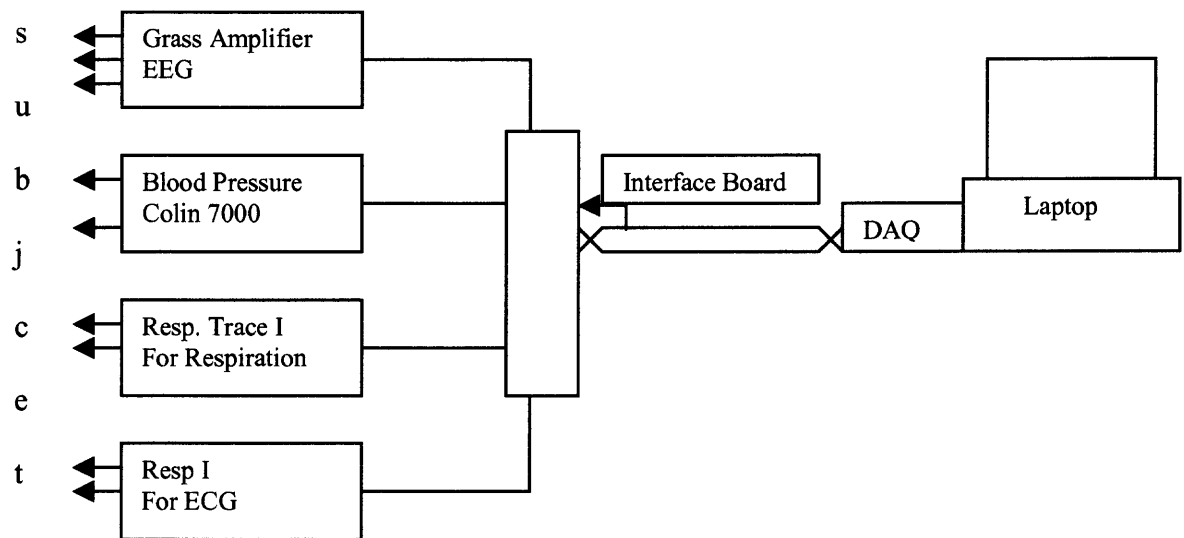
1. Future work includes an investigation of stability and specificity in the presence of other diseases known to affect the ANS as well as different sleep stages, which will help in further investigation of spectral components VLF, LF & HF.
2. Comparison of two different subject's result may not be a good idea as each person has different physiological and cardiovascular phenomena. It would be more interesting to compare the same

person's data while the subject is in normal sleep and with sleep apnea.

3. A correct detection of R peaks of the QRS complexes is believed to require a sampling rate of 500-1000 Hz [35]. The sampling rate has to be increased from the current 250 samples per second to provide finer resolution in R wave peak detection.
4. To make these studies more objective, future data collection should be done at the patient home. This could be a better solution, but its disadvantage is an increase in experiment cost. The patients may not feel comfortable in traveling to a sleep lab and hooked up with wires. The traveling itself will cause discomfort to the patient's normal sleep rather than sleep apnea. We need to find a better way of data collection with the comfort of the patient in mind.

APPENDIX A
EQUIPMENT SETUP

The diagram below shows the laboratory setup for the Sleep recording experiments at NJIT. The experienced technician setup all the leads and hock to the subject. When the subject is ready to sleep the technician will fix-up all the leads and turn off the light.



Instrument	Input	Output
Grass Amplifier	Two pair signal lead One GND lead	EEG Output to Interface Card. II channel
Resp I	Two leads connected with subject through electrode One GND lead.	Single channel ECG
Colin 7000 BP Apparatus	Blood Pressure cuff Pressure Gauge	Single channel BP
RespTrace	Chest belt/abdomen	Single channel Respiration

APPENDIX B

COMPUTER PROGRAM

Time-Frequency Analysis using Wavelet

The following program used to analysis the sleep apnea signal.

```
% d_wvlet.m

% Matlab Wavelet Toolbox 2.0.

% Modified by D. Newandee

% 7-13-2001: using time - freq spectrogram and change to run with MATLAB 6.0

% 10-23-2001: add calculation of normalized sympathovagal ratio using chosen wavelet

% This program will accept any wavelet from the Matlab Wavelet Toolbox 2.0 by
entering the wavelet

% name in '' for the 'wave' variable below.

clear all;

close all;

SIGNAL=input('Please enter name of datafile with no extension --> ','s');

filename=[SIGNAL, '.asc'];

eval(['load ' filename]);

original_rawdata=eval(SIGNAL);clear SIGNAL;

Question_1=input('Which channel do you want to analyze? [1=O2, 2=BP, 3=resp,
4=ECG] --> ','s');

if    Question_1=='1'

    rawdata=original_rawdata(1,:);

elseif Question_1=='2'
```

```

        rawdata=original_rawdata(2,:);

elseif Question_1=='3'

        rawdata=original_rawdata(3,:);

elseif Question_1=='4'

        rawdata=original_rawdata(4,:);

end

sf=input('Please enter the sampling rate of the data --> ');

sf=sf/10;           % upsampling (to get correct recording time)

%T=input('Please enter the window size in seconds --> '); % normally 10 (sec) is best

T=10.0;

nfft=input('Please enter the fft size (128, 256,512 etc.) --> '); % must be larger than

window size and in  $^{2}$ 

wave = input('Please enter name of wavelet used --> ','s');

x = decimate(rawdata,10); % decimate data array

N = length(x);           % number of samples

%*sf = 1000;           % sampling frequency

%*N = 500;           % number of samples

%%T = 1/500;           % window size in seconds (1/500 = 0.02 sec)

ws = T*sf;           % window size in samples

%*nfft = 256;           % fft size in specgram command. Must be larger than window

size in samples

%*wave = 'mexh';           % the wavelet to use (see wavelets table in Matlab Wavelet

Tool Box v 2.0

```

```

%
t = ( (1:(N)) ) * (1/sf); % times
f = ( (0:(N-1))/N ) * sf; % frequencies
index = 1:N;

% first construct the time domain and frequency domain plots
fx = abs(fft(x));

% spectrum1D.m
% function [Pyy,f]=rspec(x,Fs)
    fftsize=length(x);
% put alternative fft method here
    x=x-mean(x);
    fftx=fft(x,fftsize);
    Pyy=fftx.*conj(fftx)/fftsize;
%    f=sf*(0:(fftsize/2-1))/fftsize;
    f=sf*(0:(fftsize-1))/fftsize;

    clear fftx

    p=Pyy;

figure;
subplot(2,1,1)

    plot(t,x);

% axis([0 20 -2 5]);

    grid on;

    xlabel('Time (sec)');

```

```
ylabel('Amplitude');

title(['Raw data in time domain of ',eval('filename')]);

subplot(2,1,2);

% plot(f(400:800),p(400:800)/max(p),'r');

    plot(f(1:200),p(1:200)/max(p),'r');

axis([0 1 0 1]);

grid on;

xlabel('Frequency (Hz)');

    ylabel('Power');

    title(['Power Spectrum of ',eval('filename')]);

%subplot(3,1,3);

% plot(f(index)/10,fx(index));

% grid on;

% axis([0 2 -2 5]);

% xlabel('frequency');

% title('frequency domain');

%*orient landscape;

print -dps wvleta.eps

% construct a spectrogram with window size, ws

[B,frequencies,times] = specgram(x, nfft, sf, ws);

% plot the spectrogram

figure;

    imagesc(times, frequencies, abs(B));
```



```

axis('xy');

xlabel('Time (sec)');

ylabel('Frequency (Hz)');

title(['Spectrogram with T = ' num2str(1000*T) ' ms']);

%*orient landscape;

print -dps wvletb.eps

% make a 3D plot for better viewing

figure;

mesh(times, frequencies, abs(B));

xlabel('Time (sec)');

ylabel('Frequency (Hz)');

title(['3D Spectrogram with T = ' num2str(1000*T) ' ms']);

view(-60,30);

%*orient landscape;

print -dps wvletc.eps;

% now work out the scales at which to compute the CWT

% There is a connection between scale and frequency as follows

factor = 5/(2*pi);

% range of interested frequency

%freq = [100:100:2000]; % EMG: 100 - 2000 Hz

%freq = [1:10:100]; % EEG: 1 - 100 Hz

freq = [0.01:0.01:2.0]; % HRV: 0.01 - 2 Hz

scale = factor * sf ./ freq;

```

```

% make sure the string wave is set before executing the m-file

% compute the CWT and plot at the same time

figure;

    coef=cwt(x, scale, wave, 'plot');

    title('scalogram - Scale vs. Time');

%* orient landscape;

%% print -dps wvletd.eps;

% Extract LF and HF

[row,col]=size(rawdata');

I=1:row;

I=I(:);

A=(I/sf)/60;           % Time axis in minutes

m=512;                 % The size of the fft we will be computing.

skip=25;               % Number of points we skip to get the next segment.

k=fix((row-m)/skip);  % the number of spectra we compute

TFDs=abs(coef);

[r,C]=size(TFDs);

for i=1:C,

    W=TFDs(:,i);

    Y=(1:r)';

    M=W.*Y;

```

```

S=sum(M);

F=sum(W);

E(i)=S/F;

end

%LFC = input('Please enter the low frequency range in index numbers. ');

LFC=1:4;

symvag=sum(TFDs(LFC,1:k));

%HFC=input('Please enter the high frequency range in index numbers. ');

HFC=4:20;

vagal=sum(TFDs(HFC,1:k));

symtopar=symvag./vagal;

% Normalize

n_symvag=symvag./(symvag+vagal);

n_vagal=vagal./(symvag+vagal);

n_symtopar=n_symvag./n_vagal;

% Plotting commands

%J=[12.8+(1:k)*1.25]/60;

J=(length(x)/sf)/(k)*(0:k-1);

% Make a "spectrogram" type plot

figure;

    imagesc(t, freq, coef);

    colormap('hsv');

    colorbar('vert');

```

```
axis('xy');          % flip the vertical axis over

xlabel('Time (sec)');

ylabel('Frequency (Hz)');

title('Scalogram - Frequency vs. Time');

%* orient landscape;

print -dps wvlete.eps;

% make a 3D plot for better viewing, rotate by 45 degrees

figure;

subplot(2,1,1), mesh(t, freq, abs(coef));

%* [az,el]=view;

%*view(az+45,el);

%* view(az,el);

% axis([0 300 0 0.5 0 3]);

% view([55,15]);

% grid on;

colormap('jet');

colorbar('vert');

brighten(0.5);

shading interp;

xlabel('Time (sec)');

ylabel('Frequency (Hz)');

title(['3D scalogram of ',eval('filename'),' using ',eval('wave'),' wavelet']);
```

```
%* orient landscape;

%* print -dps wvletf.eps;

    subplot(2,1,2), contour(t, freq, abs(coef),20);

%% axis([0 300 0 .6]);

    grid on;

    xlabel('Time (sec)');

    ylabel('Frequency (Hz)');

    title(['Contour of ',eval('filename'),' using ',eval('wave'),' wavelet']);

% print -dps wvletf.eps;

figure;

subplot(2,1,1);

%plot(A,x);

plot(t,x);

title(['Detrended IIBI Plot of ',eval('filename'),' using ',eval('wave'),' wavelet']);

xlabel('Time (sec)');

ylabel('Amplitude');

subplot(2,1,2);

plot(t,E);

%plot(A,E);

%%axis([0 300 0 150]);

xlabel('Time (sec)');

ylabel('Frequency (Hz)');

title(['Instantaneous frequency Plot of ',eval('filename')]);
```

```
figure;

subplot(3,1,1);

plot(J,symvag);

%plot(A,symvag);

%gtext(top);

title(['Symp. and Parasymp Mixture (LF) Plot of ',eval('filename'),' using ',eval('wave'),'
wavelet']);

%xlabel('time (sec)');

ylabel('Amplitude');

subplot(3,1,2);

plot(J,vagal);

%plot(A,vagal);

title('Parasympathetic range (HF)');

%xlabel('time (sec)');

ylabel('Amplitude');

subplot(3,1,3)

plot(J,symtopar);

%plot(A,symtopar);

%gtext(top);

title('Ratio of LF to HF')

xlabel('Time (sec)');
```

```

ylabel('Amplitude');

%order=input('Please enter the order of the lowpass filter. ');

%freq=input('Please enter the cutoff frequency for LPF. ');

%sample=input('Please enter the sample rate of the data. ');

%order=12;

%freq=0.03;

%nfreq=freq/sf;

%[poles,zeros]=butter(order,nfreq);

%dtnd_nsymvag=filtfilt(poles,zeros,n_symvag);

%dtnd_nvagal=filtfilt(poles,zeros,n_vagal);

%dtnd_nsymtopar=filtfilt(poles,zeros,n_symtopar);

figure

subplot(3,1,1);

plot(J,n_symvag);

%plot(A,n_symvag);

%gtext(top);

title(['Normalized Symp and Parasymp Mixture (NLH) Plot of ',eval('filename'),' using
',eval('wave'),' wavelet']);

%xlabel('time (sec)');

ylabel('Amplitude');

subplot(3,1,2);

plot(J,n_vagal);

%plot(A,n_vagal);

```

```
title('Normalized Parasympathetic range (NHF)');  
  
%xlabel('time (sec)');  
  
ylabel('Amplitude');  
  
%figure  
  
subplot(313)  
  
plot(J,n_sympar);  
  
%plot(A,sympar);  
  
%gtext(top);  
  
title('Ratio of NLF to NHF')  
  
xlabel('Time (sec)');  
  
ylabel('Amplitude');  
  
figure;  
  
subplot(3,1,1);  
  
plot(J,symvag);  
  
%plot(A,symvag);  
  
%gtext(top);  
  
title(['Symp. and Parasymp Mixture (LF) Plot of ',eval('filename'),' using ',eval('wave'),'  
wavelet']);  
  
%xlabel('time (sec)');  
  
ylabel('Amplitude');  
  
  
subplot(3,1,2);  
  
plot(J,vagal);
```



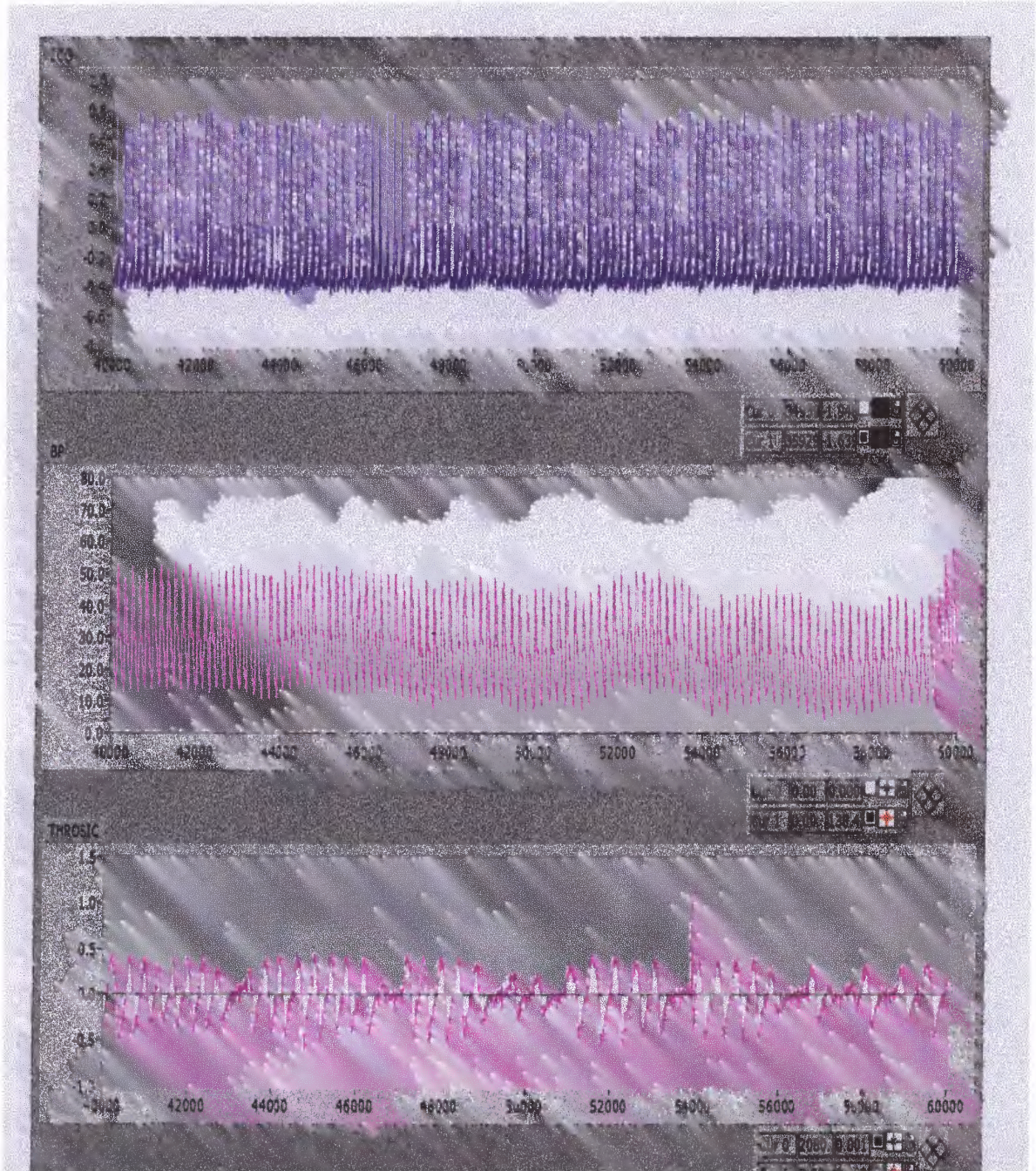
```
%plot(A,vagal);  
  
title('Parasympathetic range (HF));  
  
%xlabel('time (sec));  
  
ylabel('Amplitude');  
  
subplot(3,1,3)  
  
plot(J,symtopar);  
  
%plot(A,symtopar);  
  
%gtext(top);  
  
title('Ratio of LF to HF')  
  
xlabel('Time (sec));  
  
ylabel('Amplitude');  
  
%order=input('Please enter the order of the lowpass filter. ');  
  
%freq=input('Please enter the cutoff frequency for LPF. ');  
  
%sample=input('Please enter the sample rate of the data. ');  
  
%order=12;  
  
%freq=0.03;  
  
%nfreq=freq/sf;  
  
%[poles,zeros]=butter(order,nfreq);  
  
%dtrnd_nsymvag=filtfilt(poles,zeros,n_symvag);  
  
%dtrnd_nvagal=filtfilt(poles,zeros,n_vagal);  
  
%dtrnd_nsymtopar=filtfilt(poles,zeros,n_symtopar);  
  
figure  
  
subplot(3,1,1);
```

```
plot(J,n_symvag);  
  
%plot(A,n_symvag);  
  
%gtext(top);  
  
title(['Normalized Symp and Parasymp Mixture (NLH) Plot of ',eval('filename'),' using  
'eval('wave'),' wavelet']);  
  
%xlabel('time (sec)');  
  
ylabel('Amplitude');  
  
subplot(3,1,2);  
  
plot(J,n_vagal);  
  
%plot(A,n_vagal);  
  
title('Normalized Parasympathetic range (NHF)');  
  
%xlabel('time (sec)');  
  
ylabel('Amplitude');  
  
%figure  
  
subplot(3,1,3);  
  
plot(J,n_sympar);  
  
%plot(A,sympar);  
  
%gtext(top);  
  
title('Ratio of NLF to NHF')  
  
xlabel('Time (sec)');  
  
ylabel('Amplitude');
```

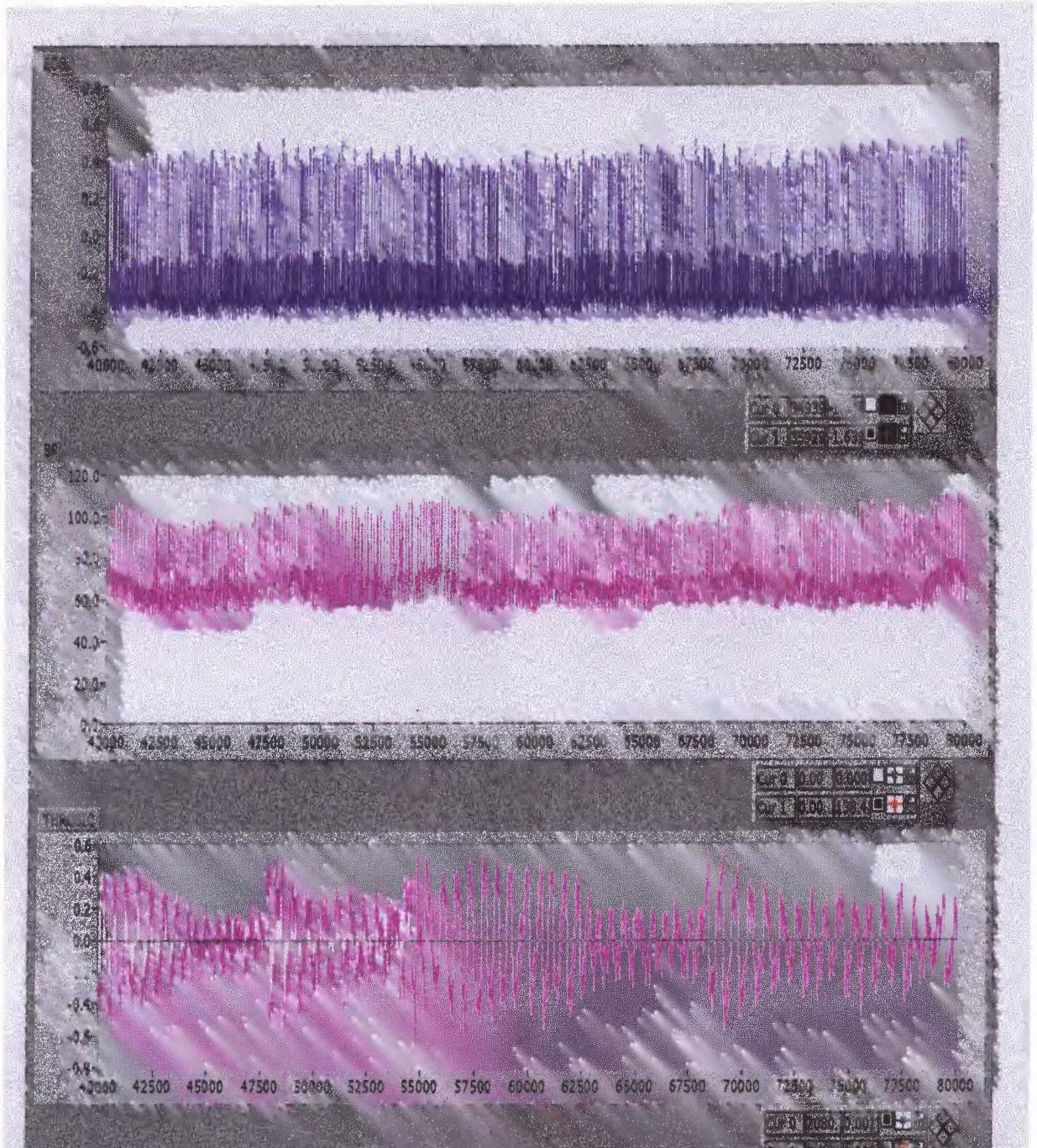
APPENDIX C

Examples of Control subjects having apnea.

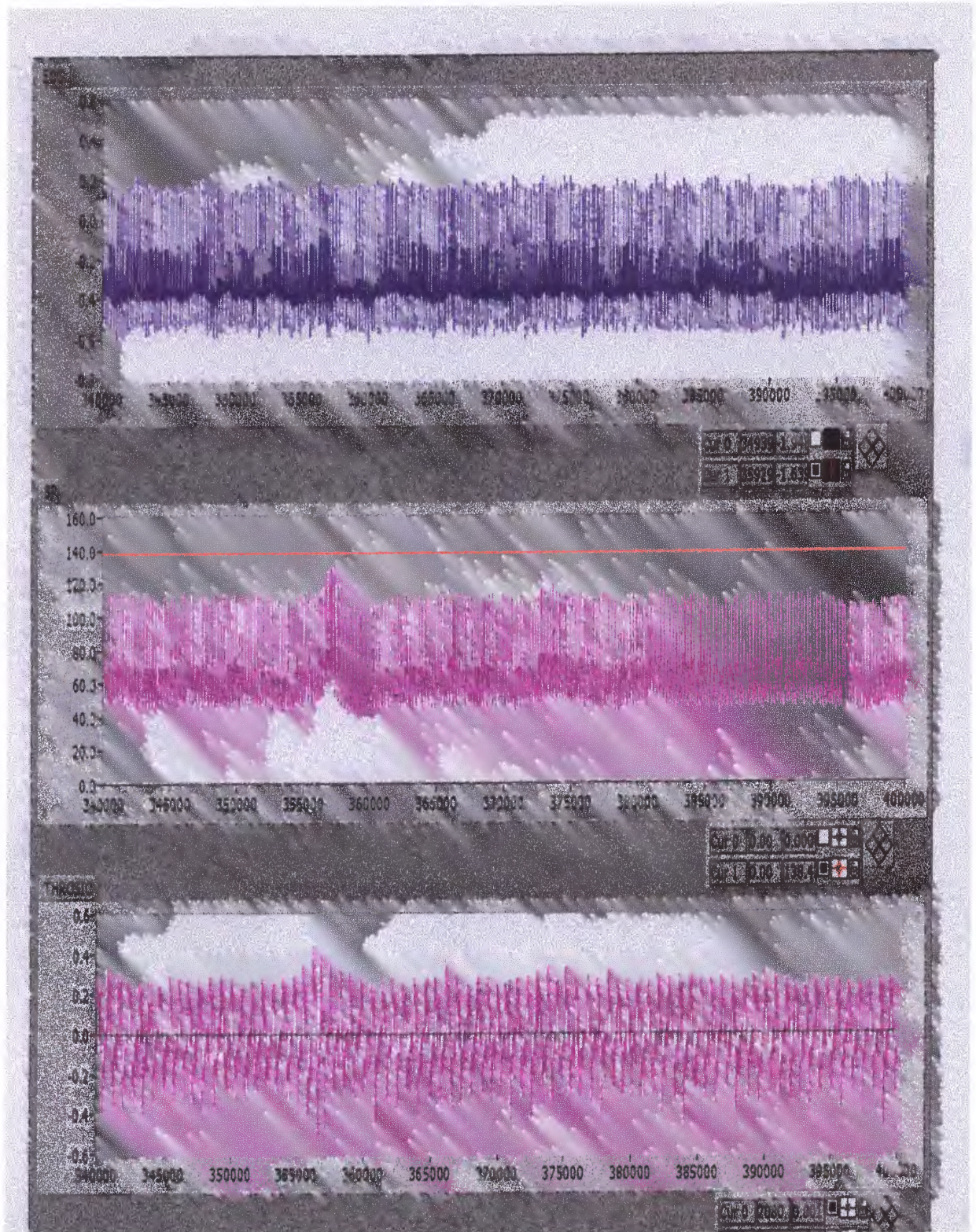
Subject: SS



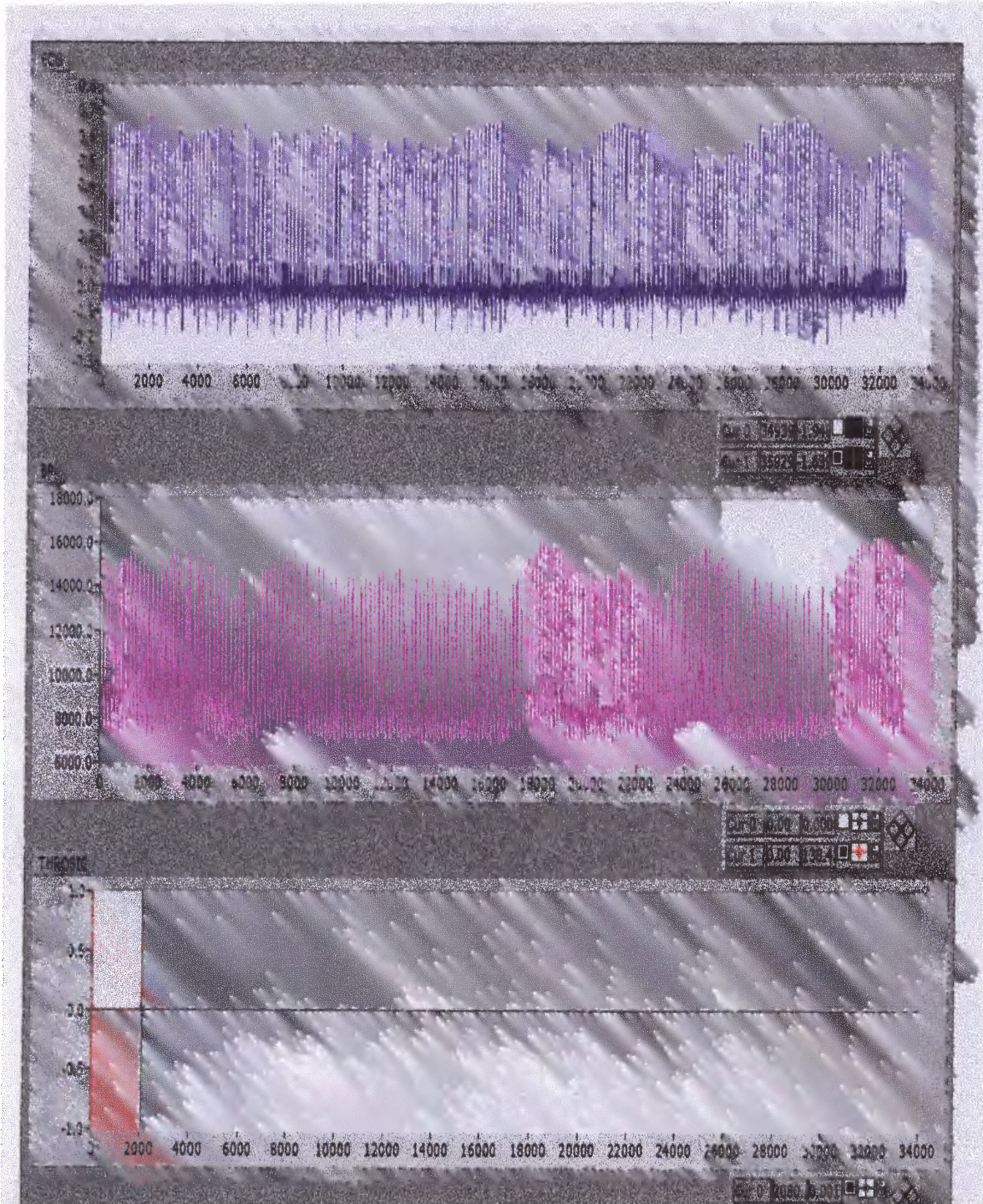
Subject: BP2



Subject: GN6



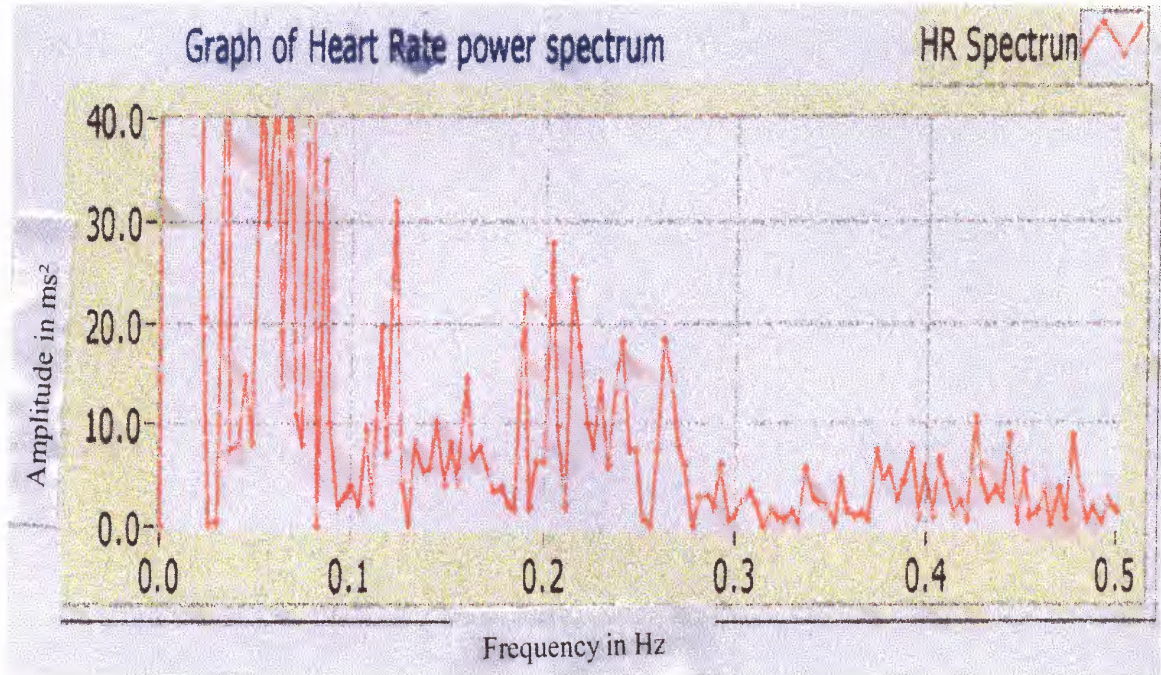
Subject: B2



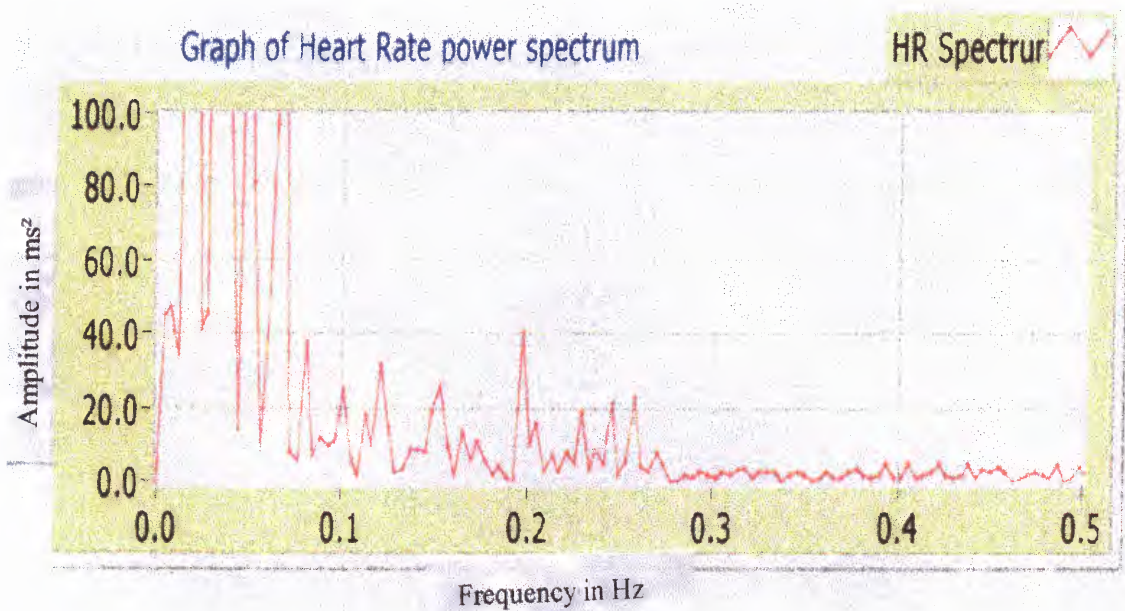
APPENDIX D

Example of Sleep Apnea Subject having spectral peak at 0.01 to 0.05 Hz.

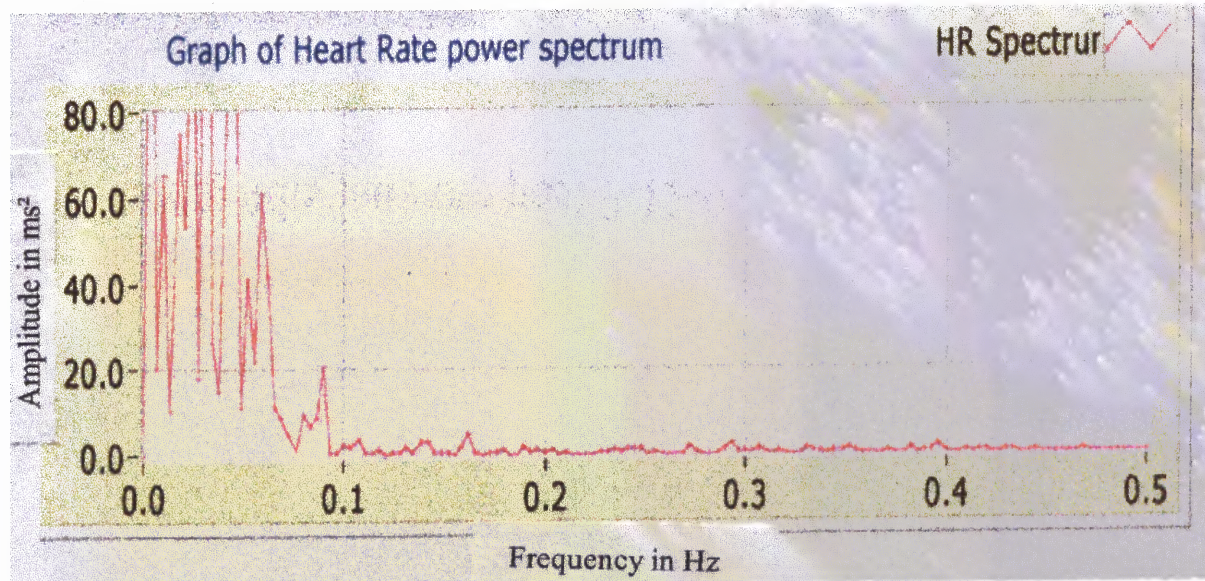
Subject: 1



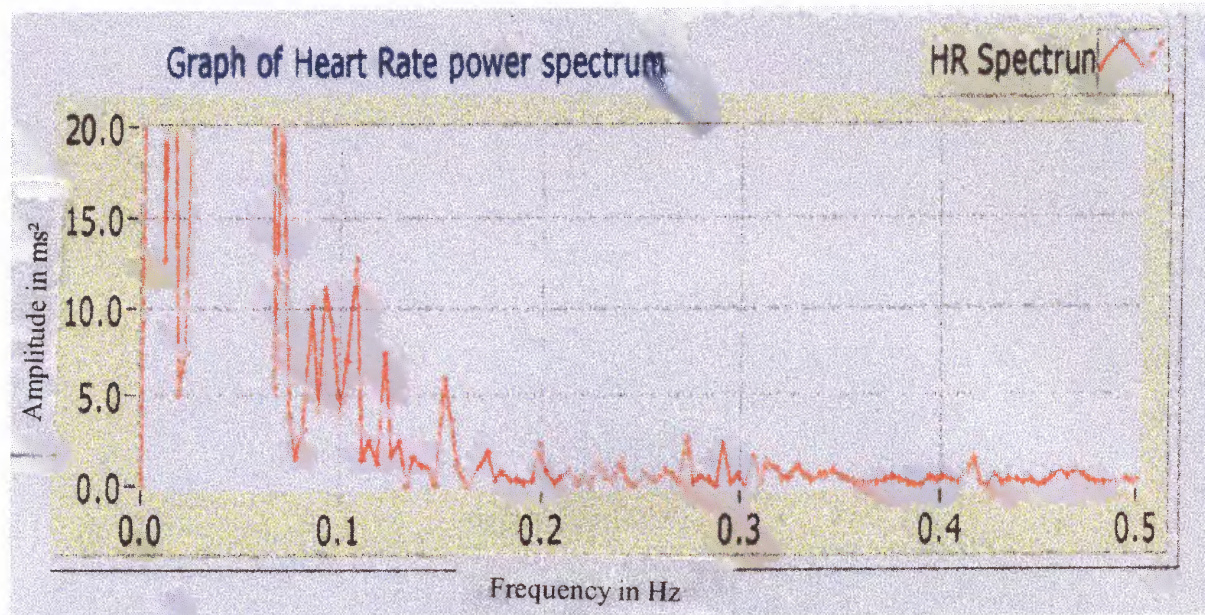
Subject: 2



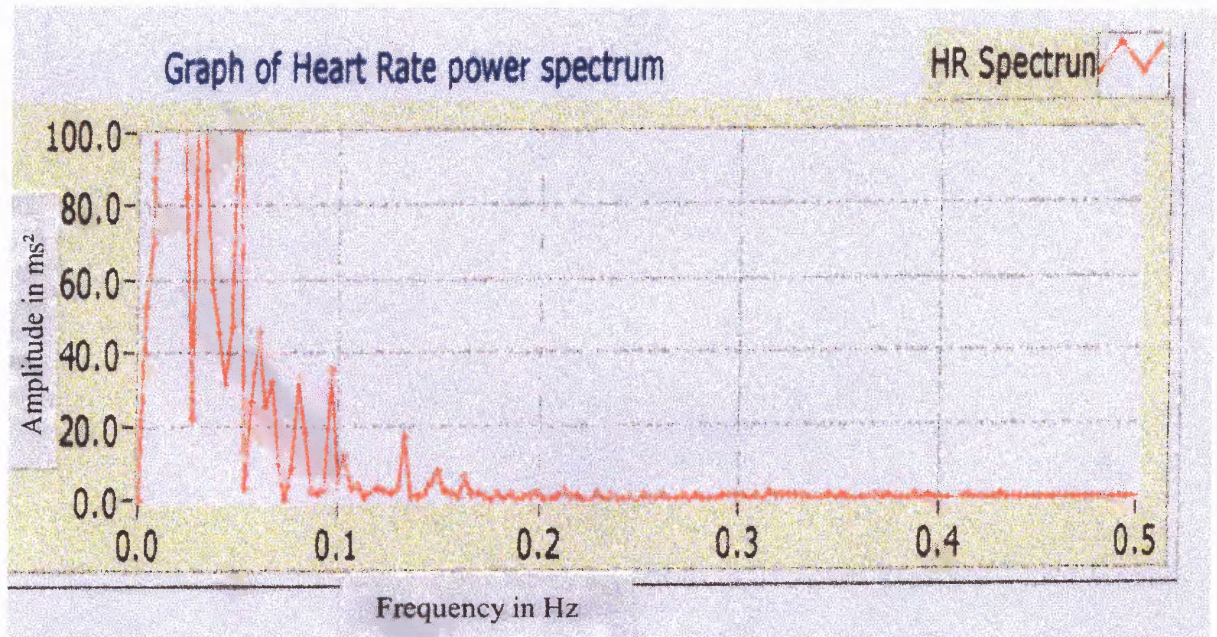
Subject: SF



Subject: KT1



Subject: KT2



APPENDIX E

t-test for normal and apnea subjects (with outlier - PW)

	Normal	Apnea	Normal	Apnea	Normal	Apnea
Name	LF	LF	HF	HF	LF/HF	LF/HF
AA		447.86		46.6		9.6
KT1		263.08		19.93		13.2
KT2		449.12		51		8.8
SIL		1310.91		347.85		3.8
LY		386.38		108.54		3.6
PW		4045.19		4727.99		0.9
SF		271.74		47.1		5.8
LE	126.91		130		0.98	
LES	343.53		151.8		2.263	
SEK	110.67		23.39		4.731	
GAN	262.57		460.9		0.569	
BV	81.98		259.64		0.315	
BP4	153.59		261.29		0.581	

t-Test: Two-Sample Assuming Unequal Variances

LF

	<i>Normal</i>	<i>Apnea</i>
Mean	179.875	1024.8971
Variance	10298.07551	1903963.1
Observations	6	7
Hypothesized Mean Difference	0	
df	6	
t Stat	-1.615183626	
P(T<=t) one-tail	0.078699071	
t Critical one-tail	1.943180905	
P(T<=t) two-tail	0.157398141	
t Critical two-tail	2.446913641	

HF

	<i>Normal</i>	<i>Apnea</i>
Mean	214.5033333	764.14429
Variance	22506.89115	3067773.8
Observations	6	7
Hypothesized Mean Difference	0	
df	6	
t Stat	-0.82673384	
P(T<=t) one-tail	0.22000993	
t Critical one-tail	1.943180905	
P(T<=t) two-tail	0.440019861	
t Critical two-tail	2.446913641	

t-Test: Two-Sample Assuming Unequal Variances**LF/HF**

	<i>Normal</i>	<i>Apnea</i>
Mean	1.573166667	6.5285714
Variance	2.875071367	17.889048
Observations	6	7
Hypothesized Mean Difference	0	
df	8	
t Stat	-2.844573683	
P(T<=t) one-tail	0.010829524	
t Critical one-tail	1.85954832	
P(T<=t) two-tail	0.021659048	
t Critical two-tail	2.306005626	

t-test for normal and apnea subjects (with outlier - PW)

DataSet	MEAN (N)	MEAN (A)	VARIANCE (N)	VARIANCE (A)	t	p
LF	179.87	1024.89	10298.07	1903963.1	-1.61	0.07
HF	214.5	764.14	22506.89	3067773.8	-0.82	0.22
LF/HF	1.57	6.52	2.87	17.88	-2.84	0.01*

*: Significant at 0.05

t-test for normal and apnea subjects (without outlier - PW)

	Normal	Apnea	Normal	Apnea	Normal	Apnea
Name	LF	LF	HF	HF	LF/HF	LF/HF
AA		447.86		46.6		9.6
KT1		263.08		19.93		13.2
KT2		449.12		51		8.8
SIL		1310.91		347.85		3.8
LY		386.38		108.54		3.6
SF		271.74		47.1		5.8
LE	126.91		130		0.98	
LES	343.53		151.8		2.263	
SEK	110.67		23.39		4.731	
GAN	262.57		460.9		0.569	
BV	81.98		259.64		0.315	
BP4	153.59		261.29		0.581	

t-Test: Two-Sample Assuming Equal Variances**LF**

	<i>Normal</i>	<i>Apnea</i>
Mean	179.875	521.515
Variance	10298.07551	156249.646
Observations	6	6
Pooled Variance	83273.86067	
Hypothesized Mean Difference	0	
df	10	
t Stat	-2.050571848	
P(T<=t) one-tail	0.033721854	
t Critical one-tail	1.812461505	
P(T<=t) two-tail	0.067443708	
t Critical two-tail	2.228139238	

t-Test: Two-Sample Assuming Equal Variances**HF**

	<i>Normal</i>	<i>Apnea</i>
Mean	214.5033333	103.503333
Variance	22506.89115	15178.2178
Observations	6	6
Pooled Variance	18842.55447	
Hypothesized Mean Difference	0	
df	10	
t Stat	1.400598692	
P(T<=t) one-tail	0.095795663	
t Critical one-tail	1.812461505	
P(T<=t) two-tail	0.191591326	
t Critical two-tail	2.228139238	

t-Test: Two-Sample Assuming Equal Variances**LF/HF**

	<i>Normal</i>	<i>Apnea</i>
Mean	1.573166667	7.46666667
Variance	2.875071367	14.0746667
Observations	6	6
Pooled Variance	8.474869017	
Hypothesized Mean Difference	0	
df	10	
t Stat	-3.506448122	
P(T<=t) one-tail	0.002832579	
t Critical one-tail	1.812461505	
P(T<=t) two-tail	0.005665158	
t Critical two-tail	2.228139238	

t-test for normal and apnea subjects (without outlier - PW)

DataSet	MEAN (N)	MEAN (A)	VARIANCE (N)	VARIANCE (A)	t	P
LF	179.87	521.51	10298.07	156249.64	-2.05	0.03
HF	214.5	103.5	22506.89	15178.21	1.4	0.09
LF/HF	1.57	7.46	2.87	14.07	-3.5	0.002*

*: Significant at 0.05

REFERENCES

1. M. F. Hilton, "Sleep Disorders Program, Division of Sleep Medicine," Brigham and Women's Hospital/Harvard Medical School, Boston, MA, 02114.
2. L. Sherwood, "Human Physiology from Cells to Systems," (Fourth Edition-© 2001). California USA: Brooke Cole.
3. P. de Chazal, C. Heneghan, E. Sheridan, R. Reilly, P. Nolan, M. O'Malley, "Automatic Classification of Sleep Apnea Epochs using the Electrocardiogram," *IEEE Computers in Cardiology*, 2000; 27:745-748.
4. J. E. Mietus, C. K. Peng, P. C. H Ivanov, A. L. Goldberger, "Detection of Obstructive Sleep Apnea from Cardiac Interbeat Interval Series," *IEEE Computers in Cardiology*, 2000; 27:753-756.
5. Y. S. Kim, S. B. Hong, J. S. Kim, "Heart rate variability and degree of sleep in different sleep stage," Sleep Disorder Center, Department of Neurology and Cardiology, Samsung Medical Center, Seoul, Korea, *Sleep Research*, 1997; 26:135-230.
6. P. Castiglioni, M. R. Bonsignore, G. Insalaco, G. Parati, M. Di Rienzo, "Signal Processing Procedures for the Evaluation of the Cardiovascular Effects in the Obstructive Sleep Apnea Syndrome," *IEEE Computers in Cardiology*, 2000; 28:221-224.
7. C. Maier, M. Baush, H. Dickhaus, "Recognition and Quantification of Sleep Apnea by Analysis of Heart Rate Variability Parameters," *IEEE Computers in Cardiology*, 2000; 27:741-744.
8. T. Penzel, A. Bunde, J. Heitmann, J. W. Kantelhardt, J. H. Peter, K. Voigt, "Sleep Stage-Dependent Heart Rate Variability in Patients with Obstructive Sleep Apnea," *IEEE Computers in Cardiology*, 1999; 26:249-252.
9. M. F. Hilton, R. A. Bates, K. R. Godfrey, R. M. Cayton, "A New Application For Heart Rate Variability: Diagnosing the Sleep Apnea Syndrome," *IEEE Computers in Cardiology*, 1998; Vol. 25.
10. Z. Shinar, A. Baharav, Y. Dagan, S. Akselord, "Automatic Detection of Slow-Wave-Sleep using Heart Rate Variability", *IEEE Computers in Cardiology*, 2001; 28:593-596.
11. A. Baharav, Z. Shinar, Y. Dagan, S. Akselord, "Impaired Autonomic Balance During Sleep in Obstructive Sleep Apnea: Origin or Result," *IEEE Computers in Cardiology*, 2001; 28: 225-228.

12. H. G. V. Steenis, W. L. J. Martens, J. H. M. Tulen, "Time-Frequency Parameters of Heart-Rate Variability," *IEEE Engineering in Medicine and Biology*, 2002; 0739-5175.
13. D. A. Newandee, S. S. Reisman, "Application of the Wavelet Transform to Heart Rate Variability (HRV)," *IEEE*, 2002; 0-7803-7419.
14. G. L. Gamero, M. Risk, J. F. Sobh, A. J. Ramirez, J. P. Saul, "Heart Rate Variability Analysis Using Wavelet Transform," *IEEE, Computers in Cardiology*, 1996; 0276-6547.
15. P. J. Strollo, R. M. Rogers, "Obstructive Sleep Apnea," *The New England Journal of Medicine*, 1996; Vol.334 No 2.
16. P. J. Hanly, "Mechanisms and Management of Central Sleep Apnea," *Lung Springer-Verlag New York Inc.*, 1992; 170:1-17.
17. J. Camm, M. Malik, "Heart Rate Variability," *European Heart Journal* 1996; 17:354-381.
18. M. V. Kamath, E. L. Fallen, "Power Spectral Analysis of Heart Rate Variability: A Noninvasive Signature of Cardiac Autonomic Function," *Critical Reviews in Biomedical Engineering*, 1993; 21(3): 245-311.
19. L. Spicuzza, L. Bernardi, A. Calciati, G. U. Maria, "Autonomic Modulation of Heart Rate During Obstructive Versus Central Apneas in Patients Sleep-disordered Breathing," *American Journal of Respiratory and Critical Care Medicine*, 2003; 167: 902-910.
20. J. A. Loadsman, "Anaesthesia and Sleep Apnea," *British Journals of Anesthesia*, 2001; 86:254-266.
21. D. Sorresso, W. Mendelson "Sleep Disorders Medicine," [Article posted on the website] Retrieved March 12th from World Wide Web: <http://sleepmed.bsd.uchicago.edu/sleepphysiology.html>
22. M. Misiti, Y. Misiti, G. Oppenheim, J. M. Poggi, "Wavelet Toolbox," September 2000; Version 2.
23. T. Penzel, G. B. Moody, R. G. Mark, A. L. Golberger, J. H. Peter, "The Apnea-ECG Database," *IEEE Computers in Cardiology*, 2000; 27: 255-258.
24. T. Penzel, A. Bunde, L. Grote, J. W. Kantelhardt, J. H. Peter, K. Voigt, "Heart Rate Variability During Sleep Stage in Normals and in Patients with Sleep Apnea,"

25. F. Ng, I. Garcia, P. Gomis, A. L. Cruz, G. Passariello, F. Mora. "Bayesian Hierarchical Model with Wavelet Transform Coefficients of the ECG in Obstructive Sleep Apnea Screening," *IEEE Computers in Cardiology*, 2000; 27: 275-278.
26. B. Raymond, R. M. Cayton, R. A. Bates, M. J. Chappell, "Screening for Obstructive Sleep Apnea Based on the Electrocardiogram," *IEEE Computers in Cardiology*, 2000; 27: 267-270.
27. Z. Shinar, A. Baharav, S. Akselord, "Obstructive Sleep Apnea Detection Based on Electrocardiogram Analysis," *IEEE Computers in Cardiology*, 2000; 27: 757-760.
28. M. J. Drinnan, J. Allen, P. Langley, A. Murray, "Detection of Sleep Apnea from Frequency Analysis of Heart Rate Variability," *IEEE Computers in Cardiology*, 2000; 27: 259-262.
29. J. G. Webster, "Medical Instrumentation Application and Design," John Wiley & Sons, Inc. Third Edition, 1998.
30. D. W. Hudgel, "Treatment of Obstructive Sleep Apnea," *CHEST*, 1996; 109:1346-58.
31. W. Weiss, S. Remburg, E. Garpestad, J. Ringler, D. Sparrow, J. A. Parker, "Hemodynamic Consequences of Obstructive Sleep Apnea," *American Sleep Disorder Association and Sleep Research Society. Sleep*, 1995: 388-397.
32. J. N. McNames, A. M. Fraser, "Obstructive Sleep Apnea Classification Based on Spectrogram Patterns in the Electrocardiogram," *IEEE Computers in Cardiology*, 2000; 27:749-752.
33. B. Hammel, "The Discrete n-Fourier Transforms," 1997. [Article posted on the website] Retrieved March 12th from World Wide Web: <http://graham.main.nc.us/~bhammel/FCCR/VII.html>
34. R. Hetzel, H. Lucking "Cerebral Haemodynamics during the Mueller manoeuvre in Humans," *Clinical Physiology*, 2000; 20(4): 292.
35. T. Penzel, J.W. Kantelhardt, L. Grote, J.H. Peter, A. Bunde, "Comparison of Detrended Fluctuation Analysis and Spectral Analysis for Heart Rate Variability in Sleep and Sleep Apnea," *IEEE Transactions on Biomedical Engineering*, 2003; 50(10): 1143-1151.